Hindawi
Journal of Function Spaces
Volume 2022, Article ID 2388557, 33 pages
https://doi.org/10.1155/2022/2388557

Research Article

A Study on the Fractal-Fractional Epidemic Probability-Based Model of SARS-CoV-2 Virus along with the Taylor Operational Matrix Method for Its Caputo Version

Shahram Rezapour,[1,2] **Sina Etemad**,[1] **İbrahim Avcı**,[3] **Hijaz Ahmad**,[4] **and Azhar Hussain**[5]

[1]*Department of Mathematics, Azarbaijan Shahid Madani University, Tabriz, Iran*
[2]*Department of Medical Research, China Medical University Hospital, China Medical University, Taichung, Taiwan*
[3]*Department of Computer Engineering, Faculty of Engineering, Final International University, Kyrenia, Northern Cyprus Mersin 10, Turkey*
[4]*Section of Mathematics, International Telematic University Uninettuno, Corso Vittorio Emanuele II, 00186 Rome, Italy*
[5]*Department of Mathematics, University of Chakwal, Chakwal 48800, Pakistan*

Correspondence should be addressed to Sina Etemad; sina.etemad@azaruniv.ac.ir

Received 4 May 2022; Revised 20 July 2022; Accepted 29 July 2022; Published 1 September 2022

Academic Editor: Yusuf Gurefe

SARS-CoV-2 is a strain of the large coronavirus family that has led to COVID-19 disease. The virus has been one of the deadliest known viruses in the world to date. Rapid mutations and the creation of new strains cause researchers to focus on the dynamic behaviors of the virus and to analyze it accurately through clinical research and mathematical models. In this paper, from the point of view of mathematical modeling, we intend to focus on the dynamic behavior of the system and examine its analytical and numerical aspects in two different structures. In other words, by recalling newly formulated hybrid fractional-fractal operators, we present a fractal-fractional probability-based model of SARS-CoV-2 virus for the first time and extract its equivalent compact fractal-fractional IVP to investigate its existence and stability criteria. A type of special admissible contractions will help us in this regard. Moreover, based on the source data, we simulate our system according to algorithms derived by Adams-Bashforth method and explain the effects of variation of the dimension of fractal and fractional order on dynamics of solutions. Finally, we transform our fractal-fractional model into a Caputo probability-based model of SARS-CoV-2 to derive solutions via the operational matrix method under Taylor's basis. The numerical simulations show close behaviors for both of models.

1. Introduction

From birth to death, humans are always at risk for a variety of diseases; the source of these infectious diseases is mainly microorganisms such as parasites, fungi, viruses, and bacteria. Over the centuries, various epidemics have killed millions of people everywhere on the planet and caused great loss of life and property to families and governments. Recently, in late 2019, the international community contracted a new type of viral respiratory disease that was reported to have originated in Wuhan, China. For the sake of rapid spread of this unknown disease in Wuhan, scientists have used a variety of terms to describe the viral cause of the disease. According to the standard classifications in virology and considering its geographical location, it was first temporarily named Wuhan coronavirus and then the new coronavirus 2019 (2019-nCov). Finally, in 2020, an international committee from the World Health Organization (WHO), which works to classify viruses, used the official title SARS-CoV-2, which interprets the severe acute respiratory syndrome of coronavirus 2 [1]; and later, in

order not to be confused with the SARS virus, the committee used the abbreviated title COVID-19 [2].

Extensive medical research was conducted worldwide to identify the nature and spread of the virus, and on January 20, human-to-human transmission of the virus was proved [3]. The virus has also been shown to be transmitted via respiratory droplets such as coughing and sneezing and even talking indoors without ventilation [4, 5]. In addition, subsequent studies have shown that the best site for infection is the nasal cavity, through which it gradually and immediately enters the lungs and infects it [6]. However, other studies have shown that some wild animals, such as bats, mice, rabbits, and mink, can also transmit the SARS-CoV-2 virus to humans [7]. In these two years, no part of the human environments has been spared from the virus, even the most remote islands. As of March 10, 2022, more than 450 million people have been infected with COVID-19, of which more than six million have died, based on the approved reports of the World Health Organization [8]. In some cases, people with the SARS-CoV-2 virus have severe clinical symptoms and are hospitalized, but in most cases, patients with the SARS-CoV-2 virus do not need to be admitted to treatment centers and are treated with antiviral drugs such as remdesivir [9].

Due to the high rate of transmission of the virus and the development of its various strains, there was a need for definitive treatment to control the epidemic. Therefore, knowledge of the pathobiology of the SARS-CoV-2 virus was essential. Because vaccines are always an important tool in the fight against all epidemics, we have also seen extensive efforts to produce safe and effective vaccines for the SARS-CoV-2 virus by large pharmaceutical companies. Of course, it should be noted that in addition to mass vaccination to eradicate the virus completely, it is necessary for human societies to continue to maintain social distance and use masks indoors. It is still unknown whether the vaccines are effective in killing the disease.

In this regard, to accurately analyze the prevalence of the SARS-CoV-2 virus worldwide and predict its upward or downward trends, researchers turned to simulating the dynamics of the virus by mathematical models. Of course, it should be noted that in recent decades, mathematical models have always been helpful in studying the dynamics of various types of diseases and engineering processes, and through various modeling, scientists and researchers have been able to achieve their study goals. In this direction, fractional mathematical models are among the most widely used methods in the field of accurate analysis and evaluation of data. Known fractional operators such as Caputo, Atangana-Baleanu, and Caputo-Fabrizio fractional derivatives are efficient mathematical tools for defining and designing mathematical systems, so that their role can be clearly observed in newly published papers, for example, the modelling of anthrax in animals [10], genetic regulatory networks [11], mumps virus [12], Zika virus [13], mosaic disease [14], computer viruses [15], thermostat control [16], pantograph equation [17], Q-fever [18], hybrid equation of p-Laplacian operators [19], geographical models [20, 21], codynamics of COVID-19 and diabetes [22], chemical compounds such as methylpropane [23], and immunogenic tumor [24]. Also, due to difficulties of solving fractional differential equations analytically, developing efficient numerical methods with different fractional operators for such equations becomes an important focus for researchers; for example, in [25], fractional derivative generalized Atangana-Baleanu differentiability has been implemented to solve fuzzy fractional differential equations. Also, in 2021, Erturk et al. [26] used fractional calculus theory to investigate the motion of a beam on an internally bent nanowire. In [27], Jajarmi et al. presented a new and general fractional formulation to investigate the complex behaviors of a capacitor microphone dynamical system. Alqhtani et al. [28] presented that two important physical examples that are of current and recurring interests are considered, in which the classical time derivative was modeled with the Caputo fractional derivative leading the system of equations to subdiffusive fractional reaction-diffusion models of predator-prey type, together with some numerical experiments. In [29], Aljhani et al. discuss a one-dimensional time-fractional Gray-Scott model with Liouville-Caputo, Caputo-Fabrizio-Caputo, and Atangana-Baleanu-Caputo fractional derivatives. They also utilize the fractional homotopy analysis transformation method to obtain approximate solutions.

Numerous articles about SARS-CoV-2 or COVID-19 have recently been published in scientific journals around the world, including a few examples: DarAssi et al. [30] presented a model of SARS-CoV-2 with hospitalization in the form of a variable-order fractional model of Caputo's differential equations, in which they studied the asymptotic stability of the system. In the same direction, Gu et al. [31] also designed the comprehensive Caputo model of SARS-CoV-2 virus in the framework of the constant-order operator and analyzed the stable solutions of the system w.r.t. the index R_0 (reproduction number). Under a five-compartmental SEIRD model, and using real data from Italian medical authorities, Rajagopal et al. [32] conducted a case study of the disease and analyzed system behavior in both classical and fractional modes. In another case research of the prevalence of SARS-CoV-2 in France and Colombia, Quintero and Gutiérrez-Carvajal [33] examined the evolution of the disease under the bound optimization method. In 2021, Zamir et al. [34] formulated a model of COVID-19 in nine subclasses and focused the elimination and control of the infection caused by COVID-19. Jain et al. [35] presented a prediction model of COVID-19 by using numerous machine learning models, such as SVM, Naïve Bayes, K-nearest neighbors, AdaBoost, gradient boosting, XGBoost, random forest, ensembles, and neural networks. Baleanu et al. [36] introduced a generalized version of fractional models for the COVID-19 pandemic, including the effects of isolation and quarantine. In [37], Ali et al. investigate the transmission dynamics of a fractional-order mathematical model of COVID-19 under five subclasses, susceptible, exposed, asymptomatic infected, symptomatic infected, and recovered, using the Caputo fractional derivative. In 2022, Ozkose et al. [38] developed a new model of the Omicron strain of SARS-CoV-2 virus and, based on data collected across the United Kingdom, studied the relationship between this strain and heart attack. They also analyzed

the sensitivity of the system and fitting of the parameters using the LCM method.

In addition to these articles, many other researchers have published articles on COVID-19 dynamics and evaluated a variety of models under different conditions and assumptions. For instances, we can mention stochastic models of COVID-19 [39], or even various case studies of COVID-19 from all over the world like [40–44]. Most researchers simultaneously studied the models of COVID-19 analytically and numerically and evaluated the types of dynamic behaviors of the solutions under singular and nonsingular systems that can be mentioned like [45, 46]. In the theoretical study of all these mentioned models, the theoretical results are among the basic parts of the analysis of mathematical models, because the existence of a solution for a system allows us to continue to study other properties such as stable solutions, equilibrium solutions, numerical solutions, and their simulations. Usually, fixed point theory is effective in this field, and its role can be observed in boundary and initial value problems [47].

By defining mathematical models and the refinement of numerical approaches, there is a need to use new mathematical operators with high computational capabilities to model processes. As a result, Atangana [48] used fractal derivatives to introduce a new type of hybrid operators and introduced fractional-fractal derivatives into the world of modeling in 2017. In fact, to define these advanced operators, he used two arguments to represent the order of the operator and the dimension of the operator, which he called the fractional order and the fractional dimension of the fractional-fractional derivatives, respectively [48]. Atangana then divided these derivatives into three different categories and, with the help of different integral kernels, extracted the numerical algorithms associated with them. Then, in the last year, these numerical techniques were used in some new studies in which researchers simulated the approximate solutions of fractional-fractal models of new infectious diseases. In 2021, Arfan et al. [49] designed a prey-predation structure for the four-compartmental fractal-fractional model of syn-ecosymbiosis and examined some conditions for species survival in an ecological system. Abdulwasaa et al. [50] conducted a case study with these fractal-fractional operators in which they examined the dynamics of new cases and the number of deaths from the COVID-19 epidemic over a specific period of time in India. Shah et al. [51] conducted the same study on a new model in Pakistan. Khan et al. [52] simulated and evaluated models of smoking at the incidence rate under the Caputo fractal-fractional derivative operator. Arif et al. [53] utilized the same fractal-fractional operators in engineering to analyze MHD stress fluid in a single channel. Alqhtani et al. [54] studied three models of fractal-fractional Michaelis-Menten enzymatic reaction (FFMMER) and presented these models based on three different kernels, namely, power law, exponential decay, and Mittag-Leffler kernels.

In this work, considering the importance of symptomatic and asymptomatic populations in spreading of virus, we present the new fractal-fractional probability-based model of SARS-CoV-2 virus by dividing the total population into four subclasses such as susceptible, asymptomatic, symptomatic, and recovered individuals. In [55], the authors designed a five-compartmental Caputo fractional epidemic model for the novel coronavirus in which the impact of environmental transmission is considered in the final result. This model motivates us to study an extended model of transmission of SARS-CoV-2 virus via advanced hybrid operators. In this paper, we get help from these newly extended hybrid fractal-fractional operators and discuss a new hybrid model of transmission of SARS-CoV-2 virus analytically and numerically. If we want to focus on the novelty and contribution of this manuscript, it is notable that for the first time, our system is a fractal-fractional probability-based model of SARS-CoV-2 virus in which we apply new hybrid fractal-fractional derivatives for modeling of the power law type kernel. Also, in this model, a probability-based structure of transmission of virus is considered. In other words, if p is the probability that both categories susceptible and infected interact and this leads to the asymptomatic category, in that case, $(1-p)$ stands for the portion of the infected persons that may automatically belong to the symptomatic category. On the other hand, it should be kept in mind that when people become infected with the SARS-CoV-2 virus, they may not have any symptoms, but at the same time, some people may experience severe complications and show specific symptoms. Therefore, the feature of our model is that we have divided the group of people infected with the virus into two categories: symptomatic and asymptomatic. Also, from mathematical point of view, a specific approach of fixed point methods is applied via ϕ-admissible ϕ-ψ-contractions to discuss the existence criterion, in which it shows the applicability of new fixed point techniques in the applied problems. Also, another novelty of this study is that in addition to fractal-fractional analysis of the SARS-CoV-2 model, we extend its Caputo-type version to compare our previous results with solutions of the fractional model under the Taylor operational matrix method. Also, note that in this paper, we consider both fractional and fractal-fractional derivatives as the full memory. We can study similar models by using the short memory. In this direction, refer to [56, 57].

In this study, from a numerical point of view, we present two numerical techniques for the approximate solution of the considered model of SARS-CoV-2 virus under two different fractional operator derivative. The first technique is the Adams-Bashforth technique which is applied to probability-based model of SARS-CoV-2 under fractal-fractional operator in this study. The ABM is a very stable technique and allows us explicitly to determine the numerical solution at an instant time from the solutions in the previous instants. Using the higher-order Adams-Bashforth method actually becomes more unstable as the timestep is reduced. So that, the corrector step need to be added to avoid much of this instability. This can be mentioned as a disadvantage of AB technique. The second method is a collocation type of the well-known spectral methods; fractional Taylor operational matrix method is applied to solve probability-based model of SARS-CoV-2 under Caputo operator first time in this paper. The main advantage of spectral methods is that they are easy to apply for both finite

and infinite intervals and when the solution of a given problem is smooth, spectral methods have very good error properties, namely, the so-called "exponential convergence." Thanks to these advantages, for solving many different types of integral and differential equations numerically, spectral methods received considerable interest in recent years. When the solution is not smooth enough, the stability and accuracy of these methods are decreasing, which is an important disadvantage because of limiting the applicability. In this work, we compare our results obtained from FTOMM with the Adams-Bashforth simulations.

The structure of the manuscript is arranged as follows: some definitions of ϕ-admissible ϕ-ψ-contractions and fractal-fractional derivatives are presented in the next section. We describe our main fractal-fractional model in Section 3 along with the meanings of parameters. Under two different fixed point methods, we guarantee the existence property for solutions of the system in Section 4. Section 5 deals with the Lipschitz and uniqueness properties. Then, in Section 6, we discuss UHR-stable solutions for each four state functions separately. To predict the future of state functions and their analysis numerically, we simulate them via the Adams-Bashforth method in two subsections of Section 7. In the next step, in Section 8, we give the Caputo-type of transmission of the SARS-CoV-2 virus, and in several subsections, we describe our method via the Taylor operational matrix technique, and after some simulations, we compare our numerical results in both fractal-fractional and fractional systems in the context of some graphs and tables. The conclusions and further study suggestions are presented in Section 9.

2. Basic Concepts

Some basic notions on the fractal-fractional operators and fixed point theory are assembled.

Let Ψ display a subclass of nondecreasing operators like $\psi : [0,\infty) \longrightarrow [0,\infty)$ s.t.

$$\sum_{j=1}^{\infty} \psi^j(\mathfrak{t}) < \infty, \psi(\mathfrak{t}) < \mathfrak{t}, \forall \mathfrak{t} > 0. \tag{1}$$

Definition 1 (see [58]). Let $\mathbb{X}$ be a normed space and $\mathcal{F} : \mathbb{X} \longrightarrow \mathbb{X}$ and $\phi : \mathbb{X}^2 \longrightarrow \mathbb{R}_{\geq 0}$.

$(p)\mathcal{F}$ is ϕ-ψ-contraction if for $\mathfrak{u}_1, \mathfrak{u}_2 \in \mathbb{X}$,

$$\phi(\mathfrak{u}_1, \mathfrak{u}_2)\mathbf{d}(\mathcal{F}\mathfrak{u}_1, \mathcal{F}\mathfrak{u}_2) \leq \psi(d(\mathfrak{u}_1, \mathfrak{u}_2)). \tag{2}$$

(q) $\mathcal{F}$ is ϕ-admissible if $\phi(\mathfrak{u}_1, \mathfrak{u}_2) \geq 1$ yields $\phi(\mathcal{F}\mathfrak{u}_1, \mathcal{F}\mathfrak{u}_2) \geq 1$.

Definition 2 (see [48]). Let $\mathcal{F}$ be fractal differentiable on (a, b) of order ν. The fractional-fractal ω^{th}-derivative of the function $\mathcal{F}$ via the power law type kernel in the Riemann-Liouville sense is defined by

$$\begin{aligned} {}^{\text{FFP}}\mathfrak{D}_{a,\mathfrak{t}}^{\omega,\nu}\mathcal{F}(\mathfrak{t}) &= \frac{1}{\Gamma(n-\omega)}\frac{\mathrm{d}}{\mathrm{d}\mathfrak{t}^{\nu}}\int_a^{\mathfrak{t}} (\mathfrak{t}-\mathfrak{m})^{n-\omega-1}\mathcal{F}(\mathfrak{m})\,\mathrm{d}\mathfrak{m}, \\ &\quad \cdot (n-1 < \omega, \nu \leq n \in \mathbb{N}), \end{aligned} \tag{3}$$

where $d\mathcal{F}(\mathfrak{m})/\mathrm{d}\mathfrak{m}^{\nu} = \lim_{\mathfrak{t}\longrightarrow\mathfrak{m}}((\mathcal{F}(\mathfrak{t}) - \mathcal{F}(\mathfrak{m}))/(\mathfrak{t}^{\nu} - \mathfrak{m}^{\nu}))$ is the fractal derivative.

It is known that if $\nu = 1$, then the fractal-fractional derivative ${}^{\text{FFP}}\mathfrak{D}_{a,\mathfrak{t}}^{\omega,\nu}$ is reduced to the standard derivative ${}^{\text{RL}}\mathfrak{D}_{a,\mathfrak{t}}^{\omega}$ of order ω.

Definition 3 (see [48]). Let $\mathcal{F}$ be continuous on (a, b). The fractional-fractal integral of the function $\mathcal{F}$ with fractional order ω and fractal order ν is

$${}^{\text{FFP}}\mathfrak{I}_{a,\mathfrak{t}}^{\omega,\nu}\mathcal{F}(\mathfrak{t}) = \frac{\nu}{\Gamma(\omega)}\int_a^{\mathfrak{t}} \mathfrak{m}^{\nu-1}(\mathfrak{t}-\mathfrak{m})^{\omega-1}\mathcal{F}(\mathfrak{m})\,\mathrm{d}\mathfrak{m}. \tag{4}$$

3. Description of the Model for SARS-CoV-2 Virus

Khan et al. [59, 60] modeled a mathematical structure of dynamics of SARS-CoV-2 virus in the form of four initial value problems equipped with four state functions $\mathcal{S}$, $\mathcal{P}_1$, $\mathcal{P}_2$, and $\mathcal{R}$, which are a part of total population. This model is

$$\begin{cases} \dfrac{\mathrm{d}\mathcal{S}(\mathfrak{t})}{\mathrm{d}\mathfrak{t}} = \Theta - r\mathcal{P}_1(\mathfrak{t})\mathcal{S}(\mathfrak{t}) - rs\mathcal{P}_2(\mathfrak{t})\mathcal{S}(\mathfrak{t}) - (b+b_1)\mathcal{S}(\mathfrak{t}), \\ \dfrac{\mathrm{d}\mathcal{P}_1(\mathfrak{t})}{\mathrm{d}\mathfrak{t}} = p[r\mathcal{P}_1(\mathfrak{t})\mathcal{S}(\mathfrak{t}) + rs\mathcal{P}_2(\mathfrak{t})\mathcal{S}(\mathfrak{t})] - (b_1+b_2+r_1)\mathcal{P}_1(\mathfrak{t}), \\ \dfrac{\mathrm{d}\mathcal{P}_2(\mathfrak{t})}{\mathrm{d}\mathfrak{t}} = (1-p)[r\mathcal{P}_1(\mathfrak{t})\mathcal{S}(\mathfrak{t}) + rs\mathcal{P}_2(\mathfrak{t})\mathcal{S}(\mathfrak{t})] + qr_1\mathcal{P}_1(\mathfrak{t}) - (b_1+b_3+r_2)\mathcal{P}_2(\mathfrak{t}), \\ \dfrac{\mathrm{d}\mathcal{R}(\mathfrak{t})}{\mathrm{d}\mathfrak{t}} = r_1(1-q)\mathcal{P}_1(\mathfrak{t}) + r_2\mathcal{P}_2(\mathfrak{t}) + b\mathcal{S}(\mathfrak{t}) - b_1\mathcal{R}(\mathfrak{t}), \end{cases} \tag{5}$$

where $\mathcal{S}(\mathfrak{t})$ stands for the people belonging to the susceptible category, $\mathcal{P}_1(\mathfrak{t})$ is the people belonging to the asymptomatic category, $\mathcal{P}_2(\mathfrak{t})$ is the people belonging to the symptomatic category, and $\mathcal{R}(\mathfrak{t})$ stands for the people belonging to the recovered category at the time $\mathfrak{t} \in \mathbb{J} := [0, T]$, $(T > 0)$. Based on these assumptions, the infected categories are taken to be symptomatic class and asymptomatic class, because asymptomatic persons are considered as the main factor of transmission of disease. It is to be noted that the variables, constants, and parameters are nonnegative.

Inspired by the aforesaid standard epidemic model, we here consider the fractal-fractional epidemic probability-based model of the SARS-CoV-2 virus in the following structure:

$$\begin{cases} {}^{\mathrm{FFP}}\mathfrak{D}_{0,\mathfrak{t}}^{\omega,\nu}\mathcal{S}(\mathfrak{t}) = \Theta - r\mathcal{P}_1(\mathfrak{t})\mathcal{S}(\mathfrak{t}) - rs\mathcal{P}_2(\mathfrak{t})\mathcal{S}(\mathfrak{t}) - (b + b_1)\mathcal{S}(\mathfrak{t}), \\ {}^{\mathrm{FFP}}\mathfrak{D}_{0,\mathfrak{t}}^{\omega,\nu}\mathcal{P}_1(\mathfrak{t}) = p[r\mathcal{P}_1(\mathfrak{t})\mathcal{S}(\mathfrak{t}) + rs\mathcal{P}_2(\mathfrak{t})\mathcal{S}(\mathfrak{t})] - (b_1 + b_2 + r_1)\mathcal{P}_1(\mathfrak{t}), \\ {}^{\mathrm{FFP}}\mathfrak{D}_{0,\mathfrak{t}}^{\omega,\nu}\mathcal{P}_2(\mathfrak{t}) = (1-p)[r\mathcal{P}_1(\mathfrak{t})\mathcal{S}(\mathfrak{t}) + rs\mathcal{P}_2(\mathfrak{t})\mathcal{S}(\mathfrak{t})] + qr_1\mathcal{P}_1(\mathfrak{t}) - (b_1 + b_3 + r_2)\mathcal{P}_2(\mathfrak{t}), \\ {}^{\mathrm{FFP}}\mathfrak{D}_{0,\mathfrak{t}}^{\omega,\nu}\mathcal{R}(\mathfrak{t}) = r_1(1-q)\mathcal{P}_1(\mathfrak{t}) + r_2\mathcal{P}_2(\mathfrak{t}) + b\mathcal{S}(\mathfrak{t}) - b_1\mathcal{R}(\mathfrak{t}), \end{cases} \tag{6}$$

subject to

$$\begin{aligned} \mathcal{S}(0) &= \mathcal{S}_0 > 0, \\ \mathcal{P}_1(0) &= \mathcal{P}_{1,0} \geq 0, \\ \mathcal{P}_2(0) &= \mathcal{P}_{2,0} \geq 0, \\ \mathcal{R}(0) &= \mathcal{R}_0 \geq 0, \end{aligned} \tag{7}$$

where ${}^{\mathrm{FFP}}\mathfrak{D}_{0,\mathfrak{t}}^{\omega,\nu}$ is the fractional-fractal derivative of the fractional order $\omega \in (0, 1]$ and the fractal order $\nu \in (0, 1]$ via the power law type kernel. We have

$$\mathcal{N}(\mathfrak{t}) = \mathcal{S}(\mathfrak{t}) + \mathcal{P}_1(\mathfrak{t}) + \mathcal{P}_2(\mathfrak{t}) + \mathcal{R}(\mathfrak{t}), \tag{8}$$

in which as we said above, $\mathcal{N}(\mathfrak{t})$ means the total population at the time $\mathfrak{t} \in \mathbb{J} := [0, T]$, $(T > 0)$.

About parameters, the total natural death rate along with the rate of disease-related death for both infected groups is specified by the symbols b_1, b_2, and b_3, respectively. We show the rate of transmission of disease by r, and its reduced rate is denoted by the symbol s. The vaccination rate is given by b, and Θ stands for the newborn rate. The probability of the asymptomatic persons is illustrated by p, and the probability of these persons that recover in the symptomatic step is specified by q. Moreover, r_2 is the recovery rate in relation to asymptomatic persons and accordingly, and r_1 is the recovery rate in relation to the symptomatic persons.

4. Existence of Solutions

In this position, we shall get help fixed point theory to the suggested fractal-fractional IVP (6). For the qualitative analysis, we define the Banach space $\mathbb{X} = \mathbb{Y}^4$, where $\mathbb{Y} = C(\mathbb{J}, \mathbb{R})$, as

$$\begin{aligned} \|\mathcal{X}\|_{\mathbb{X}} &= \|(\mathcal{S}, \mathcal{P}_1, \mathcal{P}_2, \mathcal{R})\|_{\mathbb{X}} \\ &= \max\{|\mathcal{S}(\mathfrak{t})| + |\mathcal{P}_1(\mathfrak{t})| + |\mathcal{P}_2(\mathfrak{t})| + |\mathcal{R}(\mathfrak{t})| : \mathfrak{t} \in \mathbb{J}\}. \end{aligned} \tag{9}$$

We write the R.H.S. of model (6) by

$$\begin{cases} \mathcal{F}_1(\mathfrak{t}, \mathcal{S}(\mathfrak{t}), \mathcal{P}_1(\mathfrak{t}), \mathcal{P}_2(\mathfrak{t}), \mathcal{R}(\mathfrak{t})) = \Theta - r\mathcal{P}_1(\mathfrak{t})\mathcal{S}(\mathfrak{t}) - rs\mathcal{P}_2(\mathfrak{t})\mathcal{S}(\mathfrak{t}) - (b + b_1)\mathcal{S}(\mathfrak{t}), \\ \mathcal{F}_2(\mathfrak{t}, \mathcal{S}(\mathfrak{t}), \mathcal{P}_1(\mathfrak{t}), \mathcal{P}_2(\mathfrak{t}), \mathcal{R}(\mathfrak{t})) = p[r\mathcal{P}_1(\mathfrak{t})\mathcal{S}(\mathfrak{t}) + rs\mathcal{P}_2(\mathfrak{t})\mathcal{S}(\mathfrak{t})] - (b_1 + b_2 + r_1)\mathcal{P}_1(\mathfrak{t}), \\ \mathcal{F}_3(\mathfrak{t}, \mathcal{S}(\mathfrak{t}), \mathcal{P}_1(\mathfrak{t}), \mathcal{P}_2(\mathfrak{t}), \mathcal{R}(\mathfrak{t})) = (1-p)[r\mathcal{P}_1(\mathfrak{t})\mathcal{S}(\mathfrak{t}) + rs\mathcal{P}_2(\mathfrak{t})\mathcal{S}(\mathfrak{t})] + qr_1\mathcal{P}_1(\mathfrak{t}) - (b_1 + b_3 + r_2)\mathcal{P}_2(\mathfrak{t}), \\ \mathcal{F}_4(\mathfrak{t}, \mathcal{S}(\mathfrak{t}), \mathcal{P}_1(\mathfrak{t}), \mathcal{P}_2(\mathfrak{t}), \mathcal{R}(\mathfrak{t})) = r_1(1-q)\mathcal{P}_1(\mathfrak{t}) + r_2\mathcal{P}_2(\mathfrak{t}) + b\mathcal{S}(\mathfrak{t}) - b_1\mathcal{R}(\mathfrak{t}). \end{cases} \tag{10}$$

Hence,

$$\begin{cases} {}^{\mathrm{RL}}\mathfrak{D}_{0,\mathfrak{t}}^{\omega}\mathcal{S}(\mathfrak{t}) = \nu\mathfrak{t}^{\nu-1}\mathcal{F}_1(\mathfrak{t}, \mathcal{S}(\mathfrak{t}), \mathcal{P}_1(\mathfrak{t}), \mathcal{P}_2(\mathfrak{t}), \mathcal{R}(\mathfrak{t})), \\ {}^{\mathrm{RL}}\mathfrak{D}_{0,\mathfrak{t}}^{\omega}\mathcal{P}_1(\mathfrak{t}) = \nu\mathfrak{t}^{\nu-1}\mathcal{F}_2(\mathfrak{t}, \mathcal{S}(\mathfrak{t}), \mathcal{P}_1(\mathfrak{t}), \mathcal{P}_2(\mathfrak{t}), \mathcal{R}(\mathfrak{t})), \\ {}^{\mathrm{RL}}\mathfrak{D}_{0,\mathfrak{t}}^{\omega}\mathcal{P}_2(\mathfrak{t}) = \nu\mathfrak{t}^{\nu-1}\mathcal{F}_3(\mathfrak{t}, \mathcal{S}(\mathfrak{t}), \mathcal{P}_1(\mathfrak{t}), \mathcal{P}_2(\mathfrak{t}), \mathcal{R}(\mathfrak{t})), \\ {}^{\mathrm{RL}}\mathfrak{D}_{0,\mathfrak{t}}^{\omega}\mathcal{R}(\mathfrak{t}) = \nu\mathfrak{t}^{\nu-1}\mathcal{F}_4(\mathfrak{t}, \mathcal{S}(\mathfrak{t}), \mathcal{P}_1(\mathfrak{t}), \mathcal{P}_2(\mathfrak{t}), \mathcal{R}(\mathfrak{t})). \end{cases} \tag{11}$$

By (11), we derive the following IVP:

$$\begin{cases} {}^{\mathrm{RL}}\mathfrak{D}_{0,\mathfrak{t}}^{\omega}\mathscr{X}(\mathfrak{t}) = \nu\mathfrak{t}^{\nu-1}\mathscr{F}(\mathfrak{t},\mathscr{X}(\mathfrak{t})), \omega,\nu\in(0,1], \\ \mathscr{X}(0) = \mathscr{X}_0, \end{cases} \tag{12}$$

where

$$\begin{aligned} \mathscr{X}(\mathfrak{t}) &= (\mathscr{S}(\mathfrak{t}),\mathscr{P}_1(\mathfrak{t}),\mathscr{P}_2(\mathfrak{t}),\mathscr{R}(\mathfrak{t}))^T, \\ \mathscr{X}_0 &= (\mathscr{S}_0,\mathscr{P}_{1,0},\mathscr{P}_{2,0},\mathscr{R}_0)^T, \\ \mathscr{F}(\mathfrak{t},\mathscr{X}(\mathfrak{t})) &= \begin{cases} \mathscr{F}_1(\mathfrak{t},\mathscr{S}(\mathfrak{t}),\mathscr{P}_1(\mathfrak{t}),\mathscr{P}_2(\mathfrak{t}),\mathscr{R}(\mathfrak{t})), \\ \mathscr{F}_2(\mathfrak{t},\mathscr{S}(\mathfrak{t}),\mathscr{P}_1(\mathfrak{t}),\mathscr{P}_2(\mathfrak{t}),\mathscr{R}(\mathfrak{t})), \\ \mathscr{F}_3(\mathfrak{t},\mathscr{S}(\mathfrak{t}),\mathscr{P}_1(\mathfrak{t}),\mathscr{P}_2(\mathfrak{t}),\mathscr{R}(\mathfrak{t})), \\ \mathscr{F}_4(\mathfrak{t},\mathscr{S}(\mathfrak{t}),\mathscr{P}_1(\mathfrak{t}),\mathscr{P}_2(\mathfrak{t}),\mathscr{R}(\mathfrak{t})). \end{cases} \end{aligned} \tag{13}$$

Now, the fractional-fractal integral acts on (12), and it becomes

$$\mathscr{X}(\mathfrak{t}) = \mathscr{X}(0) + \frac{\nu}{\Gamma(\omega)}\int_0^{\mathfrak{t}}\mathfrak{m}^{\nu-1}(\mathfrak{t}-\mathfrak{m})^{\omega-1}\mathscr{F}(\mathfrak{m},\mathscr{X}(\mathfrak{m}))\,\mathrm{d}\mathfrak{m}. \tag{14}$$

In other words, the extended form of the above fractal-fractional integral is represented as

$$\begin{cases} \mathscr{S}(\mathfrak{t}) = \mathscr{S}_0 + \dfrac{\nu}{\Gamma(\omega)}\displaystyle\int_0^{\mathfrak{t}}\mathfrak{m}^{\nu-1}(\mathfrak{t}-\mathfrak{m})^{\omega-1}\mathscr{F}_1(\mathfrak{m},\mathscr{S}(\mathfrak{m}),\mathscr{P}_1(\mathfrak{m}),\mathscr{P}_2(\mathfrak{m}),\mathscr{R}(\mathfrak{m}))\,\mathrm{d}\mathfrak{m}, \\ \mathscr{P}_1(\mathfrak{t}) = \mathscr{P}_{1,0} + \dfrac{\nu}{\Gamma(\omega)}\displaystyle\int_0^{\mathfrak{t}}\mathfrak{m}^{\nu-1}(\mathfrak{t}-\mathfrak{m})^{\omega-1}\mathscr{F}_2(\mathfrak{m},\mathscr{S}(\mathfrak{m}),\mathscr{P}_1(\mathfrak{m}),\mathscr{P}_2(\mathfrak{m}),\mathscr{R}(\mathfrak{m}))\,\mathrm{d}\mathfrak{m}, \\ \mathscr{P}_2(\mathfrak{t}) = \mathscr{P}_{2,0} + \dfrac{\nu}{\Gamma(\omega)}\displaystyle\int_0^{\mathfrak{t}}\mathfrak{m}^{\nu-1}(\mathfrak{t}-\mathfrak{m})^{\omega-1}\mathscr{F}_3(\mathfrak{m},\mathscr{S}(\mathfrak{m}),\mathscr{P}_1(\mathfrak{m}),\mathscr{P}_2(\mathfrak{m}),\mathscr{R}(\mathfrak{m}))\,\mathrm{d}\mathfrak{m}, \\ \mathscr{R}(\mathfrak{t}) = \mathscr{R}_0 + \dfrac{\nu}{\Gamma(\omega)}\displaystyle\int_0^{\mathfrak{t}}\mathfrak{m}^{\nu-1}(\mathfrak{t}-\mathfrak{m})^{\omega-1}\mathscr{F}_4(\mathfrak{m},\mathscr{S}(\mathfrak{m}),\mathscr{P}_1(\mathfrak{m}),\mathscr{P}_2(\mathfrak{m}),\mathscr{R}(\mathfrak{m}))\,\mathrm{d}\mathfrak{m}. \end{cases} \tag{15}$$

Consider the operator $G:\mathbb{X}\longrightarrow\mathbb{X}$ as

$$G(\mathscr{X}(\mathfrak{t})) = \mathscr{X}(0) + \frac{\nu}{\Gamma(\omega)}\int_0^{\mathfrak{t}}\mathfrak{m}^{\nu-1}(\mathfrak{t}-\mathfrak{m})^{\omega-1}\mathscr{F}(\mathfrak{m},\mathscr{X}(\mathfrak{m}))\mathrm{d}\mathfrak{m}. \tag{16}$$

In the preceding, we recall the required fixed point theorem in connection with our aim for proving the existence results.

Theorem 4 (see [58]). *Assume* $(\mathbb{X},\mathbf{d})$ *as a Banach space,* $\phi:\mathbb{X}\times\mathbb{X}\longrightarrow\mathbb{R}$, $\psi\in\Psi$, *and* $\mathscr{F}:\mathbb{X}\longrightarrow\mathbb{X}$ *as an* ϕ-ψ*-contraction s.t.*

(1) $\mathscr{F}$ *is* ϕ*-admissible*

(2) $\exists u_0\in\mathbb{X}, s.t.\phi(\mathfrak{u}_0,\mathscr{F}\mathfrak{u}_0)\geq 1$

(3) for any sequence $\{\mathfrak{u}_n\}$ *in* $\mathbb{X}$ *with* $\mathfrak{u}_n\longrightarrow\mathfrak{u}$ *and* $\phi(\mathfrak{u}_n,\mathfrak{u}_{n+1})\geq 1$ *for all* $n\geq 1$, *we have* $\phi(\mathfrak{u}_n,\mathfrak{u})\geq 1,\forall n\in\mathbb{N}$

Then, $\exists\mathfrak{u}*$ *s.t.* $\mathscr{F}(\mathfrak{u}*)=\mathfrak{u}*$.

Now, the first existence result is proved here under some special operators.

Theorem 5. *Let* $\exists\mathfrak{T}:\mathbb{R}\times\mathbb{R}\longrightarrow\mathbb{R}$, $\exists$ *a continuous map* $\mathscr{F}:\mathbb{J}\times\mathbb{X}\longrightarrow\mathbb{X}$, *and* $\exists$ *a nondecreasing map* $\psi\in\Psi$. *Let* $(\mathfrak{B}_1)\forall\mathscr{X}_1,\mathscr{X}_2\in\mathbb{X}$, *and* $\mathfrak{t}\in\mathbb{J}$,

$$|\mathscr{F}(\mathfrak{t},\mathscr{X}_1(\mathfrak{t}))-\mathscr{F}(\mathfrak{t},\mathscr{X}_2(\mathfrak{t}))|\leq\tilde{\ell}\,\psi(|\mathscr{X}_1(\mathfrak{t})-\mathscr{X}_2(\mathfrak{t}|), \tag{17}$$

with $\mathfrak{T}(\mathscr{X}_1(\mathfrak{t}),\mathscr{X}_2(\mathfrak{t}))\geq 0$, *where* $\tilde{\ell}=(\Gamma(\nu+\omega))/(\nu T^{\nu+\omega-1}\Gamma(\nu))$.

($\mathfrak{B}_2$*)* $\mathscr{X}_0\in\mathbb{X}$ *exists so that* $\forall\mathfrak{t}\in\mathbb{J}$,

$$\mathfrak{T}(\mathscr{X}_0(\mathfrak{t}),G(\mathscr{X}_0(\mathfrak{t})))\geq 0, \tag{18}$$

and also, the inequality

$$\mathfrak{T}(\mathscr{X}_1(\mathfrak{t}),\mathscr{X}_2(\mathfrak{t}))\geq 0, \tag{19}$$

gives

$$\mathfrak{T}(G(\mathscr{X}_1(\mathfrak{t})),G(\mathscr{X}_2(\mathfrak{t})))\geq 0, \tag{20}$$

for any $\mathscr{X}_1,\mathscr{X}_2\in\mathbb{X}$ *and* $\mathfrak{t}\in\mathbb{J}$.

($\mathfrak{B}_3$*)*$\forall\{\mathscr{X}_n\}_{n\geq 1}$ *belonging to* $\mathbb{X}$ *with* $\mathscr{X}_n\longrightarrow\mathscr{X}$ *and*

$$\mathfrak{T}(\mathscr{X}_n(\mathfrak{t}),\mathscr{X}_{n+1}(\mathfrak{t}))\geq 0, \tag{21}$$

for each n *and* $\mathfrak{t}\in\mathbb{J}$, *we get*

$$\mathfrak{T}(\mathcal{X}_n(\mathfrak{t}), \mathcal{X}(\mathfrak{t})) \geq 0. \tag{22}$$

In such a case, $\exists$ is a solution for the fractal-fractional problem (12), and so there exists a solution for the given fractal-fractional epidemic model of SARS-CoV-2 virus (6).

Proof. Let $\mathcal{X}_1$ and $\mathcal{X}_2$ be two members belonging to $\mathbb{X}$ with

$$\mathfrak{T}(\mathcal{X}_1(\mathfrak{t}), \mathcal{X}_2(\mathfrak{t})) \geq 0, \tag{23}$$

for each $\mathfrak{t} \in \mathbb{J}$. Then, by definition of the Beta function, we may write

$$\begin{aligned}
&|G(\mathcal{X}_1(\mathfrak{t})) - G(\mathcal{X}_2(\mathfrak{t}))| \\
&\quad \leq \frac{\nu}{\Gamma(\omega)} \int_0^{\mathfrak{t}} \mathfrak{m}^{\nu-1} (\mathfrak{t} - \mathfrak{m})^{\omega-1} |\mathcal{F}(\mathfrak{m}, \mathcal{X}_1(\mathfrak{m})) - \mathcal{F}(\mathfrak{m}, \mathcal{X}_2(\mathfrak{m}))| \, \mathrm{d}\mathfrak{m} \\
&\quad \leq \frac{\nu}{\Gamma(\omega)} \int_0^{\mathfrak{t}} \mathfrak{m}^{\nu-1} (\mathfrak{t} - \mathfrak{m})^{\omega-1} \tilde{\ell} \psi(\mathcal{X}_1(\mathfrak{m}) - \mathcal{X}_2(\mathfrak{m})) \mathrm{d}\mathfrak{m} \\
&\quad \leq \frac{\nu \tilde{\ell} T^{\nu+\omega-1} \mathbb{B}(\nu, \omega)}{\Gamma(\omega)} \psi(\|\mathcal{X}_1 - \mathcal{X}_2\|_{\mathbb{X}}) \\
&\quad = \frac{\nu T^{\nu+\omega-1} \Gamma(\nu)}{\Gamma(\nu + \omega)} \tilde{\ell} \psi(\|\mathcal{X}_1 - \mathcal{X}_2\|_{\mathbb{X}}).
\end{aligned} \tag{24}$$

Consequently, we have

$$\begin{aligned}
\|G(\mathcal{X}_1) - G(\mathcal{X}_2)\|_{\mathbb{X}} &\leq \frac{\nu T^{\nu+\omega-1} \Gamma(\nu)}{\Gamma(\nu + \omega)} \tilde{\ell} \psi(\|\mathcal{X}_1 - \mathcal{X}_2\|_{\mathbb{X}}) \\
&= \psi(\|\mathcal{X}_1 - \mathcal{X}_2\|_{\mathbb{X}}).
\end{aligned} \tag{25}$$

Now, $\phi : \mathbb{X} \times \mathbb{X} \longrightarrow [0,\infty)$ is introduced by the this rule:

$$\phi(\mathcal{X}_1, \mathcal{X}_2) = \begin{cases} 1 \text{ if } \mathfrak{T}(\mathcal{X}_1(\mathfrak{t}), \mathcal{X}_2(\mathfrak{t})) \geq 0, \\ 0 \text{ otherwise.} \end{cases} \tag{26}$$

Then, for every $\mathcal{X}_1, \mathcal{X}_2 \in \mathbb{X}$, we will get

$$\phi(\mathcal{X}_1, \mathcal{X}_2) \mathbf{d}(G(\mathcal{X}_1), G(\mathcal{X}_2)) \leq \psi(\mathbf{d}(\mathcal{X}_1, \mathcal{X}_2)). \tag{27}$$

Thus, G is found as an ϕ-ψ-contraction. To verify that G is ϕ-admissible, let $\mathcal{X}_1, \mathcal{X}_2 \in \mathbb{X}$ be arbitrary and $\phi(\mathcal{X}_1, \mathcal{X}_2) \geq 1$. By definition of ϕ, we have

$$\mathfrak{T}(\mathcal{X}_1(\mathfrak{t}), \mathcal{X}_2(\mathfrak{t})) \geq 0. \tag{28}$$

Then, by $(\mathfrak{P}_2)$, $\mathfrak{T}(G(\mathcal{X}_1(\mathfrak{t})), G(\mathcal{X}_2(\mathfrak{t}))) \geq 0$ is satisfied. Again, the definition of ϕ gives $\phi(G(\mathcal{X}_1), G(\mathcal{X}_2)) \geq 1$. Thus, G is ϕ-admissible.

On the other hand, the condition $(\mathfrak{P}_2)$ guarantees the existence of $\mathcal{X}_0 \in \mathbb{X}$. In this case, for each $\mathfrak{t} \in \mathbb{J}$, $\mathfrak{T}(\mathcal{X}_0(\mathfrak{t}), G(\mathcal{X}_0(\mathfrak{t}))) \geq 0$ holds. Clearly, we get $\phi(\mathcal{X}_0, G(\mathcal{X}_0)) \geq 1$. These show that the conditions (1) and (2) of Theorem 4 are fulfilled.

Now, we assume that $\{\mathcal{X}_n\}_{n\geq 1}$ is a sequence in $\mathbb{X}$ s.t. $\mathcal{X}_n \longrightarrow \mathcal{X}$, and for all n, $\phi(\mathcal{X}_n, \mathcal{X}_{n+1}) \geq 1$. By virtue of definition of ϕ,

$$\mathfrak{T}(\mathcal{X}_n(\mathfrak{t}), \mathcal{X}_{n+1}(\mathfrak{t})) \geq 0. \tag{29}$$

Therefore, in the light of hypothesis $(\mathfrak{P}_3)$, we obtain

$$\mathfrak{T}(\mathcal{X}_n(\mathfrak{t}), \mathcal{X}(\mathfrak{t})) \geq 0. \tag{30}$$

This indicates that $\phi(\mathcal{X}_n, \mathcal{X}) \geq 1$ for every n. This guarantees the condition (3) of Theorem 4. Ultimately, by utilizing Theorem 4, we conclude that it found a fixed point for G like $\mathcal{X}^* \in \mathbb{X}$. This implies that $\mathcal{X}^* = (\mathcal{S}^*, \mathcal{P}_1^*, \mathcal{P}_2^*, \mathcal{R}^*)^T$ is interpreted as a solution of the fractal-fractional model of SARS-CoV-2 (6) and the argument is finally completed. □

In the sequel, we use the Leray-Schauder criterion to prove the existence result.

Theorem 6 (see [61]). *Regard $\mathbb{X}$ as a Banach space, $\mathbb{E}$ as a bounded closed set in $\mathbb{X}$ with the convexity property, and an open set $\mathbb{O} \subseteq \mathbb{E}$ with $0 \in \mathbb{O}$. The compact continuous map $G : \bar{\mathbb{O}} \longrightarrow \mathbb{E}$, either*

(i) G possesses fixed point in $\bar{\mathbb{O}}$ or

(ii) $\exists \in \partial\mathbb{O}$ and $\mu \in (0, 1)$ s.t. $\varkappa = \mu G(\varkappa)$.

Theorem 7. *Assume $\mathcal{F} \in C(\mathbb{J} \times \mathbb{X}, \mathbb{X})$ along with the following:*

(C1): $\varphi \in L^1(\mathbb{J}, \mathbb{R}^+)$ and an increasing map $B \in C([0,\infty), (0,\infty))$ exist provided that

$$|\mathcal{F}(\mathfrak{t}, \mathcal{X}(\mathfrak{t}))| \leq \varphi(\mathfrak{t}) B(|\mathcal{X}(\mathfrak{t})|) \tag{31}$$

(C2): There exist $\gamma > 0$ with

$$\frac{\gamma}{\Lambda + \Delta \varphi_0^* B(\gamma)} > 1, \tag{32}$$

in which $\varphi_0^* = \sup_{\mathfrak{t}\in\mathbb{J}} |\varphi((t))|$ and Λ, Δ are given in () and ()

Then, a solution exists for fractal-fractional problem (12), and so a solution exists for the given fractal-fractional model of SARS-CoV-2 virus (6) on $\mathbb{J}$.

Proof. We define a map $G : \mathbb{X} \longrightarrow \mathbb{X}$ as in (15) and the ball

$$V_\varepsilon = \{\mathcal{X} \in \mathbb{X} : \|\mathcal{X}\|_{\mathbb{X}} \leq \varepsilon\}, \tag{33}$$

for some $\varepsilon > 0$. From the continuity of $\mathcal{F}$, we yield the continuity of operator G. (C1) gives

$$
\begin{aligned}
|G(\mathcal{X}(\mathfrak{t}))| &\le |\mathcal{X}(0)| + \frac{\nu}{\Gamma(\omega)}\int_0^t m^{\nu-1}(\mathfrak{t}-\mathfrak{m})^{\omega}|\mathcal{F}(\mathfrak{m},\mathcal{X}(\mathfrak{m}))|\mathbf{d}\mathfrak{m}\\
&\le \mathcal{X}_0 + \frac{\nu}{\Gamma(\omega)}\int_0^t m^{\nu-1}(\mathfrak{t}-\mathfrak{m})^{\omega}\varphi(\mathfrak{m})B(\mathcal{X}(\mathfrak{m}))\mathbf{d}\mathfrak{m}\\
&\le \mathcal{X}_0 + \frac{\nu T^{\nu+\omega-1}\mathbb{B}(\nu,\omega)}{\Gamma(\omega)}\,\varphi_0^* B(\|\mathcal{X}\|_{\mathbb{X}})\\
&\le \mathcal{X}_0 + \frac{\nu T^{\nu+\omega-1}\Gamma(\nu)}{\Gamma(\nu+\omega)}\,\varphi_0^* B(\varepsilon),
\end{aligned}
\tag{34}
$$

for $\mathcal{X} \in V_\varepsilon$. Consequently, we obtain

$$
\|G(\mathcal{X}(\mathfrak{t}))\| \le \mathcal{X}_0 + \frac{\nu T^{\nu+\omega-1}\Gamma(\nu)}{\Gamma(\nu+\omega)}\varphi_0^* B(\varepsilon) < \infty. \tag{35}
$$

This gives the uniformally boundedness of the operator G on $\mathbb{X}$. We now verify the equicontinuity of operator G. For the purpose, arbitrarily, take $\mathfrak{t}, \mathfrak{t}' \in [0, T]$ such that $\mathfrak{t} < \mathfrak{t}'$ and $\mathcal{X} \in V_\varepsilon$. Assuming

$$
\sup_{\mathfrak{t},\mathcal{X}\in\mathbb{J}\times\mathbb{V}_\varepsilon} |\mathcal{F}(\mathfrak{t},\mathcal{X}(\mathfrak{t}))| = \mathcal{F}^* < \infty, \tag{36}
$$

estimate

$$
\begin{aligned}
&\left|G\left(\mathcal{X}\left(\mathfrak{t}'\right)\right) - G(\mathcal{X}(\mathfrak{t}))\right|\\
&= \left|\frac{\nu}{\Gamma(\omega)}\int_0^{\mathfrak{t}'} m^{\nu-1}\left(\mathfrak{t}'-\mathfrak{m}\right)^{\omega-1}|\mathcal{F}(\mathfrak{m},\mathcal{X}(\mathfrak{m}))|\mathbf{d}\mathfrak{m}\right.\\
&\quad \left. - \frac{\nu}{\Gamma(\omega)}\int_0^{\mathfrak{t}} m^{\nu-1}(\mathfrak{t}-\mathfrak{m})^{\omega-1}|\mathcal{F}(\mathfrak{m},\mathcal{X}(\mathfrak{m}))|\mathbf{d}\mathfrak{m}\right|\\
&\le \frac{\nu\mathcal{F}^*}{\Gamma(\omega)}\left(\int_0^{\mathfrak{t}'} m^{\nu-1}\left(\mathfrak{t}'-\mathfrak{m}\right)^{\omega-1}\mathbf{d}\mathfrak{m} - \int_0^{\mathfrak{t}} m^{\nu-1}(\mathfrak{t}-\mathfrak{m})^{\omega}\mathbf{d}\mathfrak{m}\right)\\
&\le \frac{\nu\mathcal{F}^*\mathbb{B}(\nu,\omega)}{\Gamma(\omega)}\left[\mathfrak{t}'^{\nu+\omega-1} - \mathfrak{t}^{\nu+\omega-1}\right]\\
&= \frac{\nu\mathcal{F}^*\Gamma(\nu)}{\Gamma(\nu+\omega)}\left[\mathfrak{t}'^{\nu+\omega-1} - \mathfrak{t}^{\nu+\omega-1}\right],
\end{aligned}
\tag{37}
$$

which is independent of $\mathcal{X}$, as $\mathfrak{t}' \longrightarrow \mathfrak{t}$, the R.H.S. of above, tends to 0. It implies that

$$
\left\|G\left(\mathcal{X}\left(\mathfrak{t}'\right)\right) - G(\mathcal{X}(\mathfrak{t}))\right\|_{\mathbb{X}} \longrightarrow 0. \tag{38}
$$

This confirms the equicontinuity of G. Arzelà-Ascoli's theorem implies the compactness of operator G on V_ε. The hypothesis of Theorem 6 on the operator G has now been verified. Utilizing (C2), we construct

$$
\mathbb{P} = \left\{\mathcal{X} \in \mathbb{X} : \|\mathcal{X}\|_{\mathbb{X}} < \gamma\right\}, \tag{39}
$$

for some $\gamma > 0$ via

$$
\mathcal{X}_0 + \frac{\nu T^{\nu+\omega-1}\Gamma(\nu)}{\Gamma(\nu+\omega)}\varphi_0^* B(\gamma) < \gamma. \tag{40}
$$

Utilizing (C1) and by (35), we write

$$
\|G\mathcal{X}\|_{\mathbb{X}} \le \mathcal{X}_0 + \frac{\nu T^{\nu+\omega-1}\Gamma(\nu)}{\Gamma(\nu+\omega)}\varphi_0^* B(\mathcal{X}). \tag{41}
$$

Now, we assume the existence of $\mathcal{X} \in \partial\mathbb{P}$ and $\alpha \in (0,1)$ subject to $\mathcal{X} = \alpha G(\mathcal{X})$. For such α and $\mathcal{X}$, by (41), one may write that

$$
\begin{aligned}
\gamma = \|\mathcal{X}\|_{\mathbb{X}} &= \alpha\|G\mathcal{X}\|_{\mathbb{X}}\\
&< \mathcal{X}_0 + \frac{\nu T^{\nu+\omega-1}\Gamma(\nu)}{\Gamma(\nu+\omega)}\varphi_0^* B(\|\mathcal{X}\|_{\mathbb{X}})\\
&< \mathcal{X}_0 + \frac{\nu T^{\nu+\omega-1}\Gamma(\nu)}{\Gamma(\nu+\omega)}\varphi_0^* B(\gamma) < \gamma,
\end{aligned}
\tag{42}
$$

which is impossible. Therefore, (ii) is not valid, and by Theorem 6, G possesses a fixed point in $\overline{\mathbb{P}}$. Therefore, the fractal-fractional model of SARS-CoV-2 virus (6) admits a solution and so proof is complete. □

5. Uniqueness Result

Lemma 8. *Assume* $\mathcal{S}, \mathcal{P}_1, \mathcal{P}_2, \mathcal{R}, \mathcal{S}^*, \mathcal{P}_1^*, \mathcal{P}_2^*, \mathcal{R}^* \in \mathbb{Y} = C(\mathbb{J}, \mathbb{R})$. *Let (H1)* $\|\mathcal{S}\| \le \lambda_1$, $\|\mathcal{P}_1\| \le \lambda_2$, $\|\mathcal{P}_1\| \le \lambda_3$, *and* $\|\mathcal{R}\| \le \lambda_4$ *for some* $\lambda_1, \lambda_2, \lambda_3, \lambda_4 > 0$.

Then, the kernels $\mathcal{F}_1$, $\mathcal{F}_2$, $\mathcal{F}_3$, *and* $\mathcal{F}_4$ *given in (10) satisfied the Lipschitz property w.r.t. the corresponding components if* $\varpi_1, \varpi_2, \varpi_3, \varpi_4 < 1$, *where*

$$
\begin{aligned}
\varpi_1 &= q\lambda_1 + r,\\
\varpi_2 &= r + s,\\
\varpi_3 &= r + b,\\
\varpi_4 &= r.
\end{aligned}
\tag{43}
$$

Proof. Starting from the kernel $\mathcal{F}_1$, for each $\mathcal{S}, \mathcal{S}^* \in \mathbb{Y}$, we estimate

$$
\begin{aligned}
&\|\mathcal{F}_1(\mathfrak{t},\mathcal{S}(\mathfrak{t}),\mathcal{P}_1(\mathfrak{t}),\mathcal{P}_2(\mathfrak{t}),\mathcal{R}(\mathfrak{t}))\\
&\quad - \mathcal{F}_1(\mathfrak{t},\mathcal{S}^*(\mathfrak{t}),\mathcal{P}_1(\mathfrak{t}),\mathcal{P}_2(\mathfrak{t}),\mathcal{R}(\mathfrak{t}))\|\\
&= \|(p - q\mathcal{S}(\mathfrak{t})\mathcal{P}_2(\mathfrak{t}) - r\mathcal{S}(\mathfrak{t}))\\
&\quad - (p - q\mathcal{S}^*(\mathfrak{t})\mathcal{P}_2(\mathfrak{t}) - r\mathcal{S}^*(\mathfrak{t}))\|\\
&\le [q\|\mathcal{P}_2(\mathfrak{t})\| + r]\|\mathcal{S}(\mathfrak{t}) - \mathcal{S}^*(\mathfrak{t})\|\\
&\le [q\lambda_3 + r]\|\mathcal{S}(\mathfrak{t}) - \mathcal{S}^*(\mathfrak{t})\|\\
&= \varpi_1\|\mathcal{S}(\mathfrak{t}) - \mathcal{S}^*(\mathfrak{t})\|.
\end{aligned}
\tag{44}
$$

This shows that the kernel $\mathcal{F}_1$ is Lipschitz w.r.t. $\mathcal{S}$ with constant $\varpi_1 < 1$. Regarding the kernel function $\mathcal{F}_2$, for each $\mathcal{P}_1, \mathcal{P}_1^* \in \mathbb{Y} \coloneqq C(\mathbb{J}, \mathbb{R})$, we estimate

$$\begin{aligned}
&\|\mathscr{F}_2(\mathbf{t},\mathcal{S}(\mathbf{t}),\mathscr{P}_1(\mathbf{t}),\mathscr{P}_2(\mathbf{t}),\mathscr{R}(\mathbf{t}))\\
&\quad-\mathscr{F}_2(\mathbf{t},\mathcal{S}(\mathbf{t}),\mathscr{P}_1^*(\mathbf{t}),\mathscr{P}_2(\mathbf{t}),\mathscr{R}(\mathbf{t}))\|\\
&=\|(q\mathcal{S}(\mathbf{t})\mathscr{P}_2(\mathbf{t})-(r+s)\mathscr{P}_1(\mathbf{t}))\\
&\quad-(q\mathcal{S}^*(\mathbf{t})\mathscr{P}_2(\mathbf{t})-(r+s)\mathscr{P}_1^*(\mathbf{t}))\|\\
&\le[r+s]\|\mathscr{P}_1(\mathbf{t})-\mathscr{P}_1^*(\mathbf{t})\|\\
&=\varpi_2\|\mathscr{P}_1(\mathbf{t})-\mathscr{P}_1^*(\mathbf{t})\|.
\end{aligned}\tag{45}$$

This leads that $\mathscr{F}_2$ is Lipschitz w.r.t. $\mathscr{P}_1$ with constant $\varpi_2<1$. Now for each $\mathscr{P}_2,\mathscr{P}_2^*\in\mathbb{Y}$, we have

$$\begin{aligned}
&\|\mathscr{F}_3(\mathbf{t},\mathcal{S}(\mathbf{t}),\mathscr{P}_1(\mathbf{t}),\mathscr{P}_2(\mathbf{t}),\mathscr{R}(\mathbf{t}))\\
&\quad-\mathscr{F}_3(\mathbf{t},\mathcal{S}(\mathbf{t}),\mathscr{P}_1(\mathbf{t}),\mathscr{P}_2^*(\mathbf{t}),\mathscr{R}(\mathbf{t}))\|\\
&=\|(s\mathscr{P}_1(\mathbf{t})-(r+b)\mathscr{P}_2(\mathbf{t}))\\
&\quad-(s\mathscr{P}_1(\mathbf{t})-(r+b)\mathscr{P}_2^*(\mathbf{t}))\|\\
&\le[r+b]\|\mathscr{P}_2(\mathbf{t})-\mathscr{P}_2^*(\mathbf{t})\|\\
&=\varpi_3\|\mathscr{P}_2(\mathbf{t})-\mathscr{P}_2^*(\mathbf{t})\|.
\end{aligned}\tag{46}$$

This shows that $\mathscr{F}_3$ is Lipschitz w.r.t. $\mathscr{P}_2$ with constant $\varpi_3<1$. Now for each $\mathscr{R},\mathscr{R}^*\in\mathbb{Y}$, we have

$$\begin{aligned}
&\|\mathscr{F}_4(\mathbf{t},\mathcal{S}(\mathbf{t}),\mathscr{P}_1(\mathbf{t}),\mathscr{P}_2(\mathbf{t}),\mathscr{R}(\mathbf{t}))\\
&\quad-\mathscr{F}_4(\mathbf{t},\mathcal{S}(\mathbf{t}),\mathscr{P}_1(\mathbf{t}),\mathscr{P}_2(\mathbf{t}),\mathscr{R}^*(\mathbf{t}))\|\\
&=\|(b\mathscr{P}_2(\mathbf{t})-r\mathscr{R}(\mathbf{t}))-(b\mathscr{P}_2(\mathbf{t})-r\mathscr{R}^*(\mathbf{t}))\|\\
&\le[r]\|\mathscr{R}(\mathbf{t})-\mathscr{R}^*(\mathbf{t})\|=\varpi_4\|\mathscr{R}(\mathbf{t})-\mathscr{R}^*(\mathbf{t})\|.
\end{aligned}\tag{47}$$

This shows that $\mathscr{F}_4$ is Lipschitz w.r.t. $\mathscr{R}$ with constant $\varpi_4<1$. From the above, we conclude that the kernels $\mathscr{F}_i, i=1,2,3,4$, are Lipschitzian w.r.t. the corresponding component with constants $\varpi_i, i=1,2,3,4$, respectively. □

We study the uniqueness result for solution to the presumed fractal-fractional model (6) based on the conclusions gained in Lemma 8.

Theorem 9. *Assume (H1), then the given fractal-fractional model of SARS-CoV-2 virus (6) has a unique solution if*

$$\frac{\nu T^{\nu+\omega-1}\Gamma(\nu)}{\Gamma(\nu+\omega)}\varpi_i<1,\ i\in 1,2,3,4.\tag{48}$$

Proof. The outcome of the theorem is assumed to be invalid. That is to say, there is another solution for the given fractional-fractal model of SARS-CoV-2 virus (6). Assume that $(\mathcal{S}^*(t),\mathscr{P}_1^*(t),\mathscr{P}_2^*(t),\mathscr{R}^*(t))$ is another solution with $(\mathcal{S}_0,,\mathscr{P}_{1,0},\mathscr{P}_{2,0},\mathscr{R})$ such that by (16), we have

$$\begin{aligned}
\mathcal{S}^*(\mathbf{t})&=\mathcal{S}_0+\frac{\nu}{\Gamma(\omega)}\int_0^{\mathbf{t}}\mathbf{m}^{\nu-1}(\mathbf{t}-\mathbf{m})^{\omega-1}\mathscr{F}_1(\mathbf{m},\mathcal{S}^*(\mathbf{m})),\mathscr{P}_1^*(\mathbf{m}),\mathscr{P}_2^*(\mathbf{m}),\mathscr{R}^*(\mathbf{m})\mathbf{d}\mathbf{m},\\
\mathscr{P}_1^*(\mathbf{t})&=\mathscr{P}_{1,0}+\frac{\nu}{\Gamma(\omega)}\int_0^{\mathbf{t}}\mathbf{m}^{\nu-1}(\mathbf{t}-\mathbf{m})^{\omega-1}\mathscr{F}_2(\mathbf{m},\mathcal{S}^*(\mathbf{m})),\mathscr{P}_1^*(\mathbf{m}),\mathscr{P}_2^*(\mathbf{m}),\mathscr{R}^*(\mathbf{m})\mathbf{d}\mathbf{m},\\
\mathscr{P}_2^*(\mathbf{t})&=\mathscr{P}_{2,0}+\frac{\nu}{\Gamma(\omega)}\int_0^{\mathbf{t}}\mathbf{m}^{\nu-1}(\mathbf{t}-\mathbf{m})^{\omega-1}\mathscr{F}_3(\mathbf{m},\mathcal{S}^*(\mathbf{m})),\mathscr{P}_1^*(\mathbf{m}),\mathscr{P}_2^*(\mathbf{m}),\mathscr{R}^*(\mathbf{m})\mathbf{d}\mathbf{m},\\
\mathscr{R}^*(\mathbf{t})&=\mathscr{R}_0+\frac{\nu}{\Gamma(\omega)}\int_0^{\mathbf{t}}\mathbf{m}^{\nu-1}(\mathbf{t}-\mathbf{m})^{\omega-1}\mathscr{F}_4(\mathbf{m},\mathcal{S}^*(\mathbf{m})),\mathscr{P}_1^*(\mathbf{m}),\mathscr{P}_2^*(\mathbf{m}),\mathscr{R}^*(\mathbf{m})\mathbf{d}\mathbf{m}.
\end{aligned}\tag{49}$$

Now, we can estimate

$$\begin{aligned}
|\mathcal{S}(t)-\mathcal{S}^*(\mathbf{t})|&\le\frac{\nu}{\Gamma(\omega)}\int_0^{\mathbf{t}}\mathbf{m}^{\nu-1}(\mathbf{t}-\mathbf{m})^{\omega-1}\\
&\quad\times|\mathscr{F}_1(\mathbf{m},\mathcal{S}(\mathbf{m}),\mathscr{P}_1(\mathbf{m}),\mathscr{P}_2(\mathbf{m}),\mathscr{R}(\mathbf{m}))\\
&\quad-\mathscr{F}_1(\mathbf{m},\mathcal{S}^*(\mathbf{m}),\mathscr{P}_1^*(\mathbf{m}),\mathscr{P}_2^*(\mathbf{m}),\mathscr{R}^*(\mathbf{m}))|\mathbf{d}\mathbf{m}\\
&\le\frac{\nu}{\Gamma(\omega)}\int_0^{\mathbf{t}}\mathbf{m}^{\nu-1}(\mathbf{t}-\mathbf{m})^{\omega-1}\varpi_1\|\mathcal{S}-\mathcal{S}^*\|\mathbf{d}\mathbf{m}\\
&\le\frac{\nu T^{\nu+\omega-1}\Gamma(\nu)}{\Gamma(\nu+\omega)}\varpi_1\|\mathcal{S}-\mathcal{S}^*\|,
\end{aligned}\tag{50}$$

and so

$$\left[1-\frac{\nu T^{\nu+\omega-1}\Gamma(\nu)}{\Gamma(\nu+\omega)}\varpi_1\right]\|\mathcal{S}-\mathcal{S}^*\|\le 0.\tag{51}$$

It is true if $\|\mathcal{S}-\mathcal{S}^*\|=0$, and accordingly, $\mathcal{S}=\mathcal{S}^*$. Next, from

$$\|\mathscr{P}_1-\mathscr{P}_1^*\|\le\left[1-\frac{\nu T^{\nu+\omega-1}\Gamma(\nu)}{\Gamma(\nu+\omega)}\varpi_2\right]\|\mathscr{P}_1-\mathscr{P}_1^*\|,\tag{52}$$

we get

$$\left[1-\frac{\nu T^{\nu+\omega-1}\Gamma(\nu)}{\Gamma(\nu+\omega)}\varpi_2\right]\|\mathscr{P}_1-\mathscr{P}_1^*\|\leq 0. \tag{53}$$

This implies that $\|\mathscr{P}_1-\mathscr{P}_1^*\|=0$ and so $\mathscr{P}_1=\mathscr{P}_1^*$. Also, we have

$$\|\mathscr{P}_2-\mathscr{P}_2^*\|\leq\left[1-\frac{\nu T^{\nu+\omega-1}\Gamma(\nu)}{\Gamma(\nu+\omega)}\varpi_3\right]\|\mathscr{P}_2-\mathscr{P}_2^*\|. \tag{54}$$

This gives

$$\left[1-\frac{\nu T^{\nu+\omega-1}\Gamma(\nu)}{\Gamma(\nu+\omega)}\varpi_3\right]\|\mathscr{P}_2-\mathscr{P}_2^*\|\leq 0. \tag{55}$$

This implies that $\|\mathscr{P}_2-\mathscr{P}_2^*\|=0$ and so $\mathscr{P}_2=\mathscr{P}_2^*$. Finally, from

$$\|\mathscr{R}-\mathscr{R}^*\|\leq\left[1-\frac{\nu T^{\nu+\omega-1}\Gamma(\nu)}{\Gamma(\nu+\omega)}\varpi_4\right]\|\mathscr{R}-\mathscr{R}^*\|, \tag{56}$$

we get

$$\left[1-\frac{\nu T^{\nu+\omega-1}\Gamma(\nu)}{\Gamma(\nu+\omega)}\varpi_4\right]\|\mathscr{R}-\mathscr{R}^*\|\leq 0. \tag{57}$$

This implies that $\|\mathscr{R}-\mathscr{R}^*\|=0$ and so $\mathscr{R}=\mathscr{R}^*$. Consequently, we get

$$(\mathscr{S}(\mathfrak{t}),\mathscr{P}_1(\mathfrak{t}),\mathscr{P}_2(\mathfrak{t}),\mathscr{R}(\mathfrak{t}))=(\mathscr{S}^*(\mathfrak{t}),\mathscr{P}_1^*(\mathfrak{t}),\mathscr{P}_2^*(\mathfrak{t}),\mathscr{R}^*(\mathfrak{t})). \tag{58}$$

This shows that the fractal-fractional model of SARS-CoV-2 virus (6) has exactly one solution. □

6. UH and UHR Stability Criterion

We now proceed to review stable solutions in the context of the Ulam-Hyers (UH) and Ulam-Hyers-Rassias (UHR) to the given fractal-fractional model of SARS-CoV-2 virus (6).

Definition 10. The fractal-fractional model of SARS-CoV-2 virus (6) is UH-stable if $\exists 0<\mathrm{M}_{\mathscr{F}_i}\in\mathbb{R}$, i = 1, 2, 3, 4 s.t. $\forall\varepsilon_i>0$ and $\forall,(\mathscr{S}^*,\mathscr{P}_1^*,\mathscr{P}_2^*,\mathscr{R}^*)\in\mathbb{X}$ fulfilling

$$\begin{cases}\left|{}^{\mathrm{FFP}}\mathfrak{D}_{0,\mathfrak{t}}^{\omega,\nu}\mathscr{S}^*(\mathfrak{t})-\mathscr{F}_1(\mathfrak{t},\mathscr{S}^*(\mathfrak{t}),\mathscr{P}_1^*(\mathfrak{t}),\mathscr{P}_2^*(\mathfrak{t}),\mathscr{R}^*(\mathfrak{t}))\right|<\varepsilon_1,\\ \left|{}^{\mathrm{FFP}}\mathfrak{D}_{0,\mathfrak{t}}^{\omega,\nu}\mathscr{P}_1^*(\mathfrak{t})-\mathscr{F}_2(\mathfrak{t},\mathscr{S}^*(\mathfrak{t}),\mathscr{P}_1^*(\mathfrak{t}),\mathscr{P}_2^*(\mathfrak{t}),\mathscr{R}^*(\mathfrak{t}))\right|<\varepsilon_2,\\ \left|{}^{\mathrm{FFP}}\mathfrak{D}_{0,\mathfrak{t}}^{\omega,\nu}\mathscr{P}_2^*(\mathfrak{t})-\mathscr{F}_3(\mathfrak{t},\mathscr{S}^*(\mathfrak{t}),\mathscr{P}_1^*(\mathfrak{t}),\mathscr{P}_2^*(\mathfrak{t}),\mathscr{R}^*(\mathfrak{t}))\right|<\varepsilon_3,\\ \left|{}^{\mathrm{FFP}}\mathfrak{D}_{0,\mathfrak{t}}^{\omega,\nu}\mathscr{R}^*(\mathfrak{t})-\mathscr{F}_4(\mathfrak{t},\mathscr{S}^*(\mathfrak{t}),\mathscr{P}_1^*(\mathfrak{t}),\mathscr{P}_2^*(\mathfrak{t}),\mathscr{R}^*(\mathfrak{t}))\right|<\varepsilon_4.\end{cases} \tag{59}$$

There exist $(\mathscr{S},\mathscr{P}_1,\mathscr{P}_2,\mathscr{R})\in\mathbb{X}$ satisfying the given fractal-fractional model of SARS-CoV-2 virus (6) with

$$\begin{cases}|\mathscr{S}^*(\mathfrak{t})-\mathscr{S}(\mathfrak{t}))|\leq M_{\mathscr{F}_1}\varepsilon_1,\forall\mathfrak{t}\in\mathbb{J},\\ |\mathscr{P}_1^*(\mathfrak{t})-\mathscr{P}_1(\mathfrak{t}))|\leq M_{\mathscr{F}_2}\varepsilon_2,\forall\mathfrak{t}\in\mathbb{J},\\ |\mathscr{P}_2^*(\mathfrak{t})-\mathscr{P}_2(\mathfrak{t}))|\leq M_{\mathscr{F}_3}\varepsilon_3,\forall\mathfrak{t}\in\mathbb{J},\\ |\mathscr{R}^*(\mathfrak{t})-\mathscr{R}(\mathfrak{t}))|\leq M_{\mathscr{F}_4}\varepsilon_4,\forall\mathfrak{t}\in\mathbb{J}.\end{cases} \tag{60}$$

Definition 11. The given fractal-fractional model of SARS-CoV-2 virus (6) is generalized UH-stable if $\exists\mathrm{M}_{\mathscr{F}_i}\in\mathrm{C}(\mathbb{R}^+,\mathbb{R}^+)$, i = 1, 2, 3, 4 with $\mathrm{M}_{\mathscr{F}_i}(0)=0$ s.t. $\forall\varepsilon_i>0$ and $\forall(\mathscr{S}^*,\mathscr{P}_1^*,\mathscr{P}_2^*,\mathscr{R}^*)\in\mathbb{X}$ fulfilling

$$\begin{cases}\left|{}^{\mathrm{FFP}}\mathfrak{D}_{0,\mathfrak{t}}^{\omega,\nu}\mathscr{S}^*(\mathfrak{t})-\mathscr{F}_1(\mathfrak{t},\mathscr{S}^*(\mathfrak{t}),\mathscr{P}_1^*(\mathfrak{t}),\mathscr{P}_2^*(\mathfrak{t}),\mathscr{R}^*(\mathfrak{t}))\right|<\varepsilon_1,\\ \left|{}^{\mathrm{FFP}}\mathfrak{D}_{0,\mathfrak{t}}^{\omega,\nu}\mathscr{P}_1^*(\mathfrak{t})-\mathscr{F}_2(\mathfrak{t},\mathscr{S}^*(\mathfrak{t}),\mathscr{P}_1^*(\mathfrak{t}),\mathscr{P}_2^*(\mathfrak{t}),\mathscr{R}^*(\mathfrak{t}))\right|<\varepsilon_2,\\ \left|{}^{\mathrm{FFP}}\mathfrak{D}_{0,\mathfrak{t}}^{\omega,\nu}\mathscr{P}_2^*(\mathfrak{t})-\mathscr{F}_3(\mathfrak{t},\mathscr{S}^*(\mathfrak{t}),\mathscr{P}_1^*(\mathfrak{t}),\mathscr{P}_2^*(\mathfrak{t}),\mathscr{R}^*(\mathfrak{t}))\right|<\varepsilon_3,\\ \left|{}^{\mathrm{FFP}}\mathfrak{D}_{0,\mathfrak{t}}^{\omega,\nu}\mathscr{R}^*(\mathfrak{t})-\mathscr{F}_4(\mathfrak{t},\mathscr{S}^*(\mathfrak{t}),\mathscr{P}_1^*(\mathfrak{t}),\mathscr{P}_2^*(\mathfrak{t}),\mathscr{R}^*(\mathfrak{t}))\right|<\varepsilon_4.\end{cases} \tag{61}$$

There exist a solution $(\mathscr{S},\mathscr{P}_1,\mathscr{P}_2,\mathscr{R})\in\mathbb{X}$ of the given fractal-fractional model of SARS-CoV-2 virus (6) with

$$\begin{cases}|\mathscr{S}^*(\mathfrak{t})-\mathscr{S}(\mathfrak{t}))|\leq M_{\mathscr{F}_1}\varepsilon_1,\forall\mathfrak{t}\in\mathbb{J},\\ |\mathscr{P}_1^*(\mathfrak{t})-\mathscr{P}_1(\mathfrak{t}))|\leq M_{\mathscr{F}_2}\varepsilon_2,\forall\mathfrak{t}\in\mathbb{J},\\ |\mathscr{P}_2^*(\mathfrak{t})-\mathscr{P}_2(\mathfrak{t}))|\leq M_{\mathscr{F}_3}\varepsilon_3,\forall\mathfrak{t}\in\mathbb{J},\\ |\mathscr{R}^*(\mathfrak{t})-\mathscr{R}(\mathfrak{t}))|\leq M_{\mathscr{F}_4}\varepsilon_4,\forall\mathfrak{t}\in\mathbb{J}.\end{cases} \tag{62}$$

Remark 12. Note that $(\mathscr{S}^*,\mathscr{P}_1^*,\mathscr{P}_2^*,\mathscr{R}^*)\in\mathbb{X}$ is a solution of (59) iff $\exists\eta_1,\eta_2,\eta_3,\eta_4\in\mathrm{C}([0,\mathrm{T}],\mathbb{R})$ (depending upon $\mathscr{S}^*$, $\mathscr{P}_1^*,\mathscr{P}_2^*,\mathscr{R}^*$, respectively) so that for all $\mathfrak{t}\in\mathbb{J}$,

(i) $|\eta_i(\mathfrak{t})|<\varepsilon_i$, $(i=1,2,3,4)$

(ii) We have

$$\begin{cases}\left|{}^{\mathrm{FFP}}\mathfrak{D}_{0,\mathfrak{t}}^{\omega,\nu}\mathscr{S}^*(\mathfrak{t})-\mathscr{F}_1(\mathfrak{t},\mathscr{S}^*(\mathfrak{t}),\mathscr{P}_1^*(\mathfrak{t}),\mathscr{P}_2^*(\mathfrak{t}),\mathscr{R}^*(\mathfrak{t}))\right|+\eta_1(\mathfrak{t}),\\ \left|{}^{\mathrm{FFP}}\mathfrak{D}_{0,\mathfrak{t}}^{\omega,\nu}\mathscr{P}_1^*(\mathfrak{t})-\mathscr{F}_2(\mathfrak{t},\mathscr{S}^*(\mathfrak{t}),\mathscr{P}_1^*(\mathfrak{t}),\mathscr{P}_2^*(\mathfrak{t}),\mathscr{R}^*(\mathfrak{t}))\right|+\eta_2(\mathfrak{t}),\\ \left|{}^{\mathrm{FFP}}\mathfrak{D}_{0,\mathfrak{t}}^{\omega,\nu}\mathscr{P}_2^*(\mathfrak{t})-\mathscr{F}_3(\mathfrak{t},\mathscr{S}^*(\mathfrak{t}),\mathscr{P}_1^*(\mathfrak{t}),\mathscr{P}_2^*(\mathfrak{t}),\mathscr{R}^*(\mathfrak{t}))\right|\eta_3(\mathfrak{t}),\\ \left|{}^{\mathrm{FFP}}\mathfrak{D}_{0,\mathfrak{t}}^{\omega,\nu}\mathscr{R}^*(\mathfrak{t})-\mathscr{F}_4(\mathfrak{t},\mathscr{S}^*(\mathfrak{t}),\mathscr{P}_1^*(\mathfrak{t}),\mathscr{P}_2^*(\mathfrak{t}),\mathscr{R}^*(\mathfrak{t}))\right|\eta_4(\mathfrak{t})\end{cases} \tag{63}$$

Definition 13. The fractal-fractional model of SARS-CoV-2 virus (6) is UHR-stable w.r.t. functions Ψ_i, i = 1, 2, 3, 4, if $\exists$ $0<\mathrm{M}_{\mathscr{F}_i,\Psi_i}\in\mathbb{R}$, i = 1, 2, 3, 4 s.t. $\forall\varepsilon_i>0$ and $\forall(\mathscr{S}^*,\mathscr{P}_1^*,\mathscr{P}_2^*,\mathscr{R}^*)\in\mathbb{X}$ fulfilling

$$\begin{cases} \left|{}^{\mathrm{FFP}}\mathfrak{D}_{0,\mathfrak{t}}^{\omega,\nu}\mathcal{S}^*(\mathfrak{t}) - \mathcal{F}_1(\mathfrak{t},\mathcal{S}^*(\mathfrak{t}),\mathcal{P}_1^*(\mathfrak{t}),\mathcal{P}_2^*(\mathfrak{t}),\mathcal{R}^*(\mathfrak{t}))\right| < \varepsilon_2\Psi_2(\mathfrak{t}). \\ \left|{}^{\mathrm{FFP}}\mathfrak{D}_{0,\mathfrak{t}}^{\omega,\nu}\mathcal{P}_1^*(\mathfrak{t}) - \mathcal{F}_2(\mathfrak{t},\mathcal{S}^*(\mathfrak{t}),\mathcal{P}_1^*(\mathfrak{t}),\mathcal{P}_2^*(\mathfrak{t}),\mathcal{R}^*(\mathfrak{t}))\right| < \varepsilon_2\Psi_2(\mathfrak{t}), \\ \left|{}^{\mathrm{FFP}}\mathfrak{D}_{0,\mathfrak{t}}^{\omega,\nu}\mathcal{P}_2^*(\mathfrak{t}) - \mathcal{F}_3(\mathfrak{t},\mathcal{S}^*(\mathfrak{t}),\mathcal{P}_1^*(\mathfrak{t}),\mathcal{P}_2^*(\mathfrak{t}),\mathcal{R}^*(\mathfrak{t}))\right| < \varepsilon_3\Psi_3(\mathfrak{t}), \\ \left|{}^{\mathrm{FFP}}\mathfrak{D}_{0,\mathfrak{t}}^{\omega,\nu}\mathcal{R}^*(\mathfrak{t}) - \mathcal{F}_4(\mathfrak{t},\mathcal{S}^*(\mathfrak{t}),\mathcal{P}_1^*(\mathfrak{t}),\mathcal{P}_2^*(\mathfrak{t}),\mathcal{R}^*(\mathfrak{t}))\right| < \varepsilon_4\Psi_4(\mathfrak{t}). \end{cases} \tag{64}$$

There exist $(\mathcal{S},\mathcal{P}_1,\mathcal{P}_2,\mathcal{R}) \in \mathbb{X}$ satisfying the given fractal-fractional model of SARS-CoV-2 virus (6) with

$$\begin{cases} |\mathcal{S}^*(\mathfrak{t}) - \mathcal{S}(\mathfrak{t}))| \le M_{\mathcal{F}_1,\Psi_1}\varepsilon_1\Psi_1(\mathfrak{t}),\forall\mathfrak{t} \in \mathbb{J}, \\ |\mathcal{P}_1^*(\mathfrak{t}) - \mathcal{P}_1(\mathfrak{t}))| \le M_{\mathcal{F}_2,\Psi_1}\varepsilon_2\Psi_2(\mathfrak{t}),\forall\mathfrak{t} \in \mathbb{J}, \\ |\mathcal{P}_2^*(\mathfrak{t}) - \mathcal{P}_2(\mathfrak{t}))| \le M_{\mathcal{F}_3,\Psi_3}\varepsilon_3\Psi_3(\mathfrak{t}),\forall\mathfrak{t} \in \mathbb{J}, \\ |\mathcal{R}^*(\mathfrak{t}) - \mathcal{R}(\mathfrak{t}))| \le M_{\mathcal{F}_4,\Psi_1}\varepsilon_4\Psi_4(\mathfrak{t}),\forall\mathfrak{t} \in \mathbb{J}. \end{cases} \tag{65}$$

Definition 14. The given fractal-fractional model of SARS-CoV-2 virus (6) is generalized UHR-stable w.r.t. Ψ_i, i = 1, 2, 3, 4, if $\exists M_{\mathcal{F}_i,\Psi_i} \in \mathbb{R}$, i = 1, 2, 3, 4 with $M_{\mathcal{F}_i}(0) = 0$ s.t. $\forall\varepsilon_i > 0$ and $\forall(\mathcal{S}^*,\mathcal{P}_1^*,\mathcal{P}_2^*,\mathcal{R}^*) \in \mathbb{X}$ fulfilling

$$\begin{cases} \left|{}^{\mathrm{FFP}}\mathfrak{D}_{0,\mathfrak{t}}^{\omega,\nu}\mathcal{S}^*(\mathfrak{t}) - \mathcal{F}_1(\mathfrak{t},\mathcal{S}^*(\mathfrak{t}),\mathcal{P}_1^*(\mathfrak{t}),\mathcal{P}_2^*(\mathfrak{t}),\mathcal{R}^*(\mathfrak{t}))\right| < \Psi_1(\mathfrak{t}), \\ \left|{}^{\mathrm{FFP}}\mathfrak{D}_{0,\mathfrak{t}}^{\omega,\nu}\mathcal{P}_1^*(\mathfrak{t}) - \mathcal{F}_2(\mathfrak{t},\mathcal{S}^*(\mathfrak{t}),\mathcal{P}_1^*(\mathfrak{t}),\mathcal{P}_2^*(\mathfrak{t}),\mathcal{R}^*(\mathfrak{t}))\right| < \Psi_2(\mathfrak{t}), \\ \left|{}^{\mathrm{FFP}}\mathfrak{D}_{0,\mathfrak{t}}^{\omega,\nu}\mathcal{P}_2^*(\mathfrak{t}) - \mathcal{F}_3(\mathfrak{t},\mathcal{S}^*(\mathfrak{t}),\mathcal{P}_1^*(\mathfrak{t}),\mathcal{P}_2^*(\mathfrak{t}),\mathcal{R}^*(\mathfrak{t}))\right| < \Psi_3(\mathfrak{t}), \\ \left|{}^{\mathrm{FFP}}\mathfrak{D}_{0,\mathfrak{t}}^{\omega,\nu}\mathcal{R}^*(\mathfrak{t}) - \mathcal{F}_4(\mathfrak{t},\mathcal{S}^*(\mathfrak{t}),\mathcal{P}_1^*(\mathfrak{t}),\mathcal{P}_2^*(\mathfrak{t}),\mathcal{R}^*(\mathfrak{t}))\right| < \Psi_4(\mathfrak{t}). \end{cases} \tag{66}$$

There exist a solution $(\mathcal{S},\mathcal{P}_1,\mathcal{P}_2,\mathcal{R}) \in \mathbb{X}$ of the given fractal-fractional model of SARS-CoV-2 virus (6) with

$$\begin{cases} |\mathcal{S}^*(\mathfrak{t}) - \mathcal{S}(\mathfrak{t}))| \le M_{\mathcal{F}_1,\Psi_1}\Psi_1(\mathfrak{t}),\forall\mathfrak{t} \in \mathbb{J}, \\ |\mathcal{P}_1^*(\mathfrak{t}) - \mathcal{P}_1(\mathfrak{t}))| \le M_{\mathcal{F}_2,\Psi_2}\Psi_2(\mathfrak{t}),\forall\mathfrak{t} \in \mathbb{J}, \\ |\mathcal{P}_2^*(\mathfrak{t}) - \mathcal{P}_2(\mathfrak{t}))| \le M_{\mathcal{F}_3,\Psi_3}\Psi_3(\mathfrak{t}),\forall\mathfrak{t} \in \mathbb{J}, \\ |\mathcal{R}^*(\mathfrak{t}) - \mathcal{R}(\mathfrak{t}))| \le M_{\mathcal{F}_4,\Psi_4}\Psi_4(\mathfrak{t}),\forall\mathfrak{t} \in \mathbb{J}. \end{cases} \tag{67}$$

Remark 15. Note that $(\mathcal{S}^*,\mathcal{P}_1^*,\mathcal{P}_2^*,\mathcal{R}^*) \in \mathbb{X}$ is a solution of (64) iff there exists $\eta_1,\eta_2,\eta_3,\eta_4 \in \mathrm{C}([0,\mathrm{T}],\mathbb{R})$ (depending upon $\mathcal{S}^*,\mathcal{P}_1^*,\mathcal{P}_2^*,\mathcal{R}^*$, respectively) so that for all $\mathfrak{t} \in \mathbb{J}$,

(i) $|\eta_i(\mathfrak{t})| < \Psi_i(\mathfrak{T})\varepsilon_i$, $(i = 1, 2, 3, 4)$

(ii) We have

$$\begin{cases} {}^{\mathrm{FFP}}\mathfrak{D}_{0,\mathfrak{t}}^{\omega,\nu}\mathcal{S}^*(\mathfrak{t}) = \mathcal{F}_1(\mathfrak{t},\mathcal{S}^*(\mathfrak{t}),\mathcal{P}_1^*(\mathfrak{t}),\mathcal{P}_2^*(\mathfrak{t}),\mathcal{R}^*(\mathfrak{t})) + \eta_1(\mathfrak{t}), \\ {}^{\mathrm{FFP}}\mathfrak{D}_{0,\mathfrak{t}}^{\omega,\nu}\mathcal{P}_1^*(\mathfrak{t}) = \mathcal{F}_2(\mathfrak{t},\mathcal{S}^*(\mathfrak{t}),\mathcal{P}_1^*(\mathfrak{t}),\mathcal{P}_2^*(\mathfrak{t}),\mathcal{R}^*(\mathfrak{t})) + \eta_2(\mathfrak{t}). \\ {}^{\mathrm{FFP}}\mathfrak{D}_{0,\mathfrak{t}}^{\omega,\nu}\mathcal{P}_2^*(\mathfrak{t}) = \mathcal{F}_3(\mathfrak{t},\mathcal{S}^*(\mathfrak{t}),\mathcal{P}_1^*(\mathfrak{t}),\mathcal{P}_2^*(\mathfrak{t}),\mathcal{R}^*(\mathfrak{t})) + \eta_3(\mathfrak{t}), \\ {}^{\mathrm{FFP}}\mathfrak{D}_{0,\mathfrak{t}}^{\omega,\nu}\mathcal{R}^*(\mathfrak{t}) = \mathcal{F}_4(\mathfrak{t},\mathcal{S}^*(\mathfrak{t}),\mathcal{P}_1^*(\mathfrak{t}),\mathcal{P}_2^*(\mathfrak{t}),\mathcal{R}^*(\mathfrak{t})) + \eta_4(\mathfrak{t}) \end{cases} \tag{68}$$

Theorem 16. *The given fractal-fractional model of SARS-CoV-2 virus (6) is UH-stable on $\mathbb{J} \coloneqq [0, T]$, and it is generalized UH-stable such that*

$$\frac{\nu T^{\nu+\omega-1}\Gamma(\nu)}{\Gamma(\nu+\omega)}\varpi_i < 1,\ i \in \{1,2,3,4\}, \tag{69}$$

where ϖ_i are given by () provided that the assumption (H1) is valid.

Proof. Let $\varepsilon_1 > 0$ and $\mathcal{S}^* \in \mathbb{Y}$ be arbitrary so that

$$\left|\ {}^{\mathrm{FFP}}\mathfrak{D}_{0,\mathfrak{t}}^{\omega,\nu}\mathcal{S}^*(\mathfrak{t}) - \mathcal{F}_1(\mathfrak{t},\mathcal{S}^*(\mathfrak{t}),\mathcal{P}_1^*(\mathfrak{t}),\mathcal{P}_2^*(\mathfrak{t}),\mathcal{R}^*(\mathfrak{t}))\right| < \varepsilon_1. \tag{70}$$

Then, in view of Remark 12, we can find a function $\eta_1(\mathfrak{t})$ satisfying

$${}^{\mathrm{FFP}}\mathfrak{D}_{0,\mathfrak{t}}^{\omega,\nu}\mathcal{S}^{ast}(\mathfrak{t}) = \mathcal{F}_1\left(\mathfrak{t},\mathcal{S}^{ast}(\mathfrak{t}),\mathcal{P}_1^{ast}(\mathfrak{t}),\mathcal{P}_2^{ast}(\mathfrak{t}),\mathcal{R}^*(\mathfrak{t})\right) + \eta_1(\mathfrak{t}), \tag{71}$$

with $|\eta_1(\mathfrak{t})| \le \varepsilon_1$. So

$$\begin{aligned} \mathcal{S}^*(\mathfrak{t}) = \mathcal{S}_0 + \frac{\nu}{\Gamma(\omega)}\int_0^{\mathfrak{t}} \mathfrak{m}^{\nu-1}(\mathfrak{t}-\mathfrak{m})^{\omega-1}\mathcal{F}_1(\mathfrak{m},\mathcal{S}^*(\mathfrak{m}),\mathcal{P}_1^* \\ \cdot(\mathfrak{m}),\mathcal{P}_2^*(\mathfrak{m}),\mathcal{R}^*(\mathfrak{m}))\mathbf{d}\mathfrak{m} \\ + \frac{\nu}{\Gamma(\omega)}\int_0^{\mathfrak{t}} \mathfrak{m}^{\nu-1}(\mathfrak{t}-\mathfrak{m})^{\omega-1}\eta_1(\mathfrak{m})\mathbf{d}\mathfrak{m}. \end{aligned} \tag{72}$$

By Theorem 9, let $\mathcal{S} \in \mathbb{Y}$ be the unique solution of the given fractal-fractional model of NOV-COV-2 virus (). Then, $\mathcal{S}(\mathfrak{t})$ is given by

$$\begin{aligned} \mathcal{S}(\mathfrak{t}) = \mathcal{S}_0 + \frac{\nu}{\Gamma(\omega)}\int_0^{\mathfrak{t}} \mathfrak{m}^{\nu-1}(\mathfrak{t}-\mathfrak{m})^{\omega-1}\mathcal{F}_1 \\ \cdot(\mathfrak{m},\mathcal{S}(\mathfrak{m}),\mathcal{P}_1(\mathfrak{m}),\mathcal{P}_2(\mathfrak{m}),\mathcal{R}(\mathfrak{m}))\mathbf{d}\mathfrak{m}. \end{aligned} \tag{73}$$

Then,

$$|\mathcal{S}^*(\mathbf{t}) - \mathcal{S}(\mathbf{t})| \leq \frac{\nu}{\Gamma(\omega)}\int_0^{\mathbf{t}} \mathbf{m}^{\nu-1}(\mathbf{t}-\mathbf{m})^{\omega-1}|\eta_1(\mathbf{m})|\mathbf{dm} + \frac{\nu}{\Gamma(\omega)}\int_0^{\mathbf{t}} \mathbf{m}^{\nu-1}(\mathbf{t}-\mathbf{m})^{\omega-1} \times |\mathcal{F}_1(\mathbf{m}, \mathcal{S}^*(\mathbf{m}), \mathcal{P}_1^*(\mathbf{m}), \mathcal{P}_2^*(\mathbf{m}), \mathcal{R}^*(\mathbf{m})) - \mathcal{F}_1(\mathbf{m}, \mathcal{S}(\mathbf{m}), \mathcal{P}_1(\mathbf{m}), \mathcal{P}_2(\mathbf{m}), \mathcal{R}(\mathbf{m}))|\mathbf{dm},$$

$$\leq \frac{\nu T^{\nu+\omega-1}\Gamma(\nu)}{\Gamma(\nu+\omega)}\varepsilon_1 + \frac{\nu T^{\nu+\omega-1}\Gamma(\nu)}{\Gamma(\nu+\omega)}\varpi_1\|\mathcal{S}^* - \mathcal{S}\|. \tag{74}$$

Hence, we get

$$\|\mathcal{S}^* - \mathcal{S}\| \leq \frac{\left(\left(\nu T^{\nu+\omega-1}\Gamma(\nu)\right)/(\Gamma(\nu+\omega))\right)\varepsilon_1}{1 - \left(\left(\nu T^{\nu+\omega-1}\Gamma(\nu)\right)/(\Gamma(\nu+\omega))\right)\varpi_1}. \tag{75}$$

If we let $M_{\mathcal{F}_1} = ((\nu T^{\nu+\omega-1}\Gamma(\nu))/(\Gamma(\nu+\omega)))/(1 - ((\nu T^{\nu+\omega-1}\Gamma(\nu))/(\Gamma(\nu+\omega)))\varpi_1)$, then $\|\mathcal{S}^* - \mathcal{S}\| \leq M_{\mathcal{F}_1}\varepsilon_1$. Similarly, we have

$$\|\mathcal{P}_1^* - \mathcal{P}_1\| \leq M_{\mathcal{F}_2}\varepsilon_2, \|\mathcal{P}_2^* - \mathcal{P}_2\| \leq M_{\mathcal{F}_3}\varepsilon_3, \|\mathcal{R}^* - \mathcal{R}\| \leq M_{\mathcal{F}_4}\varepsilon_4, \tag{76}$$

where

$$M_{\mathcal{F}_i} = \frac{\left(\nu T^{\nu+\omega-1}\Gamma(\nu)\right)/(\Gamma(\nu+\omega))}{1 - \left(\left(\nu T^{\nu+\omega-1}\Gamma(\nu)\right)/(\Gamma(\nu+\omega))\right)\varpi_i}, (i \in \{2,3,4\}). \tag{77}$$

Hence, the UH stability of the given fractal-fractional model (6) is fulfilled. Next, by assuming

$$M_{\mathcal{F}_i}(\varepsilon_i) = \frac{\left(\left(\nu T^{\nu+\omega-1}\Gamma(\nu)\right)/(\Gamma(\nu+\omega))\right)\varepsilon_i}{1 - \left(\left(\nu T^{\nu+\omega-1}\Gamma(\nu)\right)/(\Gamma(\nu+\omega))\right)\varpi_i}, (i \in \{1,2,3,4\}), \tag{78}$$

with $M_{\mathcal{F}_i}(0) = 0$, the generalized UH stability of the given fractional-fractal model (6) is fulfilled. □

In the next result, UHR stability for the given fractal-fractional model of SARS-CoV-2 (6) is studied:

Theorem 17. *The condition (H1) is assumed to be held:*

(H′): ∃ increasing mappings $\Psi_i \in C([0,T], \mathbb{R}^+)$, $(i \in \{1,2,3,4\}$ and $\exists \Lambda_{\Psi_i} > 0$ such that $\forall \mathbf{t} \in \mathbb{J}$,

$$^{\mathrm{FFP}}\mathcal{J}_{0,\mathbf{t}}^{\omega,\nu}\Psi_i(\mathbf{t}) < \Lambda_{\Psi_i}\Psi_i(\mathbf{t}), (i \in \{1,2,3,4\}). \tag{79}$$

Then, the given fractal-fractional model of SARS-CoV-2 virus (6) is UHR and generalized UHR-stable.

Proof. For every $\varepsilon_1 > 0$ and $\forall \mathcal{S}^* \in \mathbb{Y}$ satisfying

$$\left|{}^{\mathrm{FFP}}\mathcal{D}_{0,\mathbf{t}}^{\omega,\nu}\mathcal{S}^*(\mathbf{t}) - \mathcal{F}_1(\mathbf{t}, \mathcal{S}^*(\mathbf{t}), \mathcal{P}_1^*(\mathbf{t}), \mathcal{P}_2^*(\mathbf{t}), \mathcal{R}^*(\mathbf{t}))\right| < \varepsilon_1\Psi_1(\mathbf{t}), \quad \exists \eta(\mathbf{t}) \text{ s.t.}$$
$$^{\mathrm{FFP}}\mathcal{D}_{0,\mathbf{t}}^{\omega,\nu}\mathcal{S}^*(\mathbf{t}) = \mathcal{F}_1(\mathbf{t}, \mathcal{S}^*(\mathbf{t}), \mathcal{P}_1^*(\mathbf{t}), \mathcal{P}_2^*(\mathbf{t}), \mathcal{R}^*(\mathbf{t})) + \eta_1(\mathbf{t}), \tag{80}$$

with $\eta_1(\mathbf{t}) \leq \varepsilon_1\Psi_1(\mathbf{t})$. It follows that

$$\mathcal{S}^*(\mathbf{t}) = \mathcal{S}_0 + \frac{\nu}{\Gamma(\omega)}\int_0^{\mathbf{t}} \mathbf{t}^{\nu-1}(\mathbf{t}-\mathbf{t})^{\omega-1}\mathcal{F}_1(\mathbf{t}, \mathcal{S}^*(\mathbf{t}), \mathcal{P}_1^*(\mathbf{t}), \mathcal{P}_2^*(\mathbf{t}), \mathcal{R}^*(\mathbf{t}))\mathbf{dt} + \frac{\nu}{\Gamma(\omega)}\int_0^{\mathbf{t}} \mathbf{t}^{\nu-1}(\mathbf{t}-\mathbf{t})^{\omega-1}\eta_1(\mathbf{t})\mathbf{dt}. \tag{81}$$

By Theorem 9, let $\mathcal{S} \in \mathbb{Y}$ be the unique solution of the given fractal-fractional model of SARS-CoV-2 virus (6). Then, $\mathcal{S}(\mathbf{t})$ is given by

$$\mathcal{S}(\mathbf{t}) = \mathcal{S}_0 + \frac{\nu}{\Gamma(\omega)}\int_0^{\mathbf{t}} \mathbf{t}^{\nu-1}(\mathbf{t}-\mathbf{t})^{\omega-1}\mathcal{F}_1(\mathbf{t}, \mathcal{S}(\mathbf{t}), \mathcal{P}_1(\mathbf{t}), \mathcal{P}_2(\mathbf{t}), \mathcal{R}(\mathbf{t}))\mathbf{dt}. \tag{82}$$

Then, by (61),

$$\begin{aligned}|\mathcal{S}^*(\mathbf{t}) - \mathcal{S}(\mathbf{t})| &\leq \frac{\nu}{\Gamma(\omega)}\int_0^t m^{\nu-1}(\mathbf{t}-\mathbf{m})^{\omega-1}|h_1(\mathbf{m})|\mathbf{dm} + \frac{\nu}{\Gamma(\omega)}\int_0^{\mathbf{t}} \mathbf{m}^{\nu-1}(\mathbf{t}-\mathbf{m})^{\omega-1} \times |\mathcal{F}_1(\mathbf{m}, \mathcal{S}^*(\mathbf{m}), \mathcal{P}_1^*(\mathbf{m}), \mathcal{P}_2^*(\mathbf{m}), \mathcal{R}^*(\mathbf{m})) - \mathcal{F}_1(\mathbf{m}, \mathcal{S}(\mathbf{m}), \mathcal{P}_1(\mathbf{m}), \mathcal{P}_2(\mathbf{m}), \mathcal{R}(\mathbf{m}))\mathbf{dm}| \\ &\leq \frac{\varepsilon_1\nu}{\Gamma(\omega)}\int_0^{\mathbf{t}} \mathbf{m}^{\nu-1}(\mathbf{t}-\mathbf{m})^{\omega-1}\Psi_1(\mathbf{m})\mathbf{dm} + \frac{\nu T^{\nu+\omega-1}\Gamma(\nu)}{\Gamma(\nu+\omega)}\varpi_1\|\mathcal{S}^* - \mathcal{S}\| \\ &\leq \varepsilon_1\Lambda_{\Psi_1}\Psi_1 + \frac{\nu T^{\nu+\omega-1}\Gamma(\nu)}{\Gamma(\nu+\omega)}\varpi_1\|\mathcal{S}^* - \mathcal{S}\|.\end{aligned} \tag{83}$$

Accordingly, it gives

$$\|\mathcal{S}^* - \mathcal{S}\| \leq \frac{\varepsilon_1\Lambda_{\Psi_1}\Psi_1}{1 - \left(\left(\nu T^{\nu+\omega-1}\Gamma(\nu)\right)/(\Gamma(\nu+\omega))\right)\varpi_1}. \tag{84}$$

If we let

$$M_{(\mathcal{F}_1,\Psi_1)} = \frac{\Lambda_{\Psi_1}}{1 - \left(\left(\nu T^{\nu+\omega-1}\Gamma(\nu)\right)/(\Gamma(\nu+\omega))\right)\varpi_1}, \tag{85}$$

then $\|\mathcal{S}^* - \mathcal{S}\| \leq \varepsilon_1 M_{(\mathcal{F}_1,\Psi_1)}\Psi_1$. Similarly, we have

$$\begin{aligned}\|\mathcal{P}_1^* - \mathcal{P}_1\| &\leq \varepsilon_2 M_{(\mathcal{F}_2,\Psi_2)}\Psi_2, \|\mathcal{P}_2^* - \mathcal{P}_2\| \\ &\leq \varepsilon_3 M_{(\mathcal{F}_3,\Psi_3)}\Psi_3, \|\mathcal{R}^* - \mathcal{R}\| \\ &\leq \varepsilon_4 M_{(\mathcal{F}_4,\Psi_4)}\Psi_4,\end{aligned} \tag{86}$$

where

$$M_{(\mathcal{F}_i,\Psi_i)} = \frac{\Lambda_{\Psi_i}}{1 - \left(\left(\nu T^{\nu+\omega-1}\Gamma(\nu)\right)/(\Gamma(\nu+\omega))\right)\varpi_i}, (i \in \{1,2,3,4\}). \tag{87}$$

Hence, the given fractal-fractional model of SARS-CoV-2 virus (6) is stable in the sense of UHR. Along with this, by setting $\varepsilon_i = 1; (i \in \{1,2,3,4\})$, the mentioned fractal-fractional model of SARS-CoV-2 virus (6) is generalized UHR-stable. □

7. Numerical Algorithms and Simulations

7.1. Numerical Adams-Bashforth Method. In this section, we describe the numerical scheme in relation to the fractal-fractional model of SARS-CoV-2 virus (6). For this, we have taken help from the technique regarding two-step Lagrange polynomials called fractional Adams-Bashforth method (ABM). To begin this process, we follow the numerical method of fractal-fractional integral equations (15) using a new approach at $\mathbf{t}_{n+1}$. In other words, we discretize the mentioned equation (15) for $\mathbf{t} = \mathbf{t}_{n+1}$, and we have

$$\begin{cases}\mathcal{S}(\mathbf{t}_{n+1}) = \mathcal{S}_0 + \dfrac{\nu}{\Gamma(\omega)}\displaystyle\int_0^{\mathbf{t}_{n+1}} (\mathbf{t}_{n+1} - \mathfrak{m})^{\omega-1}\mathcal{H}_1(\mathfrak{m})\,\mathrm{d}\mathfrak{m}, \\ \mathcal{P}_1(\mathbf{t}_{n+1}) = \mathcal{P}_{1,0} + \dfrac{\nu}{\Gamma(\omega)}\displaystyle\int_0^{\mathbf{t}_{n+1}} (\mathbf{t}_{n+1} - \mathfrak{m})^{\omega-1}\mathcal{H}_2(\mathfrak{m})\,\mathrm{d}\mathfrak{m}, \\ \mathcal{P}_2(\mathbf{t}_{n+1}) = \mathcal{P}_{2,0} + \dfrac{\nu}{\Gamma(\omega)}\displaystyle\int_0^{\mathbf{t}_{n+1}} (\mathbf{t}_{n+1} - \mathfrak{m})^{\omega-1}\mathcal{H}_3(\mathfrak{m})\,\mathrm{d}\mathfrak{m}, \\ \mathcal{R}(\mathbf{t}_{n+1}) = \mathcal{R}_0 + \dfrac{\nu}{\Gamma(\omega)}\displaystyle\int_0^{\mathbf{t}_{n+1}} (\mathbf{t}_{n+1} - \mathfrak{m})^{\omega-1}\mathcal{H}_4(\mathfrak{m})\,\mathrm{d}\mathfrak{m}.\end{cases} \tag{88}$$

where

$$\begin{cases}\mathcal{H}_1(\mathfrak{m}) = \mathfrak{m}^{\nu-1}\mathcal{F}_1(\mathfrak{m}, \mathcal{S}(\mathfrak{m}), \mathcal{P}_1(\mathfrak{m}), \mathcal{P}_2(\mathfrak{m}), \mathcal{R}(\mathfrak{m})), \\ \mathcal{H}_2(\mathfrak{m}) = \mathfrak{m}^{\nu-1}\mathcal{F}_2(\mathfrak{m}, \mathcal{S}(\mathfrak{m}), \mathcal{P}_1(\mathfrak{m}), \mathcal{P}_2(\mathfrak{m}), \mathcal{R}(\mathfrak{m})), \\ \mathcal{H}_3(\mathfrak{m}) = \mathfrak{m}^{\nu-1}\mathcal{F}_3(\mathfrak{m}, \mathcal{S}(\mathfrak{m}), \mathcal{P}_1(\mathfrak{m}), \mathcal{P}_2(\mathfrak{m}), \mathcal{R}(\mathfrak{m})), \\ \mathcal{H}_4(\mathfrak{m}) = \mathfrak{m}^{\nu-1}\mathcal{F}_4(\mathfrak{m}, \mathcal{S}(\mathfrak{m}), \mathcal{P}_1(\mathfrak{m}), \mathcal{P}_2(\mathfrak{m}), \mathcal{R}(\mathfrak{m})).\end{cases} \tag{89}$$

By approximating above integrals, we get

$$\begin{cases}\mathcal{S}(\mathbf{t}_{n+1}) = \mathcal{S}_0 + \dfrac{\nu}{\Gamma(\omega)}\displaystyle\sum_{l=0}^{n}\int_{\mathbf{t}_l}^{\mathbf{t}_{l+1}} (\mathbf{t}_{n+1} - \mathfrak{m})^{\omega-1}\mathcal{H}_1(\mathfrak{m})\mathrm{d}\mathfrak{m}, \\ \mathcal{P}_1(\mathbf{t}_{n+1}) = \mathcal{P}_{1,0} + \dfrac{\nu}{\Gamma(\omega)}\displaystyle\sum_{l=0}^{n}\int_{\mathbf{t}_l}^{\mathbf{t}_{l+1}} (\mathbf{t}_{n+1} - \mathfrak{m})^{\omega-1}\mathcal{H}_2(\mathfrak{m})\mathrm{d}\mathfrak{m}, \\ \mathcal{P}_2(\mathbf{t}_{n+1}) = \mathcal{P}_{2,0} + \dfrac{\nu}{\Gamma(\omega)}\displaystyle\sum_{l=0}^{n}\int_{\mathbf{t}_l}^{\mathbf{t}_{l+1}} (\mathbf{t}_{n+1} - \mathfrak{m})^{\omega-1}\mathcal{H}_3(\mathfrak{m})\mathrm{d}\mathfrak{m}, \\ \mathcal{R}(\mathbf{t}_{n+1}) = \mathcal{R}_0 + \dfrac{\nu}{\Gamma(\omega)}\displaystyle\sum_{l=0}^{n}\int_{\mathbf{t}_l}^{\mathbf{t}_{l+1}} (\mathbf{t}_{n+1} - \mathfrak{m})^{\omega-1}\mathcal{H}_4(\mathfrak{m})\mathrm{d}\mathfrak{m}.\end{cases} \tag{90}$$

In the sequel, we approximate the functions $\mathcal{H}_1, \mathcal{H}_2, \mathcal{H}_3$, and $\mathcal{H}_4$, introduced by (89), on the interval $[\mathbf{t}_l, \mathbf{t}_{l+1}]$ via two-step Lagrange interpolation polynomials with the step size $\mathbf{h} = \mathbf{t}_l - \mathbf{t}_{l-1}$ as

$$\begin{aligned}\mathcal{H}_{1,l}^*(\mathfrak{m}) &\simeq \frac{\mathfrak{m} - \mathbf{t}_{l-1}}{\mathbf{h}}\mathbf{t}_l^{\nu-1}\mathcal{F}_1(\mathfrak{m}_l, \mathcal{S}_l, \mathcal{P}_{1,l}, \mathcal{P}_{2,l}, \mathcal{R}_l) \\ &\quad - \frac{\mathfrak{m} - \mathbf{t}_l}{\mathbf{h}}\mathbf{t}_{l-1}^{\nu-1}\mathcal{F}_1(\mathfrak{m}_{l-1}, \mathcal{S}_{l-1}, \mathcal{P}_{1,l-1}, \mathcal{P}_{2,l-1}, \mathcal{R}_{l-1}), \\ \mathcal{H}_{2,l}^*(\mathfrak{m}) &\simeq \frac{\mathfrak{m} - \mathbf{t}_{l-1}}{\mathbf{h}}\mathbf{t}_l^{\nu-1}\mathcal{F}_2(\mathfrak{m}_l, \mathcal{S}_l, \mathcal{P}_{1,l}, \mathcal{P}_{2,l}, \mathcal{R}_l) \\ &\quad - \frac{\mathfrak{m} - \mathbf{t}_l}{\mathbf{h}}\mathbf{t}_{l-1}^{\nu-1}\mathcal{F}_2(\mathfrak{m}_{l-1}, \mathcal{S}_{l-1}, \mathcal{P}_{1,l-1}, \mathcal{P}_{2,l-1}, \mathcal{R}_{l-1}), \\ \mathcal{H}_{3,l}^*(\mathfrak{m}) &\simeq \frac{\mathfrak{m} - \mathbf{t}_{l-1}}{\mathbf{h}}\mathbf{t}_l^{\nu-1}\mathcal{F}_3(\mathfrak{m}_l, \mathcal{S}_l, \mathcal{P}_{1,l}, \mathcal{P}_{2,l}, \mathcal{R}_l) \\ &\quad - \frac{\mathfrak{m} - \mathbf{t}_l}{\mathbf{h}}\mathbf{t}_{l-1}^{\nu-1}\mathcal{F}_3(\mathfrak{m}_{l-1}, \mathcal{S}_{l-1}, \mathcal{P}_{1,l-1}, \mathcal{P}_{2,l-1}, \mathcal{R}_{l-1}), \\ \mathcal{H}_{4,l}^*(\mathfrak{m}) &\simeq \frac{\mathfrak{m} - \mathbf{t}_{l-1}}{\mathbf{h}}\mathbf{t}_l^{\nu-1}\mathcal{F}_4(\mathfrak{m}_l, \mathcal{S}_l, \mathcal{P}_{1,l}, \mathcal{P}_{2,l}, \mathcal{R}_l) \\ &\quad - \frac{\mathfrak{m} - \mathbf{t}_l}{\mathbf{h}}\mathbf{t}_{l-1}^{\nu-1}\mathcal{F}_4(\mathfrak{m}_{l-1}, \mathcal{S}_{l-1}, \mathcal{P}_{1,l-1}, \mathcal{P}_{2,l-1}, \mathcal{R}_{l-1}).\end{aligned} \tag{91}$$

Then, we have

$$\begin{cases}\mathcal{S}(\mathbf{t}_{n+1}) = \mathcal{S}_0 + \dfrac{\nu}{\Gamma(\omega)}\displaystyle\sum_{l=0}^{n}\int_{\mathbf{t}_l}^{\mathbf{t}_{l+1}} (\mathbf{t}_{n+1} - \mathfrak{m})^{\omega-1}\mathcal{H}_{1,l}^*(\mathfrak{m})\mathrm{d}\mathfrak{m}, \\ \mathcal{P}_1(\mathbf{t}_{n+1}) = \mathcal{P}_{1,0} + \dfrac{\nu}{\Gamma(\omega)}\displaystyle\sum_{l=0}^{n}\int_{\mathbf{t}_l}^{\mathbf{t}_{l+1}} (\mathbf{t}_{n+1} - \mathfrak{m})^{\omega-1}\mathcal{H}_{2,l}^*(\mathfrak{m})\mathrm{d}\mathfrak{m}, \\ \mathcal{P}_2(\mathbf{t}_{n+1}) = \mathcal{P}_{2,0} + \dfrac{\nu}{\Gamma(\omega)}\displaystyle\sum_{l=0}^{n}\int_{\mathbf{t}_l}^{\mathbf{t}_{l+1}} (\mathbf{t}_{n+1} - \mathfrak{m})^{\omega-1}\mathcal{H}_{3,l}^*(\mathfrak{m})\mathrm{d}\mathfrak{m}, \\ \mathcal{R}(\mathbf{t}_{n+1}) = \mathcal{R}_0 + \dfrac{\nu}{\Gamma(\omega)}\displaystyle\sum_{l=0}^{n}\int_{\mathbf{t}_l}^{\mathbf{t}_{l+1}} (\mathbf{t}_{n+1} - \mathfrak{m})^{\omega-1}\mathcal{H}_{4,l}^*(\mathfrak{m})\mathrm{d}\mathfrak{m}.\end{cases} \tag{92}$$

By evaluating above integrals directly, the approximate solutions of the given fractional-fractal model of SARS-CoV-2 virus (6) are given by

$$\mathcal{S}_{n+1} = \mathcal{S}_0 + \frac{\nu \mathbf{h}^{\omega}}{\Gamma(\omega+2)} \sum_{l=0}^{n} \Big[\mathbf{t}_l^{\nu-1} \mathcal{F}_1(\mathbf{t}_l, \mathcal{S}_l, \mathcal{P}_{1,l}, \mathcal{P}_{2,l}, \mathcal{R}_l) Y_{(n,l)} - \mathbf{t}_{l-1}^{\nu-1} \mathcal{F}_1(\mathbf{t}_{l-1}, \mathcal{S}_{l-1}, \mathcal{P}_{1,l-1}, \mathcal{P}_{2,l-1}, \mathcal{R}_{l-1}) \widehat{Y}_{(n,l)} \Big],$$

$$\mathcal{P}_{1,n+1} = \mathcal{P}_{1,0} + \frac{\nu \mathbf{h}^{\omega}}{\Gamma(\omega+2)} \sum_{l=0}^{n} \Big[\mathbf{t}_l^{\nu-1} \mathcal{F}_2(\mathbf{t}_l, \mathcal{S}_l, \mathcal{P}_{1,l}, \mathcal{P}_{2,l}, \mathcal{R}_l) Y_{(n,l)} - \mathbf{t}_{l-1}^{\nu-1} \mathcal{F}_2(\mathbf{t}_{l-1}, \mathcal{S}_{l-1}, \mathcal{P}_{1,l-1}, \mathcal{P}_{2,l-1}, \mathcal{R}_{l-1}) \widehat{Y}_{(n,l)} \Big],$$

$$\mathcal{P}_{2,n+1} = \mathcal{P}_{2,0} + \frac{\nu \mathbf{h}^{\omega}}{\Gamma(\omega+2)} \sum_{l=0}^{n} \Big[\mathbf{t}_l^{\nu-1} \mathcal{F}_3(\mathbf{t}_l, \mathcal{S}_l, \mathcal{P}_{1,l}, \mathcal{P}_{2,l}, \mathcal{R}_l) Y_{(n,l)} - \mathbf{t}_{l-1}^{\nu-1} \mathcal{F}_3(\mathbf{t}_{l-1}, \mathcal{S}_{l-1}, \mathcal{P}_{1,l-1}, \mathcal{P}_{2,l-1}, \mathcal{R}_{l-1}) \widehat{Y}_{(n,l)} \Big],$$

$$\mathcal{R}_{n+1} = \mathcal{R}_0 + \frac{\nu \mathbf{h}^{\omega}}{\Gamma(\omega+2)} \sum_{l=0}^{n} \Big[\mathbf{t}_l^{\nu-1} \mathcal{F}_4(\mathbf{t}_l, \mathcal{S}_l, \mathcal{P}_{1,l}, \mathcal{P}_{2,l}, \mathcal{R}_l) Y_{(n,l)} - \mathbf{t}_{l-1}^{\nu-1} \mathcal{F}_4(\mathbf{t}_{l-1}, \mathcal{S}_{l-1}, \mathcal{P}_{1,l-1}, \mathcal{P}_{2,l-1}, \mathcal{R}_{l-1}) \widehat{Y}_{(n,l)} \Big], \tag{93}$$

where

$$Y_{(n,l)} = (n+1-l)^{\omega}(n-l+2+\omega) - (n-l)^{\omega}(n-l+2+2\omega),$$
$$\widehat{Y}_{(n,l)} = (n+1-l)^{\omega+1} - (n-l)^{\omega}(n-l+1+\omega), \tag{94}$$

where ω is the fractional order of the given fractal-fractional system (6).

7.2. Simulations Based on Adams-Bashforth Method. In this section, using the AB method for fractal-fractional, we present approximate solutions for the fractal-fractional probability-based model of SARS-CoV-2 virus (6). We demonstrate simulations to observe the behavior of four subclasses of SARS-CoV-2, which are $\mathcal{S}$, $\mathcal{P}_1$, $\mathcal{P}_2$, and $\mathcal{R}$ under the different set of parameters.

To provide a numerical simulation, we start by determining the value of the parameters by using reported cases in Turkey from 01 January 2021 to 03 July 2021. The birth rate for the Turkey in 2021 is 15.408 births per 1000 people, and the death rate is $b_1 = 5.5$ per 1000 people. The Turkey's population on 1st of January was $\mathcal{N} = 84339067$. Since we use the day as time limit, we can calculate the newborn rate as $\Theta = (84339067 \times 15.408)/(1000 \times 365)$. To estimate the remaining parameters, we use the curve fitting technique with the data reported for SARS-CoV-2. Using this method, we determine the parameters as follows: $p = 0.4$, $r = 0.003$, $s = 0.05$, $b = 0.05$, $r_1 = 0.05$, and $r_2 = 0.6$, and we assume $q = 0.2$, $b_2 = 0.04$, and $b_3 = 0.6$. Also, the stepsize for the time interval is choosen as $h = 10^{-3}$. As a first visualization, in Figure 1, we demonstrate the real data versus present model simulation. Then, behaviors of four subclasses are presented

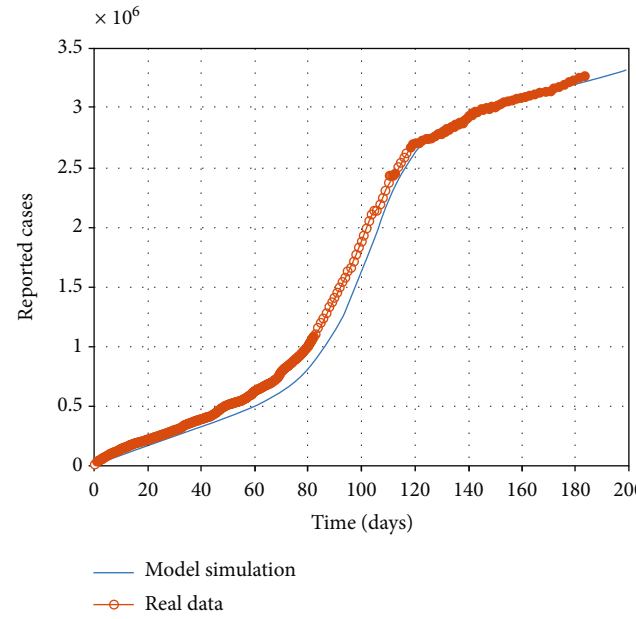

Figure 1: Simulated data vs. Real data for the SARS-CoV-2 cases in Turkey from 01 January 2021 to 03 July 2021.

in Figures 2(a)–2(d) with the chosen initial values $\mathcal{S} = 100$, $\mathcal{P}_1 = 90$, $\mathcal{P}_2 = 80$, and $\mathcal{R} = 70$, respectively, and under various fractal-fractional orders ω and ν.

Now, we simulate and discuss the dynamics of the model based on the parameters provided by [60]. Based on this source, we assume $\Theta = 30$, $r = 0.003$, $s = 0.05$, $b = 0.05$, $b_1 = 0.05$, $p = 0.4$, $b_2 = 0.04$, $r_1 = 0.05$, $q = 0.2$, $b_3 = 0.6$, and $r_2 = 0.6$. Finally, the initial values for state functions are $\mathcal{S}(0) = 0.5$, $\mathcal{P}_1(0) = 0.3$, $\mathcal{P}_2(0) = 0.2$, and $\mathcal{R}(0) = 0.1$. In different figures, we will show the behaviors of four state functions $\mathcal{S}$, $\mathcal{P}_1$, $\mathcal{P}_2$, and $\mathcal{R}$ by assuming different values for fractal and fractional orders $\omega = \nu = 1.00,0.99,0.98,0.97,0.96,0.95$.

In Figures 3(a) and 3(b), we illustrate the obtained dynamics of all four state functions $\mathcal{S}$, $\mathcal{P}_1$, $\mathcal{P}_2$, and $\mathcal{R}$ by the use of ABM with the vaccination rate (a) $b = 0.05$ and (b) $b = 0.1$, respectively. The great impact of the vaccine can be clearly observed from these illustrations as increasing the vaccination rate decreases the infected population and increases the recovered population.

In Figure 4, the susceptible subclass $\mathcal{S}(t)$ is demonstrated with the initial value $\mathcal{S}(0) = 0.5$. From this illustration, we observed that the graphs of this category of people converge quickly to a stable case at higher fractal-fractional orders and slowly to such a stable case at lower fractal-fractional orders. Also, we can see that by increasing the fractal-fractional orders, the density of $\mathcal{S}(t)$ also increases.

In Figure 5, the asymptomatic subclass $\mathcal{P}_1(t)$ is demonstrated with the initial value $\mathcal{P}_1(t) = 0.3$. From this illustration, we observed that the graphs of this category of people converge quickly to a stable case at higher fractal-fractional orders and slowly to such a stable case at lower fractal-fractional orders. Also, we can see that by increasing the fractal-fractional orders, the density of asymptomatic category $\mathcal{P}_1(t)$ also increases.

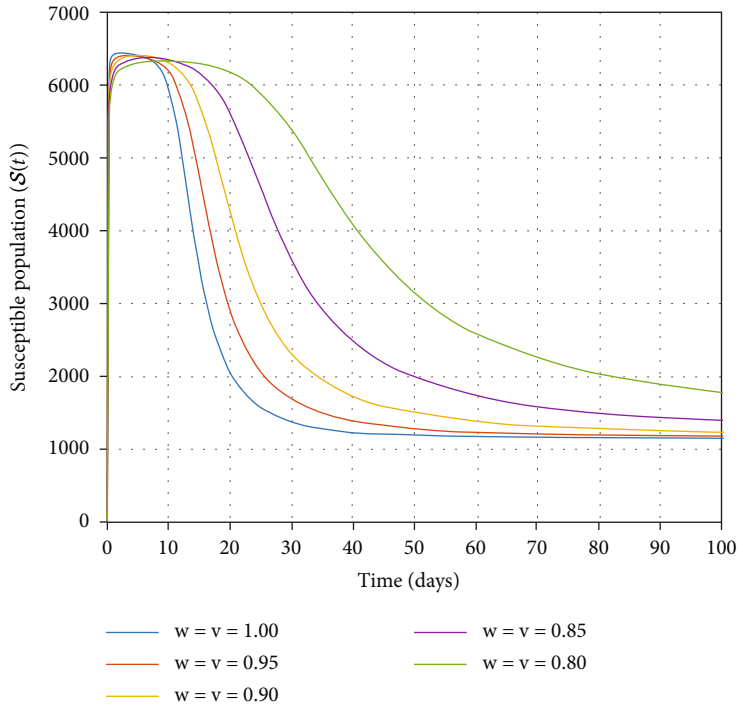

(a)

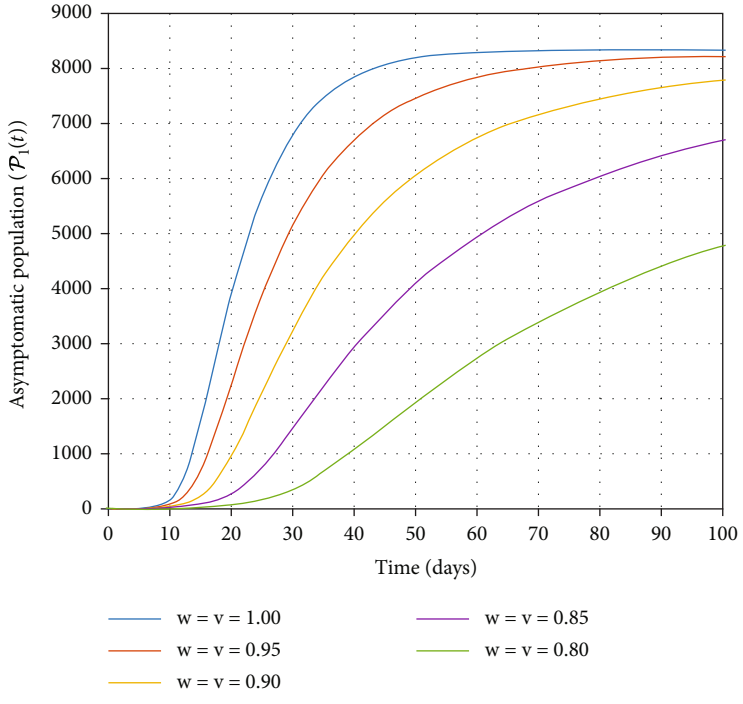

(b)

Figure 2: Continued.

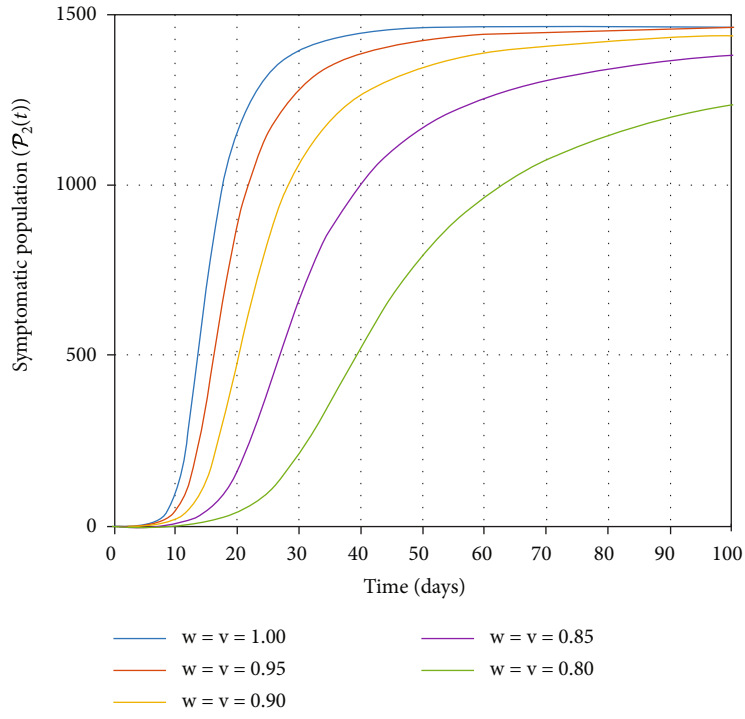

(c)

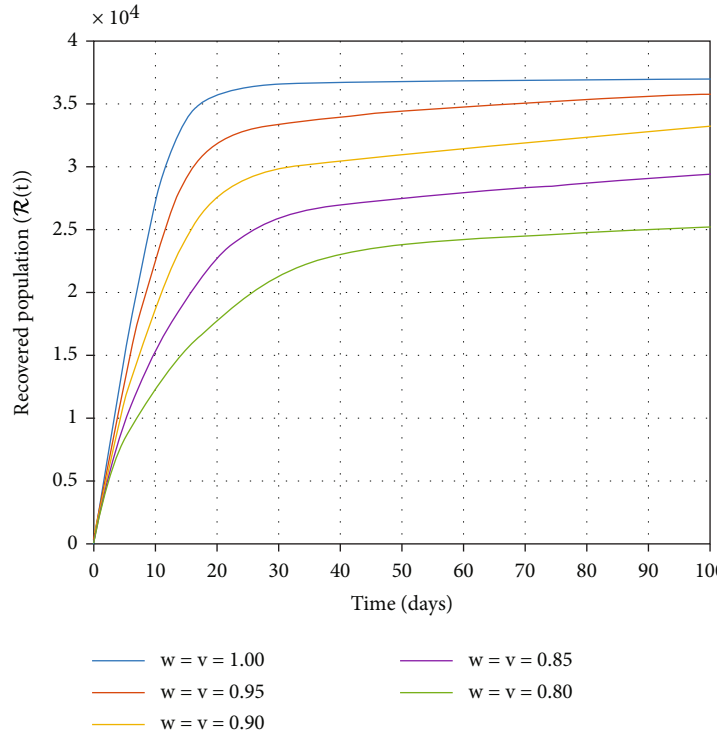

(d)

FIGURE 2: Behaviors of each compartments: (a) $\mathscr{S}(t)$, (b) $\mathscr{P}_1(t)$, (c) $\mathscr{P}_2(t)$, and (d) $\mathscr{R}(t)$ under various fractal-fractional orders $\omega = \nu =$ 1,0.95,0.90,0.85,0.80 with the estimated parameters from the reported data.

In Figure 6, the symptomatic subclass $\mathscr{P}_2(t)$ is presented with the initial value $\mathscr{P}_2(t) = 0.2$. From this illustration, we can see that the graphs of this category of people converge quickly to a stable case at higher fractal-fractional orders and slowly to such a stable case at lower fractal-fractional orders. Also, we can see that by increasing the fractal-fractional orders, the density of symptomatic category $\mathscr{P}_2(t)$ also increases.

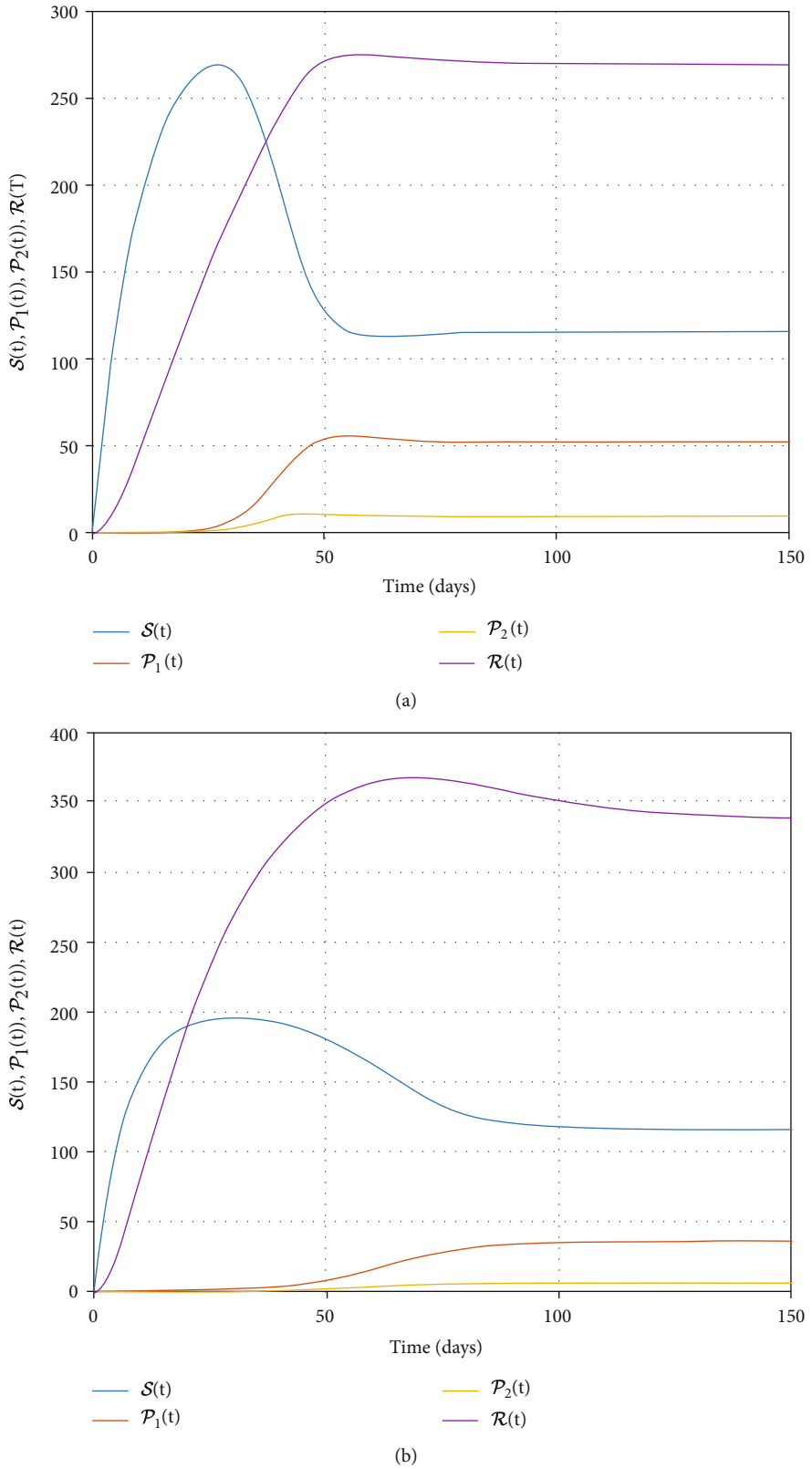

FIGURE 3: Behaviors of four trajectories for (a) vaccination rate $b = 0.05$ and (b) vaccination rate $b = 0.1$, under fractal-fractional order $\omega = \nu = 1$.

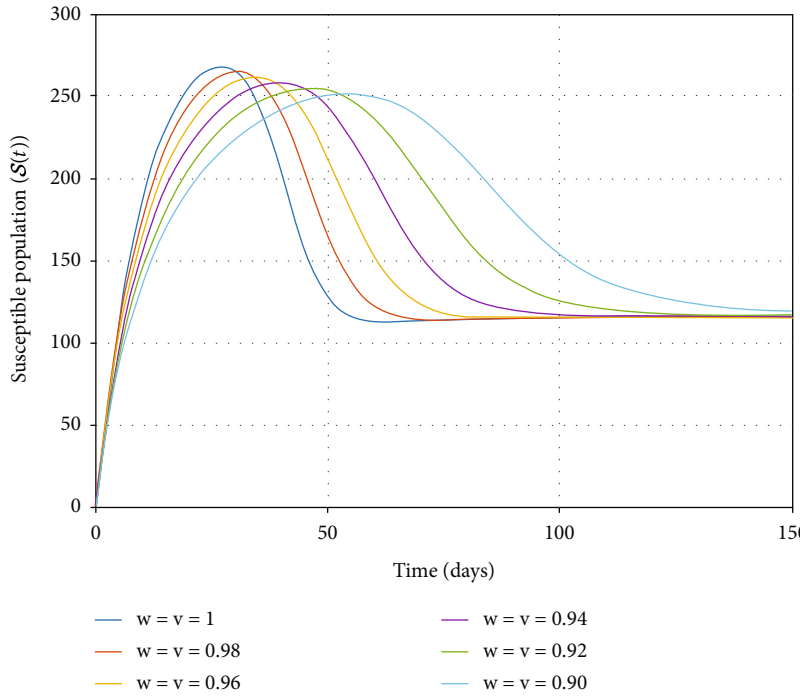

FIGURE 4: Behavior of $\mathcal{S}(t)$ by changing fractal-fractional order ω and v.

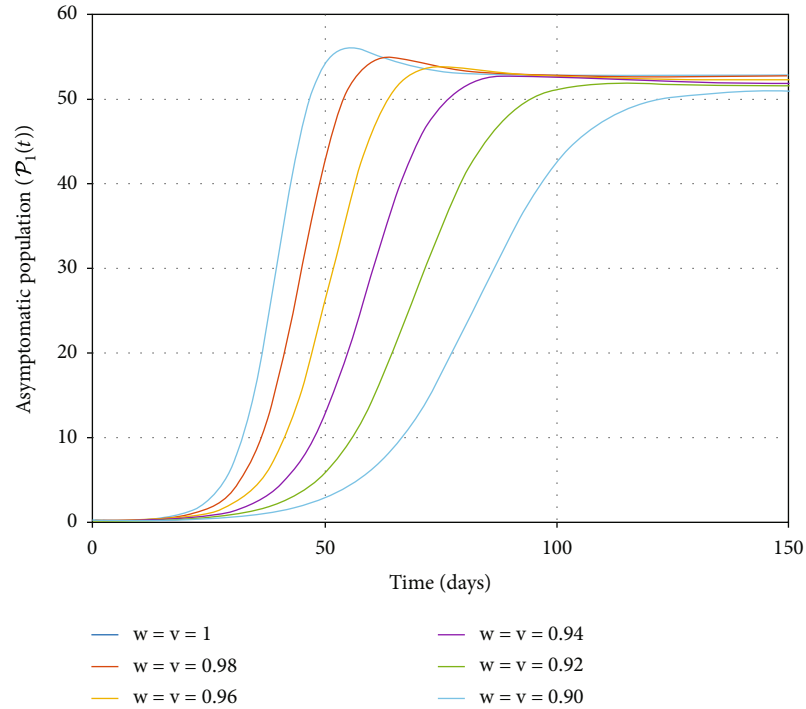

FIGURE 5: Behavior of $\mathcal{P}_1(t)$ by changing fractal-fractional order ω and v.

In Figure 7, the recovered category $\mathcal{R}(t)$ is demonstrated with the initial value $\mathcal{R}(t) = 0.1$. From this illustration, we observed that the graphs of this category of people converge quickly to a stable case at higher fractal-fractional orders and slowly to such a stable case at lower fractal-fractional orders. Also, we can see that by increasing the fractal-fractional orders, the density of recovered population $\mathcal{R}(t)$ also increases.

It is seen that the graphs of all four category of people have the similar behaviors regarding to different values of

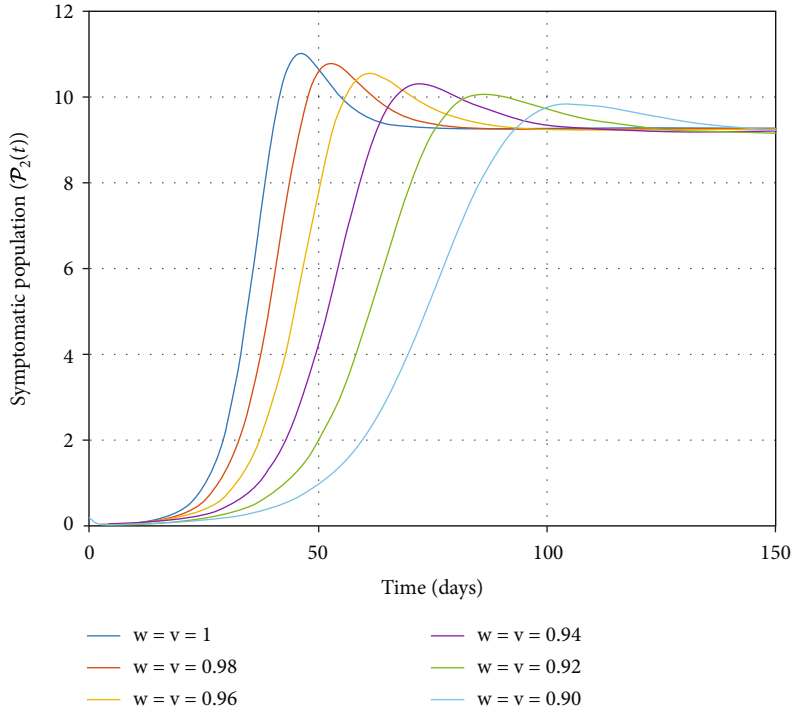

FIGURE 6: Behavior of $\mathcal{P}_2(t)$ by changing fractal-fractional order ω and ν.

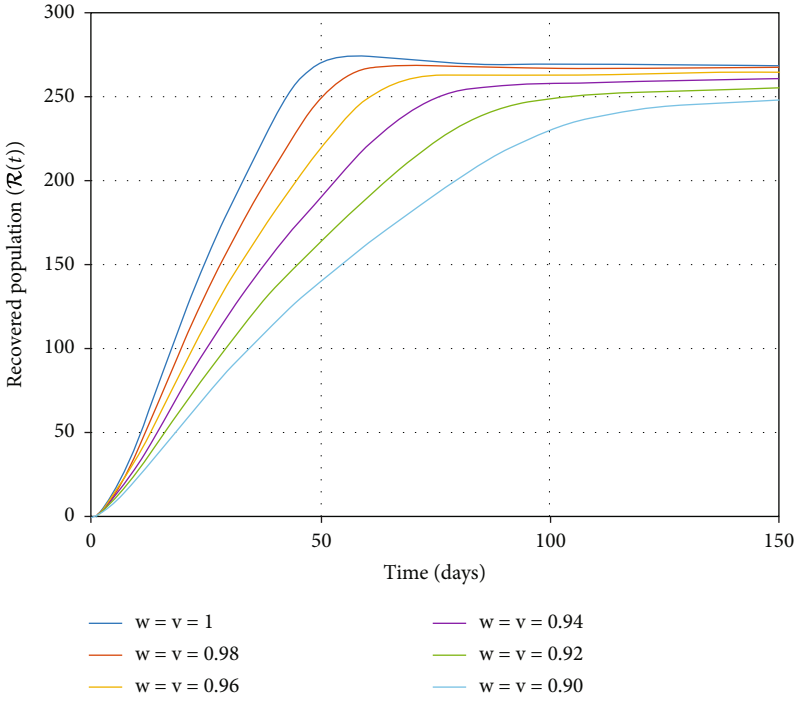

FIGURE 7: Behavior of $\mathcal{R}(t)$ by changing fractal-fractional order ω and ν.

fractal-fractional orders, and they converge quickly to a stable case at higher fractal-fractional orders and slowly to such a stable case at lower fractal-fractional orders. Also, the densities of all four group of population are increasing as the fractal-fractional order increases.

8. Model Dynamics in the Caputo Sense

In this section, we convert the presented fractal-fractional epidemic probability-based model of SARS-CoV-2 virus (6) into a Caputo-type model. The main motivation of this

replacement is to compare the proposed model in two different type and capture the memory effects on the given model by using different fractional-order dynamics. The new formulation of the proposed model is as follows:

$$\begin{cases} {}^{C}\mathfrak{D}^{\omega}_{0,\mathfrak{t}}\mathcal{S}(\mathfrak{t}) = \Theta - r\mathcal{P}_1(\mathfrak{t})\mathcal{S}(\mathfrak{t}) - rs\mathcal{P}_2(\mathfrak{t})\mathcal{S}(\mathfrak{t}) - (b + b_1)\mathcal{S}(\mathfrak{t}), \\ {}^{C}\mathfrak{D}^{\omega}_{0,\mathfrak{t}}\mathcal{P}_1(\mathfrak{t}) = p[r\mathcal{P}_1(\mathfrak{t})\mathcal{S}(\mathfrak{t}) + rs\mathcal{P}_2(\mathfrak{t})\mathcal{S}(\mathfrak{t})] - (b_1 + b_2 + r_1)\mathcal{P}_1(\mathfrak{t}), \\ {}^{C}\mathfrak{D}^{\omega}_{0,\mathfrak{t}}\mathcal{P}_2(\mathfrak{t}) = (1-p)[r\mathcal{P}_1(\mathfrak{t})\mathcal{S}(\mathfrak{t}) + rs\mathcal{P}_2(\mathfrak{t})\mathcal{S}(\mathfrak{t})] + qr_1\mathcal{P}_1(\mathfrak{t}) - (b_1 + b_3 + r_2)\mathcal{P}_2(\mathfrak{t}), \\ {}^{C}\mathfrak{D}^{\omega}_{0,\mathfrak{t}}\mathcal{R}(\mathfrak{t}) = r_1(1-q)\mathcal{P}_1(\mathfrak{t}) + r_2\mathcal{P}_2(\mathfrak{t}) + b\mathcal{S}(\mathfrak{t}) - b_1\mathcal{R}(\mathfrak{t}), \end{cases} \tag{95}$$

where

$${}^{C}\mathfrak{D}^{\omega}_{0,\mathfrak{t}}u(\mathfrak{t}) = {}^{RL}\mathfrak{J}^{\eta-\omega}_{0,\mathfrak{t}}\left(\frac{\mathrm{d}^{\eta}}{\mathrm{d}\mathfrak{t}^{\eta}}u(\mathfrak{t})\right), \eta - 1 < \omega \le \eta, \eta \in \mathbb{N}. \tag{96}$$

The Caputo fractional derivative satisfies the Newton–Leibniz formula for every $0 < \omega < 1$, that is,

$${}^{RL}\mathfrak{J}^{\omega}_{0,\mathfrak{t}}\left({}^{C}\mathfrak{D}^{\omega}_{0,\mathfrak{t}}u(\mathfrak{t})\right) = u(\mathfrak{t}) - \sum_{j=0}^{\lceil\omega\rceil-1} u^{(j)}(0)\frac{\mathfrak{t}^j}{j!}. \tag{97}$$

In recent years, many researchers have developed a number of numerical methods to solve different types of fractional-order models. In this section, our aim is to use a new method called the FTOMM (see ref. [62, 63]) method (fractional Taylor operational matrix method), to solve the probability-based model of the SARS-CoV-2 virus (95) in the Caputo settings.

8.1. Function Approximation and Operational Matrix. The Taylor vector of the fractional order is given as [64]

$$T_{n\kappa} = \left[1, \mathfrak{t}^{\kappa}, \mathfrak{t}^{2\kappa}, \cdots, \mathfrak{t}^{n\kappa}\right], \tag{98}$$

where $n \in \mathbb{N}$ and $\kappa > 0$. Let $T_{n\kappa} \subset S$ where $S \in L^2[0,1]$. For any $\varphi \in M$, since $M = \mathrm{span}\{1, \mathfrak{t}^{\kappa}, \mathfrak{t}^{2\kappa}, \cdots, \mathfrak{t}^{n\kappa}\}$ is a vector space of finite dimension in S, thus φ possesses a unique best apporoximation φ_*, that is,

$$\forall \widehat{\varphi} \in M, \|\varphi - \varphi_*\| \le \|\varphi - \widehat{\varphi}\|. \tag{99}$$

Then, the function φ is approximated by the fractional-order Taylor vector by

$$\varphi \simeq \varphi_* = \sum_{j=0}^{n} g_j\mathfrak{t}^{j\kappa} = G^T T_{n\kappa}, \tag{100}$$

where $G^T = [g_0, g_1, \cdots, g_m]$ are the unique coefficients.

Consider $F_{(\mathfrak{t},\omega)}$ as an operational matrix of ω^{th}-integration with $(m+1)^2$ dimension. Then, the ω^{th}-R-L-integration of the Taylor vector defined in equation (98) is

$${}^{RL}\mathfrak{J}^{\omega}_{0,\mathfrak{t}}T_{n\kappa}(\mathfrak{t}) = F_{(\mathfrak{t},\omega)}T_{nk}(\mathfrak{t}). \tag{101}$$

By applying the ω^{th}-R-L integral for $T_{n\kappa}$, it becomes

$${}^{RL}\mathfrak{J}^{\omega}_{0,\mathfrak{t}}(T_{n\kappa}(\mathfrak{t})) = \left[\frac{1}{\Gamma(\omega+1)}\mathfrak{t}^{\omega}, \frac{\Gamma(\kappa+1)}{\Gamma(\kappa+\omega+1)}\mathfrak{t}^{\kappa+\omega}, \cdots, \frac{\Gamma(n\kappa+1)}{\Gamma(n\kappa+\omega+1)}\mathfrak{t}^{n\kappa+\omega}\right]. \tag{102}$$

Thus, (102) can be reformulated as

$${}^{RL}\mathfrak{J}^{\omega}_{0,\mathfrak{t}}(T_{n\kappa}(\mathfrak{t})) = \mathfrak{t}^{\omega}S_{\omega}T_{n\kappa}(\mathfrak{t}), \tag{103}$$

where

$$S_{\omega} = \mathrm{diag}\left[\frac{1}{\Gamma(\omega+1)}, \frac{\Gamma(\kappa+1)}{\Gamma(\kappa+\omega+1)}, \frac{\Gamma(2\kappa+1)}{\Gamma(2\kappa+\omega+1)}, \cdots, \frac{\Gamma(n\kappa+1)}{\Gamma(n\kappa+\omega+1)}\right]. \tag{104}$$

Set $\Phi_{(\mathfrak{t},\omega)} = \mathfrak{t}^{\omega}S_{\omega}$. In this case, the fractional Taylor operational matrix of integration is reformulated by

$$F_{(\mathfrak{t},\omega)} = \mathrm{diag}\left[\Phi_{(\mathfrak{t},\omega)}, \Phi_{(\mathfrak{t},\omega)}, \cdots, \Phi_{(\mathfrak{t},\omega)}\right]. \tag{105}$$

The product of two Taylor basis vectors is

$${}^{RL}\mathfrak{J}^{\omega}_{0,\mathfrak{t}}\left(T_{n\kappa}(\mathfrak{t})T^T_{n\kappa}(\mathfrak{t})\right) = \mathfrak{t}^{\omega}P_{\omega} * \left(T_{n\kappa}(\mathfrak{t})T^T_{n\kappa}(\mathfrak{t})\right), \tag{106}$$

where

$$P_\omega = \begin{bmatrix} \frac{1}{\Gamma(\omega+1)} & \frac{\Gamma(\kappa+1)}{\Gamma(\kappa+\omega+1)} & \cdots & \frac{\Gamma(n\kappa+1)}{\Gamma(n\kappa+\omega+1)} \\ \frac{\Gamma(\kappa+1)}{\Gamma(\kappa+\omega+1)} & \frac{\Gamma(2\kappa+1)}{\Gamma(2\kappa+\omega+1)} & \cdots & \frac{\Gamma((n+1)\kappa+1)}{\Gamma((n+1)\kappa+\omega+1)} \\ \vdots & \vdots & \vdots & \vdots \\ \frac{\Gamma(n\kappa+1)}{\Gamma(\kappa+\omega+1)} & \frac{\Gamma((n+1)\kappa+1)}{\Gamma((n+1)\kappa+\omega+1)} & \cdots & \frac{\Gamma(2n\kappa+1)}{\Gamma(2n\kappa+\omega+1)} \end{bmatrix}, \tag{107}$$

$$T_{n\kappa}(\mathfrak{t})T_{n\kappa}^T(\mathfrak{t}) = \begin{bmatrix} 1 & \mathfrak{t}^\omega & \mathfrak{t}^{2\omega} & \cdots & \mathfrak{t}^{n\omega} \\ \mathfrak{t}^\omega & \mathfrak{t}^{2\omega} & \mathfrak{t}^{3\omega} & \cdots & \mathfrak{t}^{(n+1)\omega} \\ \mathfrak{t}^{2\omega} & \mathfrak{t}^{3\omega} & \mathfrak{t}^{4\omega} & \cdots & \mathfrak{t}^{(n+2)\omega} \\ \vdots & \vdots & \vdots & \vdots & \vdots \\ \mathfrak{t}^{n\omega} & \mathfrak{t}^{(n+1)\omega} & \mathfrak{t}^{(n+2)\omega} & \cdots & \mathfrak{t}^{2n\omega} \end{bmatrix}. \tag{108}$$

Again, by utilizing ${}^{\mathbf{RL}}\mathfrak{I}_{0,\mathfrak{t}}^{\omega}$ on the matrix (108), we get

$${}^{\mathbf{RL}}\mathfrak{I}_{0,\mathfrak{t}}^{\omega}\left(T_{n\kappa}(\mathfrak{t})T_{n\kappa}^T(\mathfrak{t})\right) = \begin{bmatrix} \frac{1}{\Gamma(\omega+1)} & \frac{\Gamma(\kappa+1)}{\Gamma(\kappa+\omega+1)}\mathfrak{t}^\omega & \cdots & \frac{\Gamma(n\kappa+1)}{\Gamma(n\kappa+\omega+1)}\mathfrak{t}^{n\omega} \\ \frac{\Gamma(\kappa+1)}{\Gamma(\kappa+\omega+1)}\mathfrak{t}^\omega & \frac{\Gamma(2\kappa+1)}{\Gamma(2\kappa+\omega+1)}\mathfrak{t}^{2\omega} & \cdots & \frac{\Gamma((n+1)\kappa+1)}{\Gamma((n+1)\kappa+\omega+1)}\mathfrak{t}^{(n+1)\omega} \\ \vdots & \vdots & \vdots & \vdots \\ \frac{\Gamma(n\kappa+1)}{\Gamma(\kappa+\omega+1)}\mathfrak{t}^{n\omega} & \frac{\Gamma((n+1)\kappa+1)}{\Gamma((n+1)\kappa+\omega+1)}\mathfrak{t}^{(n+1)\omega} & \cdots & \frac{\Gamma(2n\kappa+1)}{\Gamma(2n\kappa+\omega+1)}\mathfrak{t}^{2n\omega} \end{bmatrix}. \tag{109}$$

8.2. Application of FTOMM on the SARS-CoV-2 Model. In this part, the suggested FTOMM method is utilized to the model of SARS-CoV-2 virus given in (95).

We start by expanding ${}^{\mathbf{C}}\mathfrak{D}_{0,\mathfrak{t}}^{\omega}\mathcal{S}(\mathfrak{t})$, ${}^{\mathbf{C}}\mathfrak{D}_{0,\mathfrak{t}}^{\omega}\mathcal{P}_1(\mathfrak{t})$, ${}^{\mathbf{C}}\mathfrak{D}_{0,\mathfrak{t}}^{\omega}\mathcal{P}_2(\mathfrak{t})$, and ${}^{\mathbf{C}}\mathfrak{D}_{0,\mathfrak{t}}^{\omega}\mathcal{R}(\mathfrak{t})$ with the help of a fractional Taylor basis vector as following:

$$\begin{cases} {}^{\mathbf{C}}\mathfrak{D}_{0,\mathfrak{t}}^{\omega}\mathcal{S}(\mathfrak{t}) \approx C^T T_{n\kappa}(\mathfrak{t}), \\ {}^{\mathbf{C}}\mathfrak{D}_{0,\mathfrak{t}}^{\omega}\mathcal{P}_1(\mathfrak{t}) \approx K^T T_{n\kappa}(\mathfrak{t}), \\ {}^{\mathbf{C}}\mathfrak{D}_{0,\mathfrak{t}}^{\omega}\mathcal{P}_2(\mathfrak{t}) \approx L^T T_{n\kappa}(\mathfrak{t}), \\ {}^{\mathbf{C}}\mathfrak{D}_{0,\mathfrak{t}}^{\omega}\mathcal{R}(\mathfrak{t}) \approx N^T T_{n\kappa}(\mathfrak{t}). \end{cases} \tag{110}$$

Next, operating the ω^{th}-R-L integral on above equations and using initial values $\mathcal{S}(0)$,$\mathcal{P}_1(0)$,$\mathcal{P}_2(0)$, and $\mathcal{R}(0)$, we get

$$\begin{cases} \mathcal{S}(\mathfrak{t}) \approx C^T F_{(\mathfrak{t},\omega)} T_{n\kappa}(\mathfrak{t}) + \mathcal{S}(0), \\ \mathcal{P}_1(\mathfrak{t}) \approx K^T F_{(\mathfrak{t},\omega)} T_{n\kappa}(\mathfrak{t}) + \mathcal{P}_1(0), \\ \mathcal{P}_2(\mathfrak{t}) \approx L^T F_{(\mathfrak{t},\omega)} T_{n\kappa}(\mathfrak{t}) + \mathcal{P}_2(0), \\ \mathcal{R}(\mathfrak{t}) \approx N^T F_{(\mathfrak{t},\omega)} T_{n\kappa}(\mathfrak{t}) + \mathcal{R}(0). \end{cases} \tag{111}$$

Substituting (110) and (111) into SARS-CoV-2 model (95), we get

$$\begin{aligned} C^T T_{n\kappa}(\mathfrak{t}) = \Theta &- r\left[\left(K^T F_{(\mathfrak{t},\omega)} T_{n\kappa}(\mathfrak{t}) + \mathcal{S}_1(0)\right)\left(C^T F_{(\mathfrak{t},\omega)} T_{n\kappa}(\mathfrak{t}) + \mathcal{S}(0)\right)\right] \\ &- rs\left[\left(K^T F_{(\mathfrak{t},\omega)} T_{n\kappa}(\mathfrak{t}) + \mathcal{P}_1(0)\right)\left(C^T F_{(\mathfrak{t},\omega)} T_{n\kappa}(\mathfrak{t}) + \mathcal{S}(0)\right)\right] \\ &- (b+b_1)\left(C^T F_{(\mathfrak{t},\omega)} T_{n\kappa}(\mathfrak{t}) + \mathcal{S}(0)\right), \end{aligned}$$

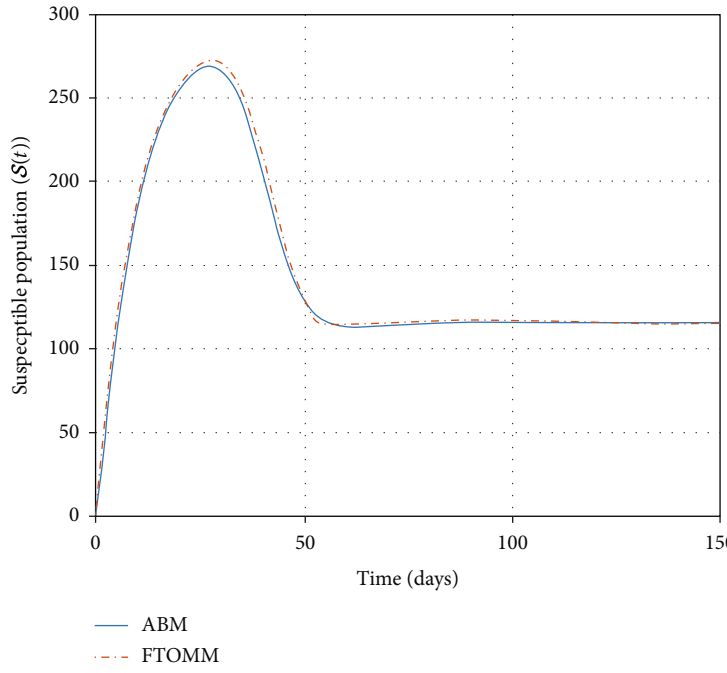

(a)

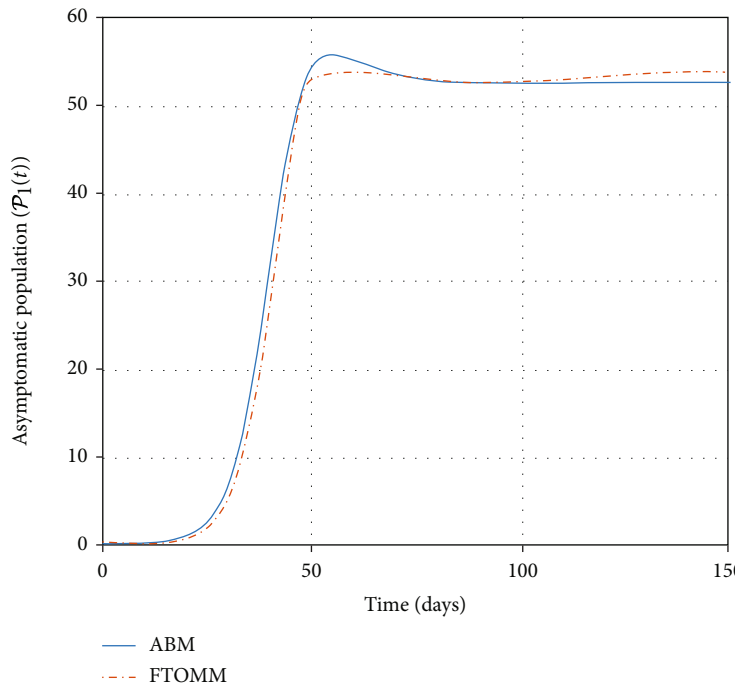

(b)

Figure 8: Continued.

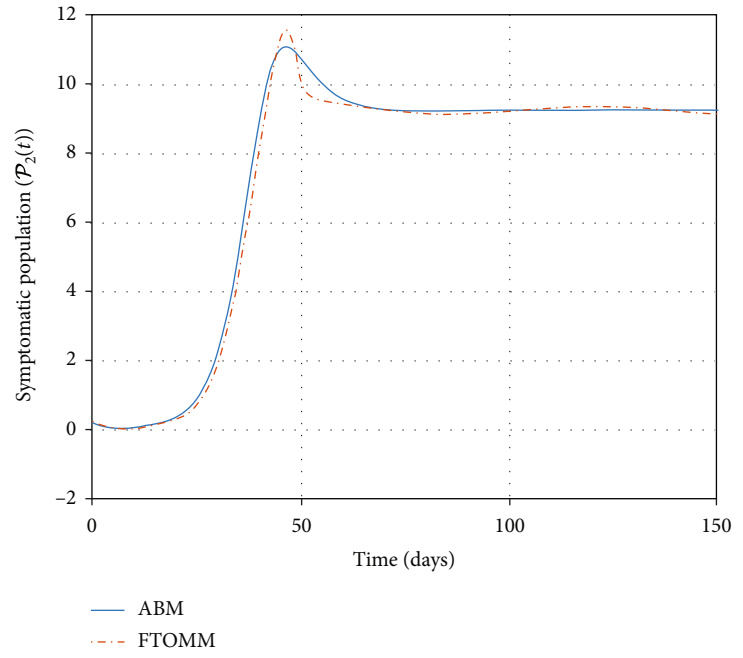

(c)

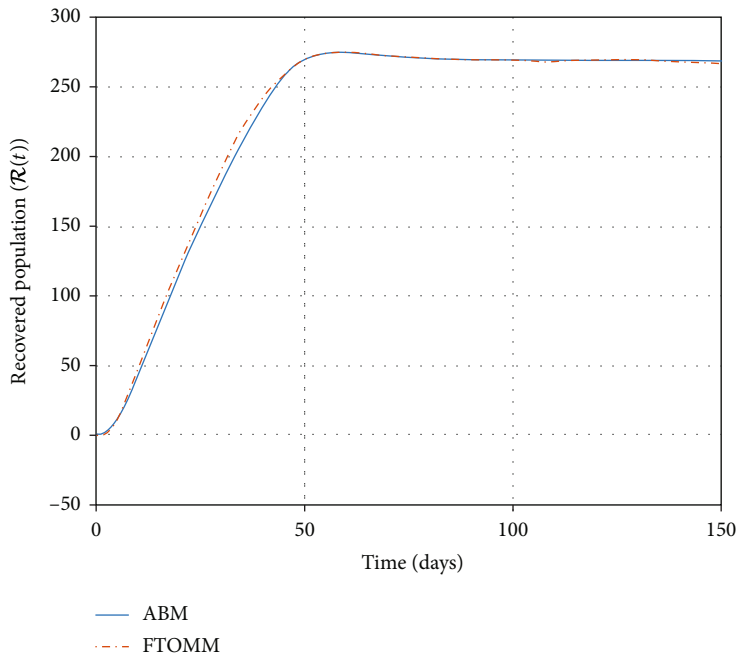

(d)

Figure 8: Comparisons between the ABM and FTOMM for the parametric values.

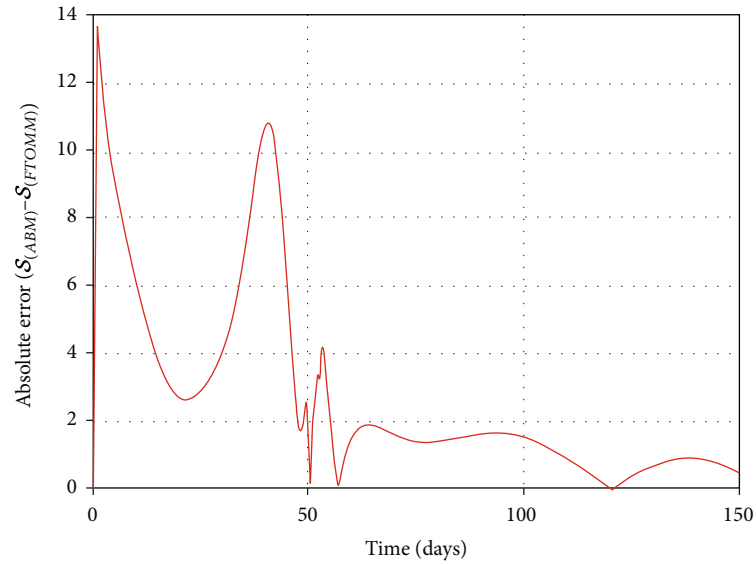

(a)

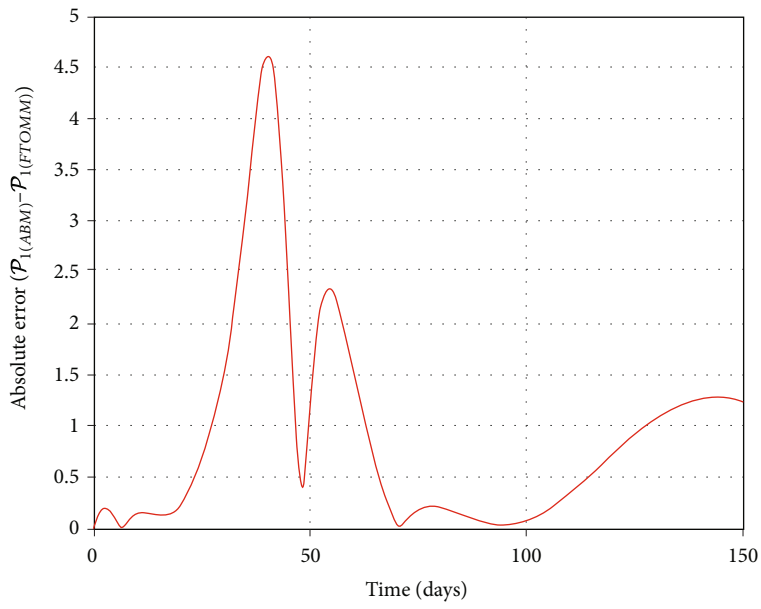

(b)

Figure 9: Continued.

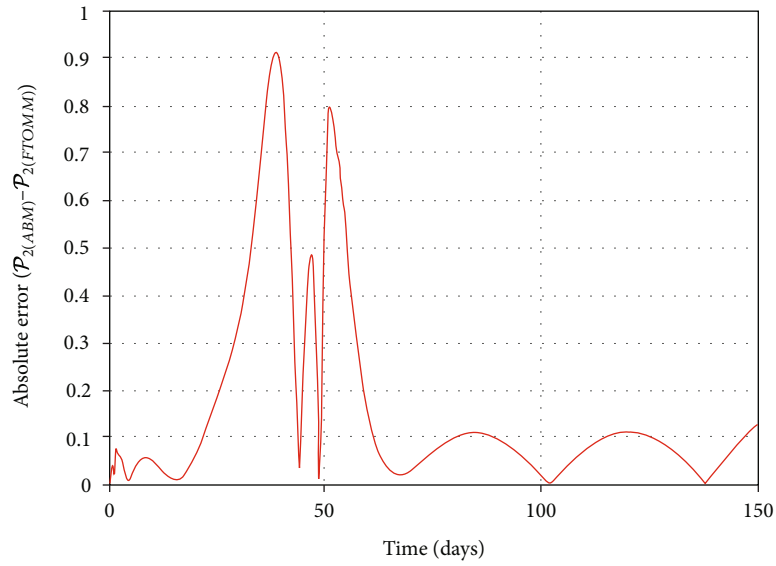

(c)

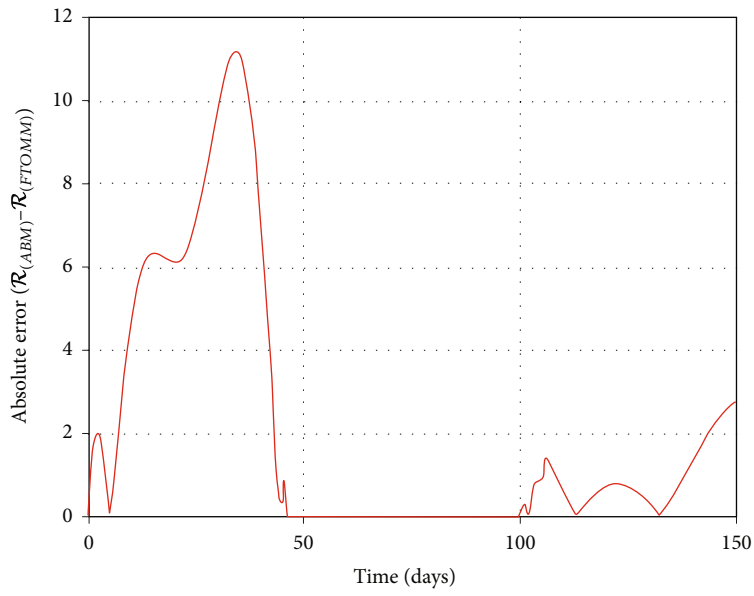

(d)

Figure 9: Absolute error comparisons between the ABM and FTOMM for the parametric values.

$$
\begin{aligned}
K^T T_{n\kappa}(\mathbf{t}) &= \mathrm{pr}\left[\left(K^T F_{(\mathbf{t},\omega)} T_{n\kappa}(\mathbf{t}) + \mathscr{P}_1(0)\right)\left(C^T F_{(\mathbf{t},\omega)} T_{n\kappa}(\mathbf{t}) + \mathscr{S}(0)\right)\right] \\
&\quad + \mathrm{prs}\left[\left(K^T F_{(\mathbf{t},\omega)} T_{n\kappa}(\mathbf{t}) + \mathscr{P}_1(0)\right)\left(C^T F_{(\mathbf{t},\omega)} T_{n\kappa}(\mathbf{t}) + \mathscr{S}(0)\right)\right] \\
&\quad - (b_1 + b_2 + r_1)\left(K^T F_{(\mathbf{t},\omega)} T_{n\kappa}(\mathbf{t}) + \mathscr{P}_1(0)\right), \\
L^T T_{n\kappa}(\mathbf{t}) &= (1-p)r\left[\left(K^T F_{(\mathbf{t},\omega)} T_{n\kappa}(\mathbf{t}) + \mathscr{P}_1(0)\right)\right. \\
&\quad \left.\cdot \left(C^T F_{(\mathbf{t},\omega)} T_{n\kappa}(\mathbf{t}) + \mathscr{S}(0)\right)\right] \\
&\quad + (1-p)rs\left[\left(K^T F_{(\mathbf{t},\omega)} T_{n\kappa}(\mathbf{t}) + \mathscr{P}_1(0)\right)\right. \\
&\quad \left.\cdot \left(C^T F_{(\mathbf{t},\omega)} T_{n\kappa}(\mathbf{t}) + \mathscr{S}(0)\right)\right] \\
&\quad + (qr_1)\left(K^T F_{(\mathbf{t},\omega)} T_{n\kappa}(\mathbf{t}) + \mathscr{P}_1(0)\right) \\
&\quad - (b_1 + b_3 + r_2)\left(L^T F_{(\mathbf{t},\omega)} T_{n\kappa}(\mathbf{t}) + \mathscr{P}_2(0)\right), \\
N^T T_{n\kappa}(\mathbf{t}) &= r_1(1-q)\left(K^T F_{(\mathbf{t},\omega)} T_{n\kappa}(\mathbf{t}) + \mathscr{P}_1(0)\right) \\
&\quad + r_2\left(L^T F_{(\mathbf{t},\omega)} T_{n\kappa}(\mathbf{t}) + \mathscr{P}_2(0)\right) \\
&\quad + b\left(C^T F_{(\mathbf{t},\omega)} T_{n\kappa}(\mathbf{t}) + \mathscr{S}(0)\right) \\
&\quad - b_1\left(N^T F_{(\mathbf{t},\omega)} T_{n\kappa}(\mathbf{t}) + \mathscr{R}(0)\right).
\end{aligned}
\tag{112}
$$

Now, by using above equations and collocation points $\mathbf{t}_j = j/n$, where $j = 0, 1, \cdots n$, we derive a system of $4n+4$ algebraic nonlinear equations with $4n+4$ unknown coefficients. This system is solved efficiently for the unknown coefficient vectors C^T, K^T, L^T, and N^T by using the Newton method in MATLAB software.

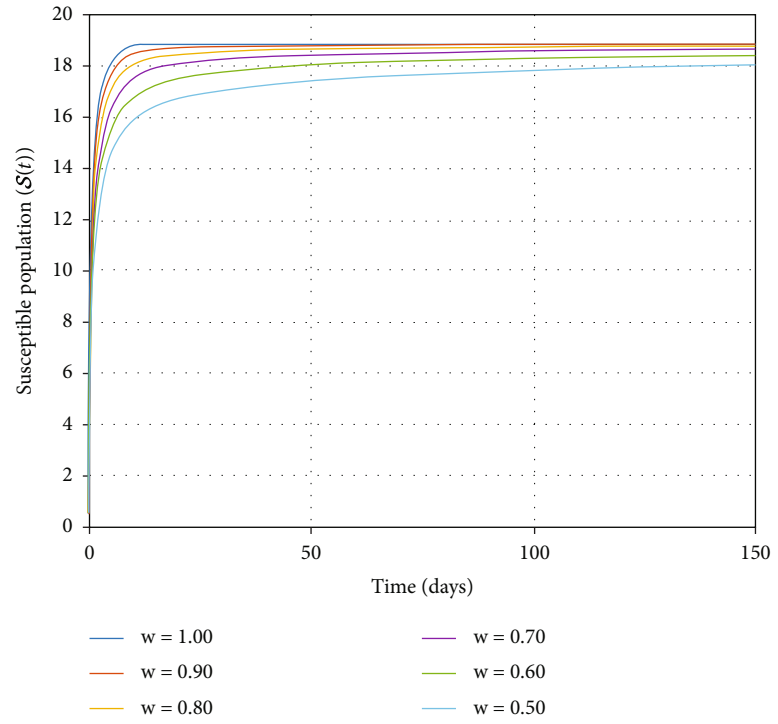

FIGURE 10: $\mathcal{S}(\mathbf{t})$ by changing ω where $m = 7$.

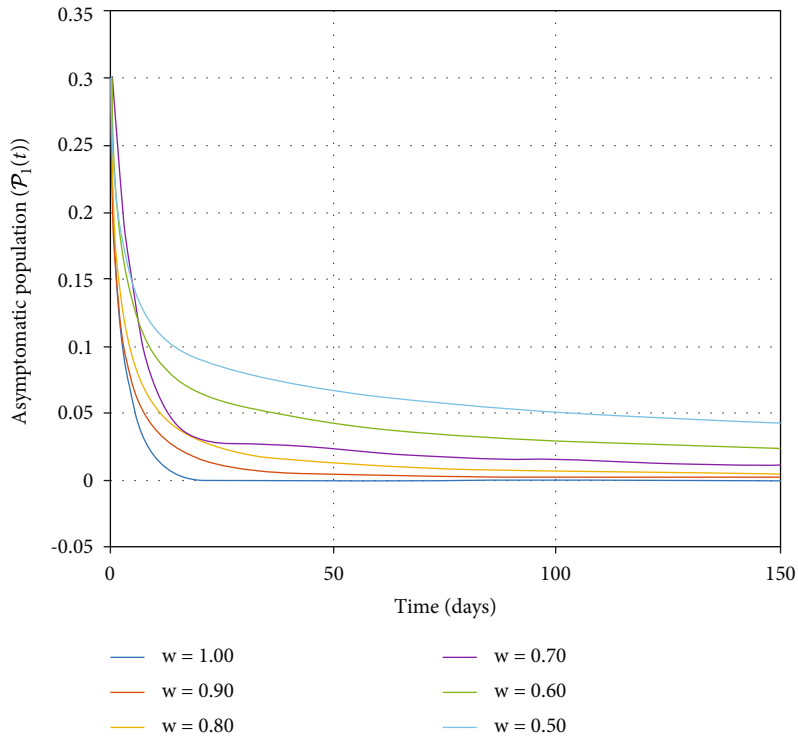

FIGURE 11: $\mathcal{P}_1(\mathbf{t})$ by changing ω where $m = 7$.

As a final step, substituting the vectors of coefficients C^T, K^T, L^T, and N^T into (111), we obtain for $\mathcal{S}(\mathbf{t})$, $\mathcal{P}_1(\mathbf{t})$, $\mathcal{P}_2(\mathbf{t})$, and $\mathcal{R}(\mathbf{t})$ approximately.

8.3. Simulations Based on FTOMM Method and Comparison with Adams-Bashforth Method. In this section, all graphical results of the fractional SARS-CoV-2 model (95) by using

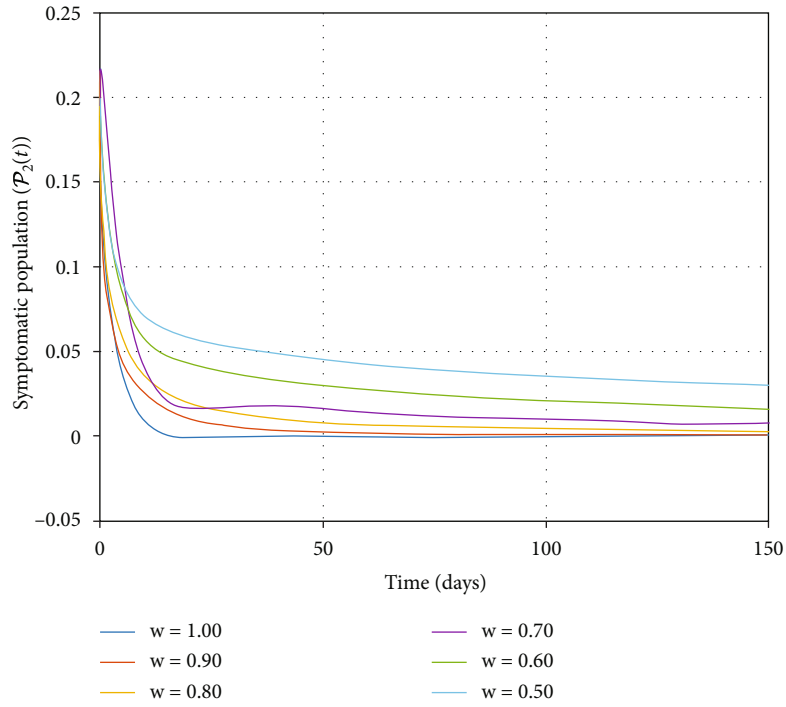

FIGURE 12: $\mathcal{P}_2(\mathbf{t})$ by changing ω where $m = 7$.

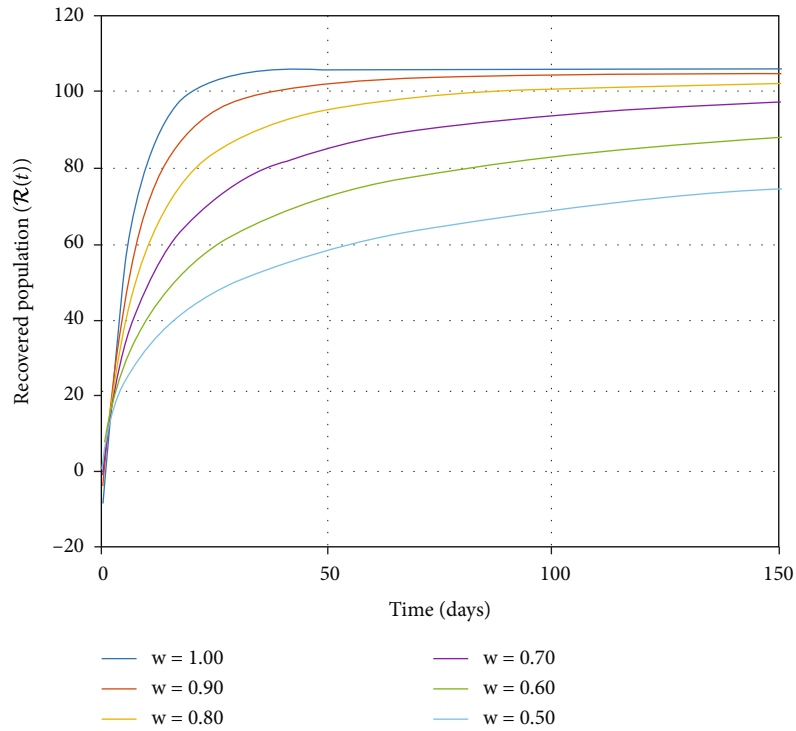

FIGURE 13: $\mathcal{R}(\mathbf{t})$ by changing ω where $m = 7$.

FTOMM and their comparison between ABM are illustrated through Figures 8–14. To see the correctness and having a comparison, we illustrate the graphical representation of the presented model at several values of ω.

In Figure 8, we present a comparison of obtained solutions by use of the ABM and FTOMM for the parametric values assumed in subsection 7.2. From Figures 8(a)–8(d), we can clearly conclude that the both acquired numerical

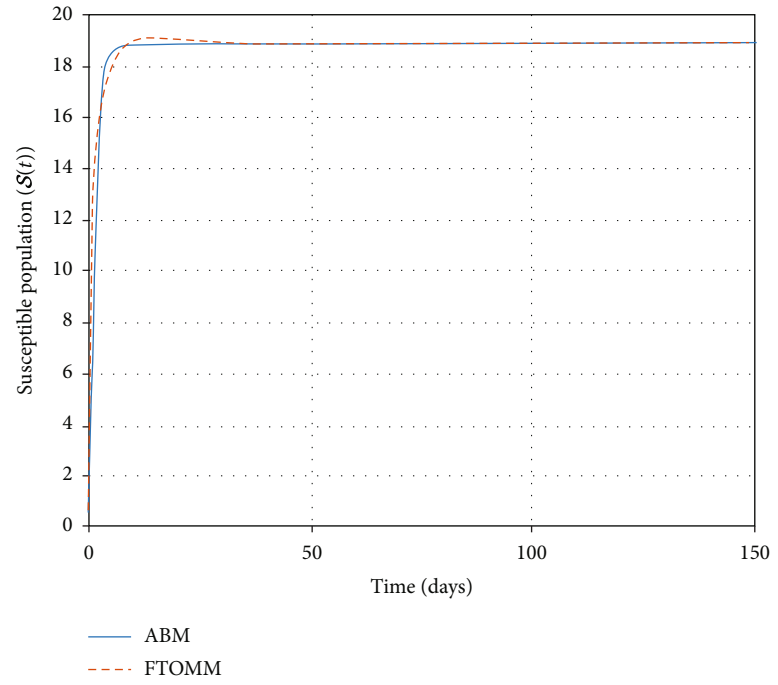

(a)

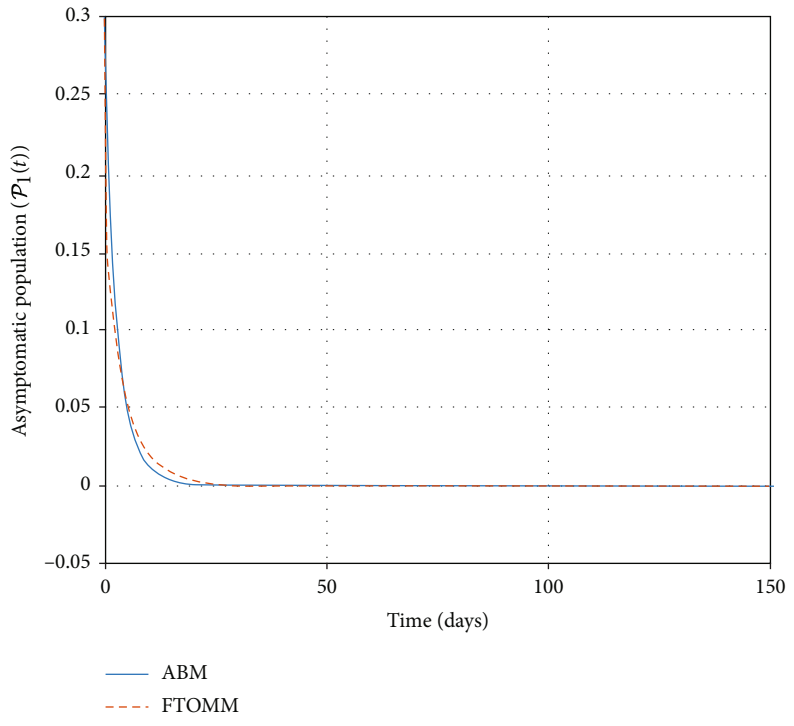

(b)

Figure 14: Continued.

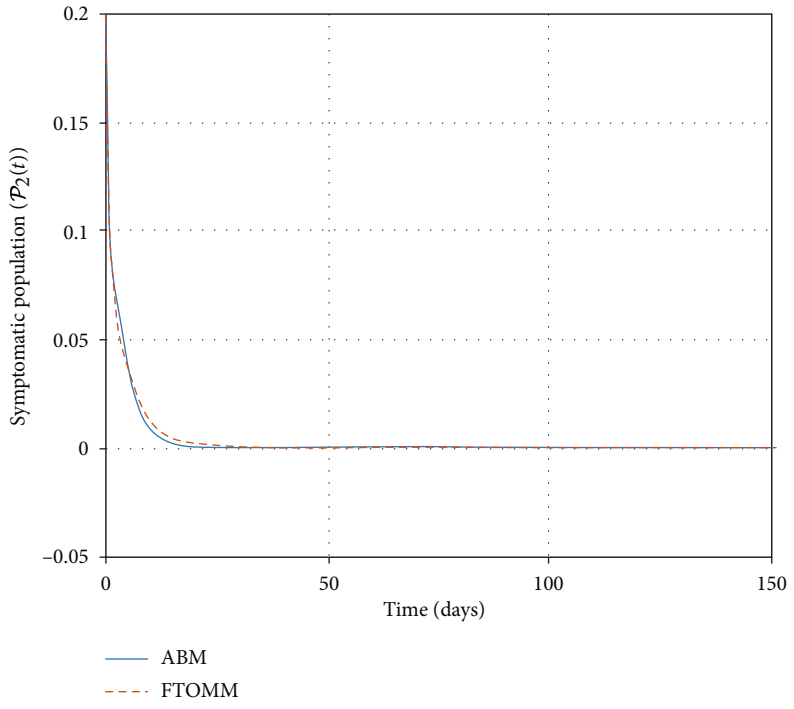

(c)

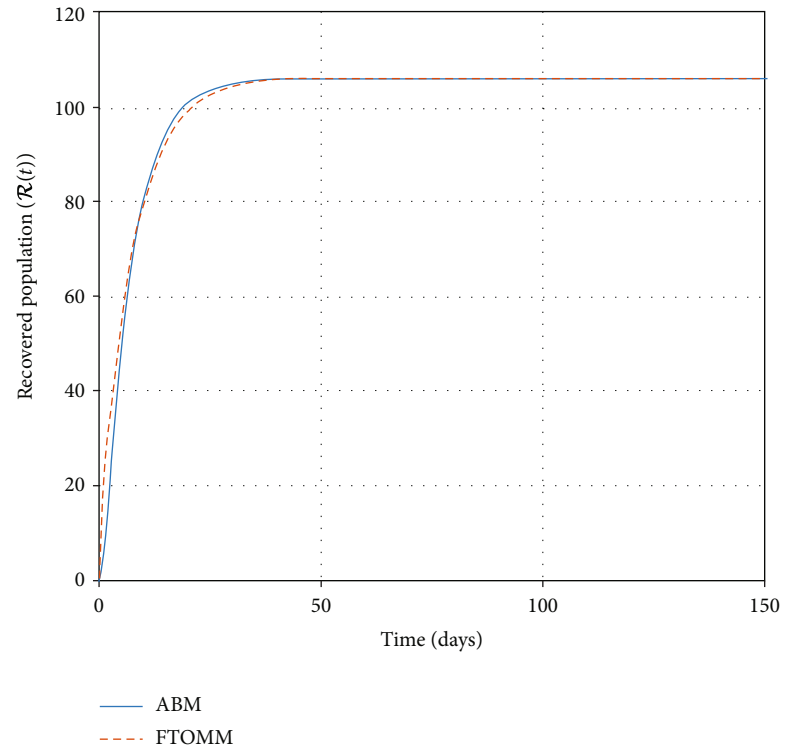

(d)

FIGURE 14: Comparisons between the ABM and FTOMM for the parametric values of S_2.

solutions of four state functions $\mathcal{S}(\mathbf{t})$, $\mathcal{P}_1(\mathbf{t})$, $\mathcal{P}_2(\mathbf{t})$, and $\mathcal{R}(\mathbf{t})$ by use of ABM and FTOMM are identical.

In Table 1, we present the solutions of four subclasses $\mathcal{S}(t)$, $\mathcal{P}_1(t)$, $\mathcal{P}_2(t)$, and $\mathcal{R}(t)$ obtained by use of the Adams-Bashforth and fractional Taylor operational matrix methods.

In Figure 9, we give the graphical illustration of the absolute errors of four subclasses $\mathcal{S}(\mathbf{t})$, $\mathcal{P}_1(\mathbf{t})$, $\mathcal{P}_2(\mathbf{t})$, and $\mathcal{R}(\mathbf{t})$

Table 1: Compared approximate results of four state functions obtained by ABM and FTOMM. (a) $\mathcal{S}$, (b) $\mathcal{P}_1$, (c) $\mathcal{P}_2$, and (d) $\mathcal{R}$.

(a)

t	$\mathcal{S}_{(\mathrm{ABM})}$	$\mathcal{S}_{(\mathrm{FTOMM})}$
0	0.50	0.50
25	266.9033	269.7917
50	129.1402	130.4819
75	114.4625	115.8542
100	115.6538	117.1644
125	115.6506	115.2917
150	115.6489	115.1839

(b)

t	$\mathcal{P}_{1(\mathrm{ABM})}$	$\mathcal{P}_{1(\mathrm{FTOMM})}$
0	0.30	0.30
25	2.6859	1.9753
50	54.1815	52.9918
75	53.1316	53.3214
100	52.6601	52.7443
125	52.6713	53.5863
150	52.6717	53.9160

(c)

t	$\mathcal{P}_{2(\mathrm{ABM})}$	$\mathcal{P}_{2(\mathrm{FTOMM})}$
0	0.20	0.20
25	1.9753	0.8732
50	10.7542	10.1061
75	9.2629	9.1954
100	9.2682	9.2501
125	9.2702	9.3729
150	9.2702	9.1423

(d)

t	$\mathcal{R}_{(\mathrm{ABM})}$	$\mathcal{R}_{(\mathrm{FTOMM})}$
0	0.10	0.10
25	150.9550	158.0875
50	270.5701	270.5721
75	271.7889	271.7783
100	269.6428	269.7108
125	269.2052	269.9315
150	269.0798	266.3295

obtained by the Adams-Bashforth and fractional Taylor operational matrix methods.

In this part, by using FTOMM, we simulate and discuss the behavior of the model based on the parametric values of the set S_2 provided by [60]. From this source, we assume the new parametric values to be $\Theta = 20$, $r = 0.079$, $s = 0.0001$, $b = 0.9$, $b_1 = 0.16$, $p = 0.29$, $b_2 = 0.11$, $r_1 = 0.45$, $q = 0.2$, $b_3 = 0.8$, and $r_2 = 0.9$. Finally, the initial values for state functions are the following:

$$\begin{aligned} \mathcal{S}(0) &= 0.5, \\ \mathcal{P}_1(0) &= 0.3, \\ \mathcal{P}_2(0) &= 0.2, \\ \mathcal{R}(0) &= 0.1. \end{aligned} \tag{113}$$

In Figures 10–13, we present the behaviors of solutions of four state functions $\mathcal{S}(\mathbf{t})$, $\mathcal{P}_1(\mathbf{t})$, $\mathcal{P}_2(\mathbf{t})$, and $\mathcal{R}(\mathbf{t})$, respectively, which are obtained by using FTOMM for some values of $\omega = 1.00,0.90,0.80,0.70,0.60,0.50$ where $\mathbf{t} \in [0,150]$.

From Figure 10, we can see the illustration of $\mathcal{S}(\mathbf{t})$ with initial value $S(0) = 0.5$ for several values of ω. It can be observed from this graph that the order of fractional derivative has an effect on convergence of people of susceptible category to stable case. Namely, at higher fractional orders, it converges slowly to a stable case, while at lower fractional order, this process is more quickly. About the density of $\mathcal{S}(\mathbf{t})$, we can observe that by increasing the fractional order, the density also increases. Also, we can clearly see that the fractional orders are highly consistent with integer order when using FTOMM.

From Figures 11–13, we can see the illustration of $\mathcal{P}_1(\mathbf{t})$, $\mathcal{P}_2(\mathbf{t})$, and $\mathcal{R}(\mathbf{t})$ with $\mathcal{P}_1(0) = 0.3$, $\mathcal{P}_2(0) = 0.2$, and $\mathcal{R}(0) = 0.1$, respectively, for some values of ω. It can be observed from these graphs that at higher fractional orders, people of asymptomatic, symptomatic, and recovered categories converge slowly to a stable case, while at lower fractional order, it is more quickly. Also, we observe that by increasing the fractional orders, the densities of $\mathcal{S}(\mathbf{t})$, $\mathcal{P}_1(\mathbf{t})$, $\mathcal{P}_2(\mathbf{t})$, and $\mathcal{R}(\mathbf{t})$ increases too.

In Figure 14, we present the comparison of the obtained solutions by use of the ABM and FTOMM for the parametric values of set S_2. From Figures 14(a)–14(d), we can clearly see that the both obtained approximate solutions of four state functions $\mathcal{S}(\mathbf{t})$, $\mathcal{P}_1(\mathbf{t})$, $\mathcal{P}_2(\mathbf{t})$, and $\mathcal{R}(\mathbf{t})$ by use of ABM and FTOMM are behaving identical.

It is clear from all figures that both obtained solutions by fractional Taylor operational matrix method and Adams-Bashforth method are identical. We can conclude that fractional Taylor operational matrix method gives almost the same results as the results acquired by Adams-Bashforth technique. Also, more accurate results can be obtained by enhancing the value of m and κ. Due to the simplicity of FTOMM, it is effective and has advantages for mathematical modelling of dynamics of SARS-CoV-2 virus.

9. Conclusions

In this manuscript, a fractal-fractional epidemic probability-based model of the SARS-CoV-2 virus with four compartments including susceptible, asymptomatic, symptomatic, and recovered was designed. By recalling a special group of contractions, named ϕ-admissible ϕ-ψ-contractionas, we proved the existence property for fixed points of a fractal-

fractional operator which is the same soultion of the mentioned system. Furthermore, other theoretical properties like stable solutions and their uniqueness for each compartments of the fractal-fractional model were established. We derived numerical solutions via the Adams-Bashforth and simulated them from several aspects such as variations of fractal-fractional dimension orders. Further, we formulated a Caputo type of the fractional model and compared its solutions obtained by the FTOMM method, with the previous ones of the fractal-fractional model. All simulations showed similar and close outcomes. From all illustrations presented in this work, we observed that the population of infected people converge quickly to a stable case at higher fractal-fractional orders and slowly to such a stable case at lower fractal-fractional orders. Also, we can see that by increasing the fractal-fractional orders, the density of susceptible population also increases. Also, from Figure 3, we can see that the probability of disease extinction increases with vaccination rate. All the numerical results and calculations are obtained with the help of MATLAB version R2019A. In the future, we aim to compare the results of our methods in the framework of other types of nonsingular kernels. Also, as a future study, the techniques introduced in this study can be modified to apply to other diseases and new variants of SARS-CoV-2 for different compartments.

Data Availability

Data sharing is not applicable to this article as no datasets were generated or analyzed during the current study.

Conflicts of Interest

The authors declare that they have no competing interests.

Authors' Contributions

The authors declare that the study was realized in collaboration with equal responsibility. All authors read and approved the final manuscript.

Acknowledgments

The first and second authors would like to thank the Azarbaijan Shahid Madani University.

References

[1] D. Fox, "What you need to know about the novel coronavirus," *Nature cell biology*, 2020.

[2] M. Hoffmann, H. Kleine-Weber, S. Schroeder et al., "SARS-CoV-2 cell entry depends on ACE2 and TMPRSS2 and is blocked by a clinically proven protease inhibitor," *Cell*, vol. 181, no. 2, pp. 271–280.e8, 2020.

[3] J. F. Chan, S. Yuan, K. H. Kok et al., "A familial cluster of pneumonia associated with the 2019 novel coronavirus indicating person-to-person transmission: a study of a family cluster," *Lancet*, vol. 395, no. 10223, pp. 514–523, 2020.

[4] M. Klompas, M. A. Baker, and C. Rhee, "Airborne transmission of SARS-CoV-2," *Journal of the American Medical Association*, vol. 324, no. 5, pp. 441-442, 2020.

[5] P. Anfinrud, C. E. Bax, and A. Bax, "Visualizing speech-generated oral fluid droplets with laser light scattering," *New England Journal of Medicine*, vol. 382, pp. 2061–2063, 2020.

[6] Y. J. Hou, K. Okuda, C. E. Edwards et al., "SARS-CoV-2 reverse genetics reveals a variable infection gradient in the respiratory tract," *Cell*, vol. 182, no. 2, pp. 429–446.e14, 2020.

[7] A. Banerjee, K. Mossman, and M. L. Baker, "Zooanthroponotic potential of SARS-CoV-2 and implications of reintroduction into human populations," *Cell Host & Microbe*, vol. 29, no. 2, pp. 160–164, 2021.

[8] http://www.covid19.who.int/, Accessed March 10, 2022.

[9] E. Mahase, "Covid-19: what treatments are being investigated?," *BMJ*, vol. 368, p. m1252, 2020.

[10] S. Rezapour, S. Etemad, and H. Mohammadi, "A mathematical analysis of a system of Caputo-Fabrizio fractional differential equations for the anthrax disease model in animals," *Advances in Difference Equations*, vol. 2020, no. 1, Article ID 481, 2020.

[11] A. Pratap, R. Raja, R. P. Agarwal, J. Alzabut, M. Niezabitowski, and E. Hincal, "Further results on asymptotic and finite-time stability analysis of fractional-order time-delayed genetic regulatory networks," *Neurocomputing*, vol. 475, pp. 26–37, 2022.

[12] H. Mohammadi, S. Kumar, S. Rezapour, and S. Etemad, "A theoretical study of the Caputo-Fabrizio fractional modeling for hearing loss due to mumps virus with optimal control," *Chaos, Solitons & Fractals*, vol. 144, article 110668, 2021.

[13] A. Ali, Q. Iqbal, J. K. K. Asamoah, and S. Islam, "Mathematical modeling for the transmission potential of Zika virus with optimal control strategies," *The European Physical Journal Plus*, vol. 137, no. 1, p. 146, 2022.

[14] P. Kumar, V. S. Erturk, and H. Almusawa, "Mathematical structure of mosaic disease using microbial biostimulants via Caputo and Atangana-Baleanu derivatives," *Results in Physics*, vol. 24, p. 104186, 2021.

[15] R. Zarin, H. Khaliq, A. Khan, D. Khan, A. Akgul, and U. W. Humphries, "Deterministic and fractional modeling of a computer virus propagation," *Results in Physics*, vol. 33, p. 105130, 2022.

[16] D. Baleanu, S. Etemad, and S. Rezapour, "A hybrid Caputo fractional modeling for thermostat with hybrid boundary value conditions," *Boundary Value Problems*, vol. 2020, no. 1, Article ID 64, 2020.

[17] J. Alzabut, G. M. Selvam, R. A. El-Nabulsi, D. Vignesh, and M. E. Samei, "Asymptotic stability of nonlinear discrete fractional pantograph equations with non-local initial conditions," *Symmetry*, vol. 13, no. 3, p. 473, 2021.

[18] J. K. K. Asamoah, E. Okyere, E. Yankson et al., "Non-fractional and fractional mathematical analysis and simulations for Q fever," *Chaos, Solitons & Fractals*, vol. 156, article 111821, 2022.

[19] H. Khan, C. Tunc, W. Chen, and A. Khan, "Existence theorems and Hyers-Ulam stability for a class of hybrid fractional differential equations with p -Laplacian operator," *Journal of Applied Analysis and Computation*, vol. 8, no. 4, pp. 1211–1226, 2018.

[20] Y. Rahmani, M. M. Alizadeh, H. Schuh, J. Wickert, and L. C. Tsai, "Probing vertical coupling effects of thunderstorms on lower ionosphere using GNSS data," *Advances in Space Research*, vol. 66, no. 8, pp. 1967–1976, 2020.

[21] Y. Rahmani and M. M. Alizadeh, "Irregularities in electron density above mesoscale thunderstorms using global navigation satellite systems measurements," in *7th Workshop on Vertical Coupling in Atmosphere-Ionosphere Systems*, GFZ, Potsdam, Germany, 2018.

[22] A. Omame, U. K. Nwajeri, M. Abbas, and C. P. Onyenegecha, "A fractional order control model for diabetes and COVID-19 co-dynamics with Mittag-Leffler function," *Alexandria Engineering Journal*, vol. 61, no. 10, pp. 7619–7635, 2022.

[23] S. Rezapour, C. T. Deressa, A. Hussain, S. Etemad, R. George, and B. Ahmad, "A theoretical analysis of a fractional multidimensional system of boundary value problems on the methylpropane graph via fixed point technique," *Mathematics*, vol. 10, no. 4, p. 568, 2022.

[24] A. Jajarmi, D. Baleanu, K. Zarghami Vahid, and S. Mobayen, "A general fractional formulation and tracking control for immunogenic tumor dynamics," *Mathematical Methods in the Applied Sciences*, vol. 45, no. 2, pp. 667–680, 2022.

[25] S. Salahshour, A. Ahmadian, B. A. Pansera, and M. Ferrara, "Uncertain inverse problem for fractional dynamical systems using perturbed collage theorem," *Communications in Nonlinear Science and Numerical Simulation*, vol. 94, no. 94, article 105553, 2021.

[26] V. S. Erturk, E. Godwe, D. Baleanu, P. Kumar, J. Asad, and A. Jajarmi, "Novel fractional-order Lagrangian to describe motion of beam on nanowire," *Acta Physica Polonica A*, vol. 140, no. 3, pp. 265–272, 2021.

[27] A. Jajarmi, D. Baleanu, K. Z. Vahid, H. M. Pirouz, and J. H. Asad, "A new and general fractional Lagrangian approach: a capacitor microphone case study," *Results in Physics*, vol. 31, p. 104950, 2021.

[28] M. Alqhtani, K. M. Owolabi, and K. M. Saad, "Spatiotemporal (target) patterns in sub-diffusive predator-prey system with the Caputo operator," *Chaos, Solitons & Fractals*, vol. 160, article 112267, 2022.

[29] S. Aljhani, M. S. Noorani, K. M. Saad, and A. K. Alomari, "Numerical solutions of certain new models of the time-fractional Gray-Scott," *Journal of Function Spaces*, vol. 2021, Article ID 2544688, 12 pages, 2021.

[30] M. H. DarAssi, M. A. Safi, M. A. Khan, A. Beigi, A. A. Aly, and M. Y. Alshahrani, "A mathematical model for SARS-CoV-2 in variable-order fractional derivative," *The European Physical Journal Special Topics*, vol. 231, no. 10, pp. 1905–1914, 2022.

[31] Y. Gu, M. A. Khan, Y. S. Hamed, and B. F. Felemban, "A comprehensive mathematical model for SARS-CoV-2 in Caputo derivative," *Fractal and Fractional*, vol. 5, no. 4, p. 271, 2021.

[32] K. Rajagopal, N. Hasanzadeh, F. Parastesh, I. I. Hamarash, S. Jafari, and I. Hussain, "A fractional-order model for the novel coronavirus (COVID-19) outbreak," *Nonlinear Dynamics*, vol. 101, no. 1, pp. 711–718, 2020.

[33] A. S. Quintero and R. E. Gutiérrez-Carvajal, "Modeling the evolution of SARS-CoV-2 using a fractional-order SIR approach," *TecnoLógicas*, vol. 24, no. 51, article e1866, 2021.

[34] M. Zamir, K. Shah, F. Nadeem et al., "Threshold conditions for global stability of disease free state of COVID-19," *Results in Physics*, vol. 21, no. 21, article 103784, 2021.

[35] N. Jain, S. Jhunthra, H. Garg et al., "Prediction modelling of COVID using machine learning methods from B-cell dataset," *Results in physics*, vol. 21, no. 21, article 103813, 2021.

[36] D. Baleanu, M. H. Abadi, A. Jajarmi, K. Z. Vahid, and J. J. Nieto, "A new comparative study on the general fractional model of COVID-19 with isolation and quarantine effects," *Alexandria Engineering Journal*, vol. 61, no. 6, pp. 4779–4791, 2022.

[37] Z. Ali, F. Rabiei, M. M. Rashidi, and T. Khodadadi, "A fractional-order mathematical model for COVID-19 outbreak with the effect of symptomatic and asymptomatic transmissions," *The European Physical Journal Plus*, vol. 137, no. 3, pp. 1–20, 2022.

[38] F. Ozkose, M. Yavuz, M. T. Senel, and R. Habbireeh, "Fractional order modelling of omicron SARS-CoV-2 variant containing heart attack effect using real data from the United Kingdom," *Chaos, Solitons & Fractals*, vol. 157, article 111954, 2022.

[39] A. Khan, H. Ullah, M. Zahri et al., "Stationary distribution and extinction of stochastic coronavirus (COVID-19) epidemic model," *Fractals*, vol. 30, no. 1, article 2240050, 2022.

[40] P. A. Naik, M. Yavuz, S. Qureshi, J. Zu, and S. Townley, "Modeling and analysis of COVID-19 epidemics with treatment in fractional derivatives using real data from Pakistan," *The European Physical Journal Plus*, vol. 135, no. 10, p. 795, 2020.

[41] M. L. Holshue, C. DeBolt, S. Lindquist et al., "First case of 2019 novel coronavirus in the United States," *New England Journal of Medicine*, vol. 382, no. 10, pp. 929–936, 2020.

[42] Z. Ali, F. Rabiei, K. Shah, and T. Khodadadi, "Qualitative analysis of fractal-fractional order COVID-19 mathematical model with case study of Wuhan," *Alexandria Engineering Journal*, vol. 60, no. 1, pp. 477–489, 2021.

[43] Z. Ali, F. Rabiei, K. Shah, and T. Khodadadi, "Modeling and analysis of novel COVID-19 under fractal-fractional derivative with case study of Malaysia," *Fractals*, vol. 29, no. 1, p. 2150020, 2021.

[44] Z. Ali, F. Rabiei, K. Shah, and Z. A. Majid, "Dynamics of SIR mathematical model for COVID-19 outbreak in Pakistan under fractal-fractional derivative," *Fractals*, vol. 29, no. 5, article 2150120, 2021.

[45] A. Din, A. Khan, A. Zeb, M. R. S. Ammi, M. Tilioua, and D. F. M. Torres, "Hybrid method for simulation of a fractional COVID-19 model with real case application," *Axioms.*, vol. 10, no. 4, p. 290, 2021.

[46] M. Rahman, S. Ahmad, R. T. Matoog, N. A. Alshehri, and T. Khan, "Study on the mathematical modelling of COVID-19 with Caputo-Fabrizio operator," *Chaos, Solitons & Fractals*, vol. 150, article 111121, 2021.

[47] M. I. Abbas and M. A. Ragusa, "Solvability of Langevin equations with two Hadamard fractional derivatives via Mittag–Leffler functions," *Applicable Analysis*, vol. 101, no. 9, pp. 3231–3245, 2022.

[48] A. Atangana, "Fractal-fractional differentiation and integration: connecting fractal calculus and fractional calculus to predict complex system," *Chaos, Solitons & Fractals*, vol. 102, pp. 396–406, 2017.

[49] M. Arfan, K. Shah, and A. Ullah, "Fractal-fractional mathematical model of four species comprising of prey-predation," *Physica Scripta*, vol. 96, no. 12, p. 124053, 2021.

[50] M. Abdulwasaa, M. S. Abdo, K. Shah et al., "Fractal-fractional mathematical modeling and forecasting of new cases and deaths of COVID-19 epidemic outbreaks in India," *Results in Physics*, vol. 20, article 103702, 2021.

[51] K. Shah, M. Arfan, I. Mahariq, A. Ahmadian, S. Salahshour, and M. Ferrara, "Fractal-fractional mathematical model addressing the situation of corona virus in Pakistan," *Results in Physics*, vol. 19, article 103560, 2020.

[52] Z. A. Khan, M. Ur Rahman, and K. Shah, "Study of a fractal-fractional smoking models with relapse and harmonic mean type incidence rate," *Journal of Function Spaces*, vol. 2021, Article ID 6344079, 11 pages, 2021.

[53] M. Arif, P. Kumam, W. Kumam, A. Akgul, and T. Sutthibutpong, "Analysis of newly developed fractal-fractional derivative with power law kernel for MHD couple stress fluid in channel embedded in a porous medium," *Scientific Reports*, vol. 11, no. 1, p. 20858, 2021.

[54] M. Alqhtani and K. M. Saad, "Fractal–fractional Michaelis–Menten enzymatic reaction model via different kernels," *Fractal and Fractional*, vol. 6, no. 1, p. 13, 2022.

[55] A. A. Khan, R. Amin, S. Ullah, W. Sumelka, and M. Altanji, "Numerical simulation of a Caputo fractional epidemic model for the novel coronavirus with the impact of environmental transmission," *Alexandria Engineering Journal*, vol. 61, no. 7, pp. 5083–5095, 2022.

[56] Y. Zhou and Y. Zhang, "Noether symmetries for fractional generalized Birkhoffian systems in terms of classical and combined Caputo derivatives," *Acta Mechanica*, vol. 231, no. 7, pp. 3017–3029, 2020.

[57] W. Sumelka, B. Luczak, T. Gajewski, and G. Z. Voyiadjis, "Modelling of AAA in the framework of time-fractional damage hyperelasticity," *International Journal of Solids and Structures*, vol. 206, pp. 30–42, 2020.

[58] B. Samet, C. Vetro, and P. Vetro, "Fixed point theorems for -ψ -contractive type mappings," *Nonlinear analysis: theory, methods & applications*, vol. 75, no. 4, pp. 2154–2165, 2012.

[59] T. Khan, R. Ullah, G. Zaman, and J. Alzabut, "A mathematical model for the dynamics of SARS-CoV-2 virus using the Caputo-Fabrizio operator," *Mathematical Biosciences and Engineering*, vol. 18, no. 5, pp. 6095–6116, 2021.

[60] T. Khan, R. Ullah, G. Zaman, and Y. El Khatib, "Modeling the dynamics of the SARS-CoV-2 virus in a population with asymptomatic and symptomatic infected individuals and vaccination," *Physica Scripta*, vol. 96, no. 10, article 104009, 2021.

[61] A. Granas and J. Dugundji, *Fixed Point Theory*, Springer-Verlag, New York, 2003.

[62] I. Avci, "Numerical simulation of fractional delay differential equations using the operational matrix of fractional integration for fractional-order Taylor basis," *Fractal and Fractional*, vol. 6, no. 1, p. 10, 2022.

[63] I. Avci and N. I. Mahmudov, "Numerical solutions for multi-term fractional order differential equations with fractional Taylor operational matrix of fractional integration," *Mathematics*, vol. 8, no. 1, p. 96, 2020.

[64] V. S. Krishnasamy, S. Mashayekhi, and M. Razzaghi, "Numerical solutions of fractional differential equations by using fractional Taylor basis," *IEEE/CAA Journal of Automatica Sinica*, vol. 4, no. 1, pp. 98–106, 2017.